UC Merced

UC Merced Previously Published Works

Title

Reconstitution of an intact clock reveals mechanisms of circadian timekeeping.

Permalink

https://escholarship.org/uc/item/7x09z73n

Journal

Science (New York, N.Y.), 374(6564)

ISSN

0036-8075

Authors

Chavan, Archana G
Swan, Jeffrey A
Heisler, Joel
et al.

Publication Date

2021-10-01

DOI

10.1126/science.abd4453

Peer reviewed

eScholarship.org Powered by the California Digital Library
University of California

RESEARCH ARTICLE SUMMARY

CIRCADIAN RHYTHMS

Reconstitution of an intact clock reveals mechanisms of circadian timekeeping

Archana G. Chavan†, Jeffrey A. Swan†, Joel Heisler†, Cigdem Sancar, Dustin C. Ernst, Mingxu Fang, Joseph G. Palacios, Rebecca K. Spangler, Clive R. Bagshaw, Sarvind Tripathi, Priya Crosby, Susan S. Golden, Carrie L. Partch*, Andy LiWang*

INTRODUCTION: Circadian clocks provide an internal representation of local time inside cells and control the timing of gene expression in anticipation of sunrise and sunset. In cyanobacteria, timekeeping is achieved by way of an oscillator comprising three Kai (meaning "cycle" in Japanese) proteins, KaiA, KaiB, and KaiC, which relay temporal information downstream through two sensor histidine kinases, SasA and CikA, to regulate the transcription factor RpaA. Identifying the specific mechanisms by which circadian clocks exert temporal control over gene expression has proven challenging in the complex milieu of cells. Thus, we reassembled an intact clock, including the core oscillator and signal transduction components, under defined conditions in vitro. Together with structural studies and biochemical analyses of partial clock reactions, we acquired insights into mechanisms by which the cyanobacterial circadian clock functions to control gene expression.

RATIONALE: Although the core oscillator can be reconstituted in vitro with just the Kai proteins, these reactions assayed by SDS–polyacrylamide gel electrophoresis report only on the phosphorylation status of KaiC and have therefore not offered mechanistic insight into clock protein interactions or signal transduction. Thus, we developed a fluorescence polarization–based in vitro whole-clock system that includes the KaiABC oscillator, SasA and/or CikA, RpaA, and a clock promoter–bearing DNA fragment. This in vitro clock (IVC) oscillates autonomously for days and allows monitoring of each component individually in real time, revealing the formation and phase of macromolecular assemblies from the timekeeper to DNA binding by RpaA.

RESULTS: The IVC was used to examine the sufficiency of SasA or CikA to maintain clock output under constant conditions and identify how each contributes to the phase of DNA binding by RpaA; it even allowed the dissection of the breakdown in signaling of an arrhythmic mutant of RpaA. We challenged a long-standing paradigm that timekeeping by the oscillator depends solely on the Kai proteins, with SasA and CikA providing only input-output signaling. The in vitro oscillator is known to function under a relatively narrow set of Kai protein concentrations; we show here that a KaiABC-only mixture that fails to oscillate in a sustained manner owing to limiting levels of KaiB can be rescued by SasA, which acts to recruit KaiB to the KaiC hexamer through heterotropic cooperativity. Cooperativity is based on structural mimicry between SasA and KaiB, and mutations that eliminate heterocooperativity in vitro profoundly affect circadian rhythms in vivo. CikA also rescues period defects under low levels of KaiA. Together, our data help to explain how the clock compensates in vivo for changes in concentrations of oscillator components that occur as part of the transcription-translation feedback loop and protein turnover. The intimate coupling between oscillator and input-output components blurs their distinction, although the extent to which this coupling can be generalized to eukaryotic clocks remains an open question.

CONCLUSION: We developed the reconstituted IVC to establish causal links between clock biochemistry and in vivo phenotypes. Our system provides a powerful platform to explore, for example, how changes in factors such as temperature or adenosine triphosphate levels are compensated to allow generation of reliable circadian rhythms of transcription.

In fact, this IVC is just a starting point, one with many possibilities. For example, the real-time data presented here will allow mathematical models of the cyanobacterial clock to extend beyond the KaiABC oscillator to address the events that effect temporal control of physiology and metabolism. As a next step, transplanting this IVC to artificial cells could enable single-cell microscopy experiments of this streamlined clock under conditions that are much closer to physiological. In an artificial cellular system, transcriptional and translational networks could be included, allowing higher-complexity customized frequencies and outputs to be engineered, opening the door to synthetic biology applications. ■

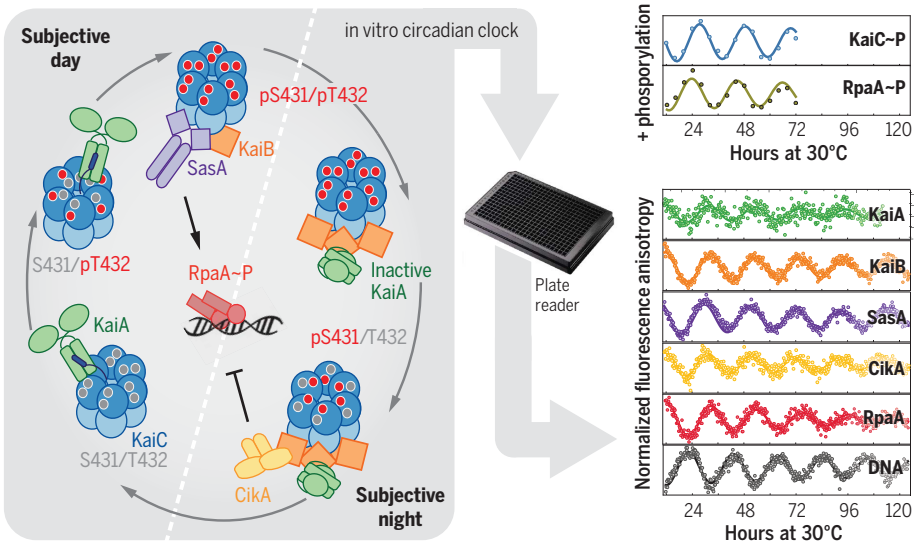

Reconstituting an intact clock in vitro. Cyanobacterial circadian proteins KaiA, KaiB, KaiC, SasA, CikA, RpaA, and a promoter-bearing DNA fragment were reconstituted into an in vitro clock. Together with structural studies and biochemical assays, this system allowed dissection of a circadian clock system to demonstrate that the concept of the core oscillator should be extended to include output proteins SasA and CikA. The dashed line separates subjective day and subjective night, which refer to the halves of a circadian period under constant conditions that correspond to day and night in a light-dark cycle. S, serine; T, threonine; p, phosphorylated.

The list of author affiliations is available in the full article online.
*Corresponding author. Email: aliwang@ucmerced.edu (A.L.); cpartch@ucsc.edu (C.L.P.)
†These authors contributed equally to this work.
Cite this article as A. G. Chavan *et al.*, *Science* **374**, eabd4453 (2021). DOI: 10.1126/science.abd4453

READ THE FULL ARTICLE AT
https://doi.org/10.1126/science.abd4453

Downloaded from https://www.science.org at University of California Merced on October 09, 2021

RESEARCH ARTICLE

CIRCADIAN RHYTHMS

Reconstitution of an intact clock reveals mechanisms of circadian timekeeping

Archana G. Chavan[1]†, Jeffrey A. Swan[2]†, Joel Heisler[3]†, Cigdem Sancar[4], Dustin C. Ernst[4], Mingxu Fang[4], Joseph G. Palacios[2], Rebecca K. Spangler[2], Clive R. Bagshaw[2], Sarvind Tripathi[2], Priya Crosby[2], Susan S. Golden[4,5], Carrie L. Partch[2,4]*, Andy LiWang[1,3,4,6,7]*

Circadian clocks control gene expression to provide an internal representation of local time. We report reconstitution of a complete cyanobacterial circadian clock in vitro, including the central oscillator, signal transduction pathways, downstream transcription factor, and promoter DNA. The entire system oscillates autonomously and remains phase coherent for many days with a fluorescence-based readout that enables real-time observation of each component simultaneously without user intervention. We identified the molecular basis for loss of cycling in an arrhythmic mutant and explored fundamental mechanisms of timekeeping in the cyanobacterial clock. We find that SasA, a circadian sensor histidine kinase associated with clock output, engages directly with KaiB on the KaiC hexamer to regulate period and amplitude of the central oscillator. SasA uses structural mimicry to cooperatively recruit the rare, fold-switched conformation of KaiB to the KaiC hexamer to form the nighttime repressive complex and enhance rhythmicity of the oscillator, particularly under limiting concentrations of KaiB. Thus, the expanded in vitro clock reveals previously unknown mechanisms by which the circadian system of cyanobacteria maintains the pace and rhythmicity under variable protein concentrations.

Circadian clocks are intracellular systems that provide organisms with an internal representation of local time and have profound consequences to health (*1*). The clock in the cyanobacterium *Synechococcus elongatus* generates circadian rhythms of genetic, physiological, and metabolic activities that enhance fitness (*2*, *3*). The core circadian clock genes of cyanobacteria, *kaiA*, *kaiB*, and *kaiC*, are essential for rhythmic gene expression (*4*), and their proteins generate an autonomous ~24-hour rhythm of KaiC phosphorylation in vivo (*5*), which can be recapitulated in vitro (*6*). Ordered phosphorylation of KaiC at residues S431 and T432 (*7*, *8*), stimulated by KaiA during the day (*9*, *10*) and suppressed by KaiB at night (*11*, *12*), helps set the circadian pace and phase of the oscillator (*13*–*15*). The input-output sensor histidine kinases, *Synechococcus* adaptive sensor A, SasA (*16*), and circadian input kinase A, CikA (*17*), interact with Kai proteins (*14*, *18*) to regulate the master transcription factor, RpaA (*19*), and generate circadian rhythms of gene expression in cyanobacteria (*20*, *21*).

Although the reconstituted KaiABC oscillator has been a powerful tool to study mechanisms of circadian timekeeping in cyanobacteria (*6*, *15*, *22*–*24*), it does not include the signal transduction machinery necessary to provide a readout of timing encoded by the biochemical oscillator. To explore how each component interacts in the network and how output proteins integrate with the core oscillator, we reconstituted clock-controlled DNA binding in a cell-free system that enables real-time reporting from different partners. In addition to the core oscillator components KaiA, KaiB, and KaiC, this in vitro clock (IVC) includes SasA and/or CikA, RpaA, and a DNA duplex that carries a clock-controlled promoter, demonstrating that these components are sufficient to form the fundamental regulatory network for autonomous timekeeping and temporal relay to downstream events. We then use this IVC to identify how a loss-of-function allele in RpaA disrupts circadian rhythms, highlighting its power to provide mechanistic insight for in vivo studies. Moreover, through careful deconstruction of our expanded IVC, we discovered that SasA helps to cooperatively recruit KaiB to the KaiC hexamer, thus defining a previously unknown role for SasA in the core oscillator that it is required for proper circadian rhythms in vivo.

Signal transduction in a reconstituted IVC

To monitor protein interactions in the IVC, we attached fluorescent probes (*25*) to each of the individual clock protein components, KaiA, KaiB, SasA, CikA, and RpaA (see methods in the supplementary materials and tables S1 to S3) using sortase A–mediated ligation (*26*, *27*) and monitored their association into larger complexes using fluorescence anisotropy (FA) (Fig. 1, A to C, and fig. S1).

Fluorescently labeled synthetic double-stranded DNA representing the promoter sequence of the *kaiBC* operon, P*kaiBC*, was used as a representative RpaA target (*20*), and each labeled species was monitored in separate but parallel clock reactions (table S4). Control experiments were performed to verify the specific binding events that cause changes in FA of each labeled species (figs. S2 and S3), assigning their corresponding peaks to known interactions and circadian properties.

We used a multimode microplate reader to monitor in vitro oscillations in parallel, with individual reactions containing 50 to 100 nM of a single fluorescently labeled species for each protein or DNA monitored, as well as physiological concentrations (*20*) of each unlabeled clock protein. This method allowed measurement of FA for each clock component in a single plate and in real time over a duration of several days.

The data from these experiments were fit to a damped cosine function to extract period and phase relative to maximal KaiC phosphorylation, which was referenced to its peak at circadian time (CT) 14 in vivo (*9*), with CT 0 and CT 12 representing subjective dawn and dusk, respectively, under constant lab conditions. Combining FA measurements with traditional time courses of RpaA and KaiC phosphorylation rhythms measured in parallel by gel electrophoresis (Fig. 1 and figs. S4 and S5), we present a comprehensive view of a fully reconstituted IVC.

KaiC adenosine triphosphatase (ATPase) activity was monitored in real time by proton nuclear magnetic resonance (^{1}H-NMR) imaging (Fig. 1D and fig. S6) (*28*) using the core oscillator to avoid conflation with ATP consumption by the output kinases. We found that the ATPase activity of KaiC peaks during subjective midday with the hydrolysis of ~13 to 18 ATPs per KaiC monomer per day but decreases to a nadir of ~7 or 8 ATPs per KaiC monomer per day during subjective night, which is consistent with earlier studies (*29*). Using this information, we next established the phase relationships of all the clock components under each IVC condition (Fig. 1, E to G). We found that the FA of RpaA increased when it was dephosphorylated or interacting with SasA in the absence of KaiC and that it decreased when RpaA was phosphorylated by CikA or a SasA-KaiC complex (fig. S3), which explains the observed phase reversal between peak RpaA anisotropy and RpaA phosphorylation.

[1]School of Natural Sciences, University of California, Merced, CA 95343, USA. [2]Department of Chemistry and Biochemistry, University of California, Santa Cruz, CA 95064, USA. [3]Department of Chemistry and Biochemistry, University of California, Merced, CA 95343, USA. [4]Center for Circadian Biology, University of California, San Diego, La Jolla, CA 92093, USA. [5]Division of Biological Sciences, University of California, San Diego, La Jolla, CA 92093, USA. [6]Center for Cellular and Biomolecular Machines, University of California, Merced, CA 95343, USA. [7]Health Sciences Research Institute, University of California, Merced, CA 95343, USA.
*Corresponding author. Email: aliwang@ucmerced.edu (A.L.); cpartch@ucsc.edu (C.L.P.)
†These authors contributed equally to this work.

Downloaded from https://www.science.org at University of California Merced on October 09, 2021

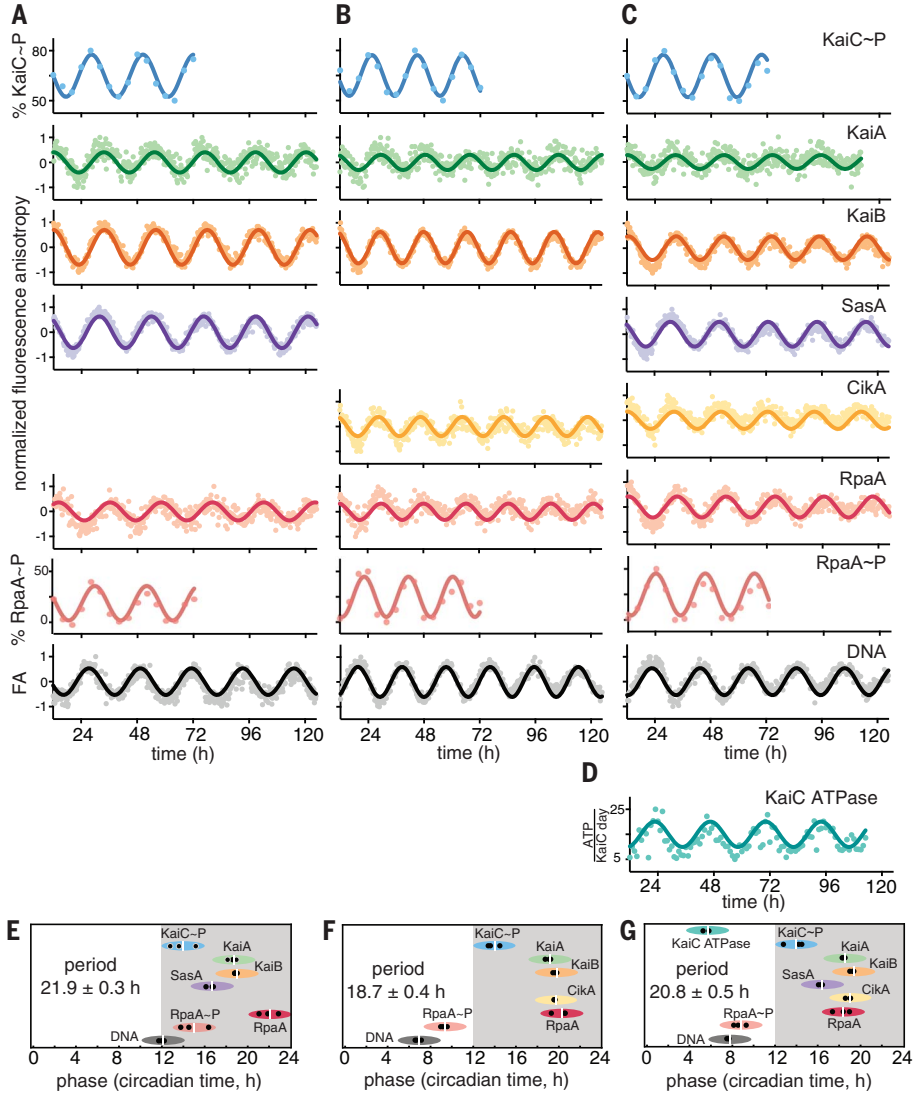

Fig. 1. Reconstitution of an intact clock that controls rhythmic DNA binding in vitro. (**A** to **C**) IVC reactions containing KaiA, KaiB, KaiC, RpaA, P*kaiBC* DNA, 1 mM ATP, 5 mM $MgCl_2$, and SasA and/or CikA. 50 nM fluorescently labeled KaiA (green), KaiB (orange), SasA (purple), CikA (yellow), RpaA (red), or 100 nM P*kaiBC* (gray) were included in separate reactions, and their fluorescence anisotropies (FA) were measured in a microplate reader at 30°C. For phosphorylation experiments, KaiC~P (blue) and RpaA~P (salmon) were quantified by gel electrophoresis on SDS-PAGE and Zn^{2+}-Phos-tag gels respectively. After truncating the first 12 hours of data collection during which samples approached stable limit cycles, data were baseline-corrected and fit to a damped cosine function to calculate periods and phases (see materials and methods in the supplementary materials). FA values were normalized before fitting. (**D**) KaiC-ATPase was measured by real-time ^{1}H-NMR in a KaiABC-only reaction to isolate the KaiC ATPase activity. (**E** to **G**) Relative phases for each component in (A) to (C), determined from three separate experiments, are shown by black dots, with the average denoted by a white vertical line, and the peak of KaiC~P is referenced to CT14 (*9*). The width of each ellipse is ±2 hours centered at the peak. Full dataset is available in data S1.

Exploring clock output by SasA and CikA

Transcriptional output in cyanobacterial circadian rhythms is based on the antagonistic activity of two sensor histidine kinases; SasA is a KaiC-dependent kinase that phosphorylates RpaA to stimulate DNA binding and activate gene expression at dusk, whereas CikA is stimulated to act as a phosphatase that dephosphorylates RpaA when it associates with the Kai complex at night (*16*, *17*, *19*, *21*, *30*). To better understand the activities of each sensor histidine kinase in clock output, we first studied the reconstituted clock under conditions where only one was present at a time. In an IVC that contained KaiA, KaiB, KaiC, and SasA alone with RpaA and DNA (Fig. 1A), the relative phases of the protein interaction rhythms (Fig. 1E) were largely consistent with those reported in vivo (*31*). For example, FA rhythms of KaiA, KaiB, and SasA peaked from CT 15 to 22, indicating the formation of large protein complexes during subjective night owing to interaction with KaiC. These proteins also form large complexes in vivo around Zeitgeber time (ZT) 16 to 22 (*32*), where ZT 0 and ZT 12 correspond to dawn and dusk, respectively, under a light-dark cycle. Although SasA and KaiB bind to overlapping sites on KaiC (*33*), we observed that the rhythms of SasA binding to KaiC peak ~3 hours earlier than those of KaiB (Fig. 1, A and E). In principle, this phase difference could provide a temporal window for the KaiC-dependent activation of SasA autophosphorylation (*20*), allowing the phosphoryl transfer from SasA to RpaA (*19*) that is observed around subjective dusk in the IVC (Fig. 1E). RpaA dephosphorylation in the SasA-only IVC is likely due to a combination of the inherent autophosphatase activity typically seen in response regulators (*34*, *35*) and weak phosphatase activity of SasA (*21*).

When SasA was replaced by CikA in the IVC, we still saw circadian rhythms in the interaction of KaiA and KaiB with KaiC in the same relative phase with KaiC phosphorylation (Fig. 1, B and F), although the period was ~3 hours shorter. The FA of CikA peaked in phase with KaiB, consistent with recruitment of the pseudoreceiver (PsR) domain of CikA to the KaiB-KaiC complex in the subjective night (*36*). We verified that formation of this complex stimulates the phosphatase activity of CikA toward RpaA and that CikA can act as an RpaA kinase when not associated with the KaiB-KaiC complex (figs. S7 and S8), as previously reported (*21*, *37*). The bifunctional switching of CikA between phosphatase and kinase in the IVC likely causes the phase advance in the rhythms of RpaA phosphorylation and DNA binding relative to the SasA-only IVC by ~5 hours (Fig. 1F and fig. S9). CikA levels in vivo are normally low under high-intensity light (*38*) (fig. S10, B and C), suggesting that it may be limited to acting predominantly as a phosphatase at night. However, Δ*sasA* strains generate circadian rhythms in low light (*16*), suggesting that environmental conditions that favor CikA stability can rescue circadian rhythms. We demonstrated robust CikA-dependent circadian rhythms in strains that lack SasA but still express CikA and in which KaiB and KaiC were boosted to wild-type (WT) levels by circumventing autoregulation; notably, these rhythms occurred with a phase advance similar to that of the CikA-only IVC (fig. S10A). Taken with the observation that Δ*sasA*Δ*cikA* strains are arrhythmic (*39*), these data suggest that the circadian rhythms observed in Δ*sasA* strains arise from a CikA-mediated regulatory circuit on RpaA. When CikA is present constitutively in the IVC, it can drive rhythms of RpaA

Downloaded from https://www.science.org at University of California Merced on October 09, 2021

phosphorylation both in the absence (Fig. 1B) and presence of SasA (Fig. 1C) to push the phase of peak DNA binding to midday instead of dusk (Fig. 1, F and G). Thus, the IVC recapitulates to a reasonable extent the relative in vivo phases of the circadian clock of *S. elongatus* and enables aspects of the clock—input (*40*, *41*), oscillator (*6*), and output (*20*, *21*, *39*, *42*)—to be measured under defined conditions with multiple readouts simultaneously in real time, including the phosphorylation-dependent interactions of RpaA (fig. S11) with a cognate promoter element in DNA.

Leveraging the extended oscillator to study clock mechanisms

Reconstitution of the cyanobacterial clock offers the possibility to ask questions about how downstream signal transduction components are coupled to the KaiABC oscillator to provide deeper mechanistic insight into circadian biology. First, we sought to explore the mechanistic origins of clock disruption in an arrhythmic *S. elongatus* strain that was originally reported as a *crm1* transposon-insertion allele (*43*). However, in addition to disruption of *crm1*, we also noted a single-nucleotide polymorphism in the *rpaA* gene located immediately downstream, resulting in an Arg^{121}→Gln (R121Q) amino acyl substitution in RpaA. When we reconstructed the allele of *rpaA-R121Q* in a WT reporter strain by markerless CRISPR-Cas12a editing (*44*), it displayed the same arrhythmic phenotype (Fig. 2A), demonstrating that mutation of *rpaA*, not *crm1*, disrupted clock function. Despite having a WT RpaA phosphorylation pattern (Fig. 2B and fig. S12), the mutant strain did not produce rhythmic gene expression (Fig. 2A). We used the IVC to test the hypothesis that the RpaA-R121Q variant is deficient in DNA binding, even in its phosphorylated form. Although we observed circadian rhythms of FA (fig. S13) and phosphorylation (Fig. 2B and fig. S14) in the mutant that were similar to WT RpaA, the R121Q mutant bound poorly to the P*kaiBC* promoter, as indicated by the low amplitude of DNA FA (Fig. 2C). Thus, the IVC helped to identify the mechanism of clock disruption by the R121Q amino acyl substitution in RpaA—it does not hinder regulatory interactions with SasA or CikA but instead prevents the phosphorylated sensor domain from regulating its DNA binding domain.

Effect of protein concentrations on rhythmicity and period of the clock

The core oscillator has a well-established, albeit relatively narrow, range of concentrations of KaiA, KaiB, and KaiC under which sustained biochemical rhythms can be observed in vitro (*45*). Using our newly developed fluorescence-based readout, we next measured how rhythms in the core oscillator depend on concentrations of KaiA and KaiB (Fig. 3). We found a notable

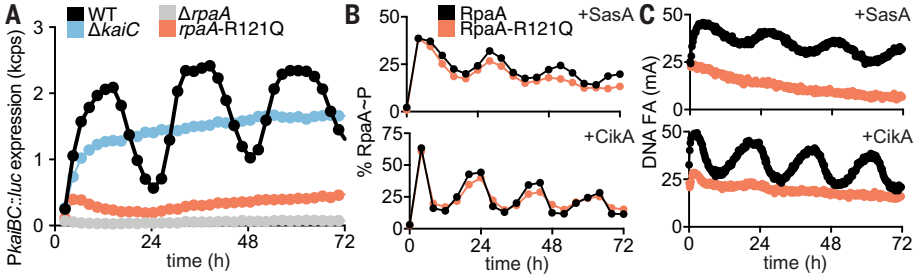

Fig. 2. The IVC reveals a defect in DNA binding by the RpaA-R121Q mutant. (**A**) Rhythms of bioluminescence generated by P*kaiBC::luc* expression were monitored for entrained WT (black), Δ*kaiC* (blue), Δ*rpaA* (gray), and *rpaA*-R121Q (salmon) cyanobacterial strains. Each plot represents an average of six biological replicates. kcps, kilocounts per second. (**B**) Rhythms of RpaA phosphorylation or (**C**) FA of P*kaiBC* DNA in IVC reactions containing either SasA or CikA, as in Fig. 1, A and B.

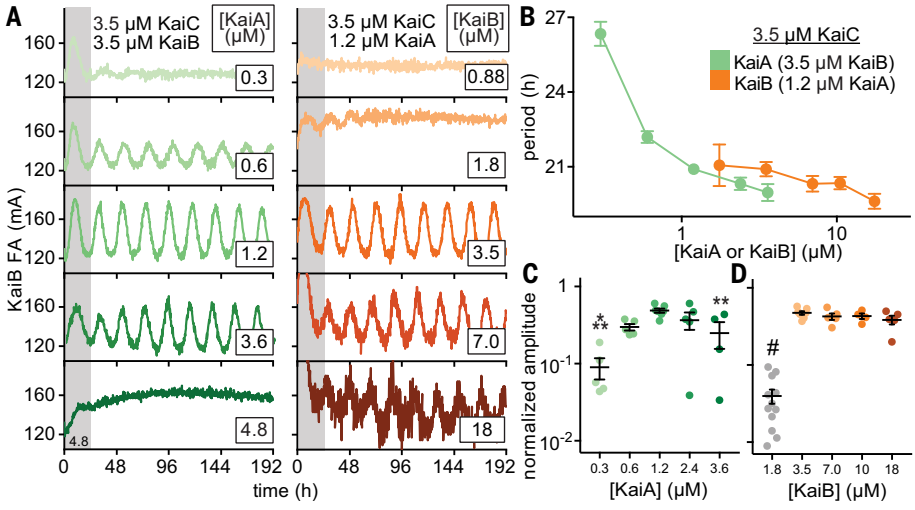

Fig. 3. Rhythmicity and period of the oscillator depend in different ways on the concentrations of KaiA and KaiB. (**A**) In vitro oscillator reactions containing 3.5 μM KaiC, 3.5 μM KaiB (including 50 nM fluorescently labeled KaiB as a probe), and titrations of KaiA from 0.3 to 6.0 μM (green scale, left column). Representative assay from $n = 3$ are shown; the first 24 hours of the reactions are shaded gray. Assays were also performed with 3.5 μM KaiC, 1.2 μM KaiA, and titrations of KaiB from 0.7 to 18 μM (orange scale, right panel). FA data were fit to a cosine function to extract period (**B**) and amplitude (**C** and **D**) as a function of KaiA or KaiB concentration. Amplitudes for KaiB titrations were normalized to account for an increasing ratio of unlabeled KaiB to fluorescently labeled probe KaiB. Reactions that did not oscillate were not included. Data are shown as mean ± SD ($n \geq 3$). One-way analysis of variance (ANOVA) with Dunnett's multiple comparisons test was used for comparison of each suboptimal condition with the 1.2 μM KaiA, 3.5 μM KaiB condition: $^{*}P < 0.05$; $^{**}P < 0.01$; $^{***}P < 0.001$; #$P < 0.0001$. Where no symbol is shown, differences were determined not to be statistically significant. Full datasets are available in data S2 and S3.

convergence with previous studies monitoring rhythms of KaiC phosphorylation by SDS–polyacrylamide gel electrophoresis (SDS-PAGE) (*45*). Because the fluorescence-based oscillator can be monitored noninvasively in a 384-well format, we could follow rhythms for many days longer than is practical for the KaiC phosphorylation assay and quantify sensitivity of oscillation amplitude and period to concentrations of the oscillator components. In general, the oscillator functions well with substoichiometric concentrations of KaiA, although the period lengthened as KaiA concentration was decreased (Fig. 3, A to C, and table S5). By contrast, oscillator period was not affected by titrating KaiB, although there was a clear requirement for KaiB to be present at concentrations at least equivalent to that of KaiC (Fig. 3D).

At one-half stoichiometry of KaiB relative to KaiC (1.75 μM KaiB and 3.5 μM KaiC), the oscillator functioned at low amplitude for only a few days with a normal circadian period before significantly damping to arrhythmicity (Fig. 3A). As KaiB is found in slight excess over KaiC in vivo (*11*, *46*), it may be essential for the KaiC hexamer to recruit a full stoichiometric complement of six molecules of KaiB to stably

Downloaded from https://www.science.org at University of California Merced on October 09, 2021

sequester KaiA and facilitate the KaiC dephosphorylation phase in subjective night. Consistent with this model, rhythms abruptly diminished as the concentration of KaiA exceeded that of KaiC (Fig. 3A) (*45*, *47*).

CikA rescues oscillator period under limiting concentrations of KaiA

Although CikA is primarily considered an input-output protein (*17*, *21*, *39*), it is known to affect circadian period in vivo and was recently shown to regulate the period of the core oscillator in vitro (*37*, *48*). We previously determined that the PsR domain of CikA competes for the KaiA binding site on the KaiB-KaiC nighttime complex (*36*). This competition likely underlies period control by CikA; by displacing KaiA from the repressive complex, CikA promotes the activating potential of KaiA to stimulate KaiC phosphorylation (*48*). Using our extended oscillator system, we found that increasing concentrations of CikA led to progressive period shortening, particularly under limiting concentrations of KaiA, bringing it in line with the period found under idealized oscillator conditions (Fig. 4A). This result demonstrates one way that competitive mechanisms can compensate for fluctuating in vivo concentrations of oscillator proteins to influence timekeeping by the cyanobacterial clock.

SasA rescues oscillations under limiting concentrations of KaiB

SasA was originally described as an amplifier of circadian rhythms needed to maintain robust, high-amplitude rhythms, presumably by controlling rhythmic transcription of the *kaiBC* cluster (*16*). In contrast to the effect we observed with CikA, the addition of SasA led to progressive lengthening of the period (Fig. 4A and table S5). The isolated thioredoxin-like domain of SasA was much less effective at lengthening the period than was the full-length SasA dimer, consistent with the avidity observed in binding studies between KaiC and full-length SasA (fig. S15). It should be noted that addition of the isolated PsR domain or full-length CikA caused concentration-dependent changes in period length in vitro that are apparently balanced out by period changes imparted by SasA (Fig. 4 and fig. S16). These data support a model in which the proteins that impart output contribute substantively to the timing of the clock through interactions with the Kai proteins.

In exploring the combined effects of KaiB and SasA concentrations on oscillator period, we unexpectedly observed that amplitude and damping in a weak oscillator with suboptimal concentrations of KaiB could be rescued through the addition of SasA (Figs. 4, B to D). To better understand this phenomenon, we set up assays with increasing concentrations of SasA under typical in vitro oscillator conditions (*6*) as well as two concentrations where KaiB was limiting relative to KaiC. When KaiB concentrations were too low to support oscillations, we observed low FA values for KaiB, consistent with incomplete recruitment of labeled KaiB to KaiC hexamers (Fig. 4C, top left column). Addition of SasA up to 1 μM increased KaiB FA, demonstrating that SasA enhances KaiB binding to KaiC. However, as the concentration of SasA approached or exceeded that of KaiC, FA values for KaiB dropped, demonstrating that SasA eventually outcompetes KaiB for binding to the KaiC hexamer, as previously observed (*36*, *49*).

Using a KaiB concentration equal to half that of KaiC, we saw rapidly damping, low-amplitude rhythms (Fig. 4C, middle column). We also found that addition of substoichiometric amounts of SasA restored full amplitude and eliminated damping of the oscillations. Increasing SasA concentrations from 0.1 to 1 μM under these conditions did not further influence amplitude, and higher concentrations of SasA attenuated oscillations by outcompeting KaiB for binding to KaiC, as reflected by low anisotropy levels of the labeled KaiB. Under standard oscillator conditions with stoichiometric KaiB and KaiC, the amplitude of oscillation was affected by addition of SasA only at 1.0 μM and higher (Fig. 4, B and C, right column). The sharp drop in oscillator amplitude and KaiB FA levels demonstrates that a functional switch from recruitment to competition by SasA occurs at around ~0.65 to 1 μM, depending on the exact oscillator conditions. This setpoint is close to the concentration of SasA in vivo estimated by quantitative Western blotting to be around 0.6 μM (*21*).

We hypothesized that SasA expands the range of permissive KaiB concentrations for biochemical oscillation by directly enhancing the interaction of KaiB and KaiC. As a test, we used a partial oscillator experiment in which unlabeled KaiB was omitted from the reaction, and association of the 50 nM labeled KaiB probe was measured as phosphorylated KaiC accumulated upon stimulation by KaiA (Fig. 4E). We observed a concentration-dependent enhancement in KaiB association as SasA concentration approached the physiological value of ~0.65 μM. This finding suggests that, aside from its role in regulating transcriptional output from the oscillator (*16*), SasA also directly modulates KaiBC association to control formation of the nighttime repressive state and stability of the clock itself. Moreover, we observed a delay in KaiB association with KaiC when SasA was present at higher concentrations, consistent with the period-lengthening effects observed with SasA in the IVC (Fig. 4A and fig. S16).

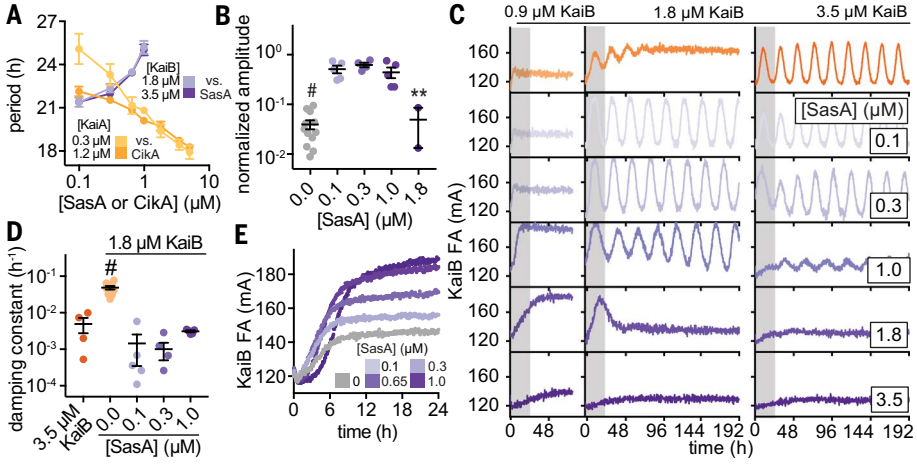

Fig. 4. Output proteins compensate for period and amplitude defects in suboptimal in vitro oscillators. (**A**) Period of clock reactions with varied concentrations of KaiA (light and dark yellow) or KaiB (light and dark purple) supplemented as a function of CikA or SasA concentration, respectively. (**B**) Amplitudes of rhythms with probe KaiB + 1.8 μM unlabeled KaiB in the presence of SasA (gray for KaiB alone; light to dark purple for SasA). Reactions that could not be fit to a sine function because they did not oscillate were not plotted. Statistical analysis was performed exactly as described in Fig. 3, C and D. (**C**) In vitro oscillator assays with 3.5 μM KaiC, 1.2 μM KaiA, and the indicated concentrations of KaiB as well as various amounts of full-length SasA ranging from 0.1 to 3.5 μM. Representative assay from $n \geq 3$ shown; the first 24 hours of the time course are shaded gray. (**D**) Damping constants derived from least-squares fitting of the FA data from (C). Full datasets are available in data S2 and S3. (**E**) "Partial oscillator" reactions containing 50 nM KaiB, 3.5 μM KaiC, and 1.2 uM KaiA with various amounts of SasA.

Structural mimicry in the KaiC-binding region of SasA and KaiB

During subjective day, when KaiB is free, it exists in a distinctive ground-state fold, but the fold-switched monomer that binds KaiC at subjective night is thioredoxin-like, which is the same fold adopted by the KaiC-binding domain of SasA ($SasA_{trx}$) (*37*). A high-resolution crystal structure of the subcomplex comprising a

Downloaded from https://www.science.org at University of California Merced on October 09, 2021

single KaiC-CI domain and a fold-switch-locked mutant KaiB I88A from the related thermophilic species *T. elongatus* (*36*) (I87A in *S. elongatus*, referred to herein as fsKaiB) illustrates how KaiB docks onto the exposed B-loop of the CI domain (Fig. 5, A and B). To better understand the relationship between SasA and KaiB recruitment to KaiC, we solved a crystal structure of $SasA_{trx}$ bound to the KaiC-CI domain from *T. elongatus* to reveal that SasA binds the B-loop in a similar orientation to KaiB (Fig. 5C and table S6). To investigate the importance of this interface, we probed substitutions in several KaiC residues in the B-loop using affinity assays to KaiC hexamer (Fig. 5D). We performed equilibrium binding assays using the KaiC phosphomimetic mutants KaiC-EE and KaiC-EA, where X and Y in KaiC-XY represent amino acyl residues at positions 431 and 432, respectively. Glutamyl/glutamyl (EE) and glutamyl/alanyl (EA) substitutions at these positions are widely used to approximate the dusk-like phosphoserine/phosphothreonine (pS/pT) and nighttime-like phosphoserine (pS/T) states (*8*). Using these mimetics, we found that KaiB has similar affinity for both states, whereas SasA has a preference for the pS/pT state (fig. S17), consistent with prior results (*50*) and its earlier phase of binding in the IVC (Fig. 1, A and E). Furthermore, although the isolated $SasA_{trx}$ domain is necessary and sufficient for binding to KaiC (*16*), avidity effects in the full-length dimer enhanced affinity for KaiC-EE by at least two orders of magnitude compared with the isolated, monomeric $SasA_{trx}$ domain (fig. S17).

Comparing the KaiB and SasA binding interfaces on KaiC, we found that substitutions at sites conserved between *S. elongatus* and *T. elongatus* (KaiC F122 and D123) decrease affinity for both KaiB and $SasA_{trx}$ (Fig. 5, D to F). We then examined how differences in the structures of KaiB and SasA or their orientations on the B-loop might influence binding to adjacent subunits of the KaiC hexamer (fig. S18). Small changes in the length and orientation of the C-terminal helix between the $SasA_{trx}$ and KaiB could lead to steric clashes of $SasA_{trx}$ with a neighboring subunit. Consistent with this idea, saturation binding experiments showed that $SasA_{trx}$ domains cannot fully occupy all six binding sites on the KaiC hexamer (fig. S18).

SasA enhances KaiBC interaction through heterotropic cooperativity

Six monomers of the active, thioredoxin-like form of KaiB assemble onto the KaiC hexamer of *S. elongatus* (*36*, *51*) to nucleate formation of the nighttime repressive state. Prior native mass spectrometry analyses demonstrated that KaiB binds to the KaiC hexamer with positive homotropic cooperativity (*52*, *53*). Given the similarity between the SasA-KaiC and KaiB-KaiC interactions, we speculated that SasA could facilitate KaiB-KaiC interactions through positive heterotropic cooperativity. We developed an assay to test directly for cooperativity by monitoring 50 nM fluorescently labeled KaiB probe with KaiC-EE using unlabeled SasA or fsKaiB as a secondary titrant (Fig. 6, A and B). Although these assay conditions do not assess the degree of homotropic cooperativity for KaiC-EE with the KaiB probe alone, we found that low concentrations (50 to 100 nM) of SasA or fsKaiB significantly increased binding

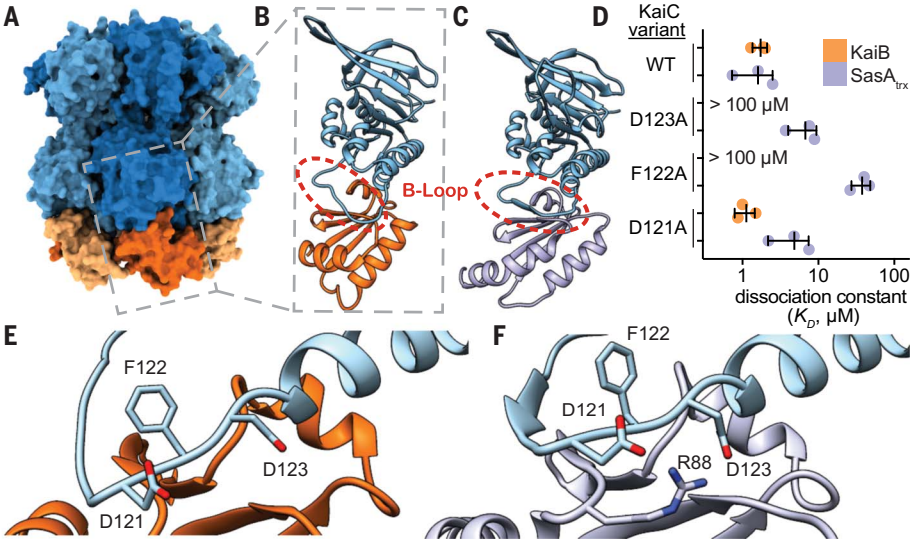

Fig. 5. SasA and KaiB bind to the same site on KaiC. (**A**) The KaiB-KaiC heterododecamer [Protein Data Bank (PDB) ID 5JWQ] with subunits of the KaiC ring depicted in alternating light and dark blue, and fsKaiB subunits in alternating light and dark orange. The gray box indicates the position of (**B**) the isolated KaiC-CI domain–fsKaiB subcomplex (PDB ID 5JWO). (**C**) The KaiC-CI domain–$SasA_{trx}$ subcomplex (PDB ID 6X61), with KaiC (blue) and SasA (purple). (**D**) Equilibrium dissociation constants (K_D) for KaiB (orange) or $SasA_{trx}$ (purple) binding to KaiC-EE mutants (mean ± SD, n = 3). Where indicated, binding was too weak for curve fitting, and K_D is reported as >100 μM. Single-letter abbreviations for the amino acid residues are as follows: A, Ala; C, Cys; D, Asp; E, Glu; F, Phe; G, Gly; H, His; I, Ile; K, Lys; L, Leu; M, Met; N, Asn; P, Pro; Q, Gln; R, Arg; S, Ser; T, Thr; V, Val; W, Trp; and Y, Tyr. (**E** and **F**) The interface of KaiC-CI with fsKaiB (E) or $SasA_{trx}$ (F) with key residues highlighted.

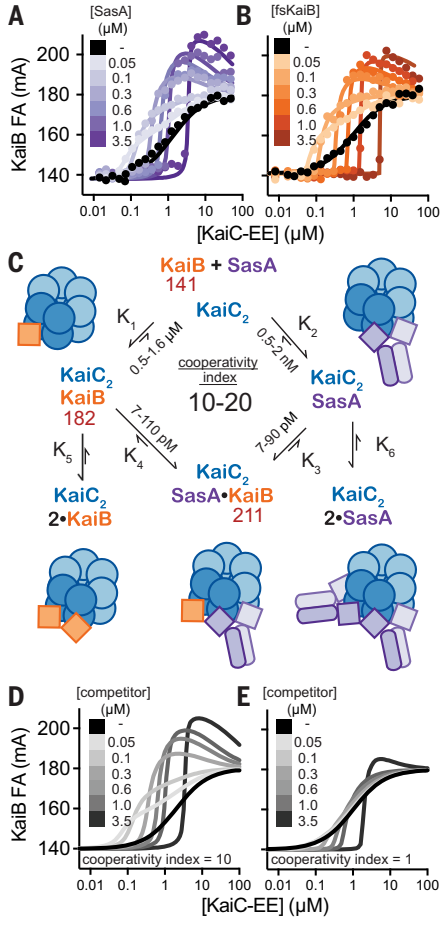

Fig. 6. The thioredoxin-like fold of SasA and fsKaiB cooperatively recruits KaiB to the KaiC hexamer. (**A** and **B**) Equilibrium binding assays of fluorescently labeled KaiB with KaiC-EE in the absence (black) or presence of (A) unlabeled SasA (light to dark purple) or (B) fsKaiB (light to dark orange). Each 2D titration is shown from representative assays with best fit lines from global curve-fitting. (**C**) Summary of a two-site thermodynamic model for SasA heterocooperativity, and mean equilibrium constants derived from least-squares fitting of SasA 2D titration assays (n = 3); values in red are mean peak anisotropy values observed from fitting of all SasA 2D titration datasets using DynaFit software. The cooperativity index is defined as the ratio $K_1/K_3 = K_2/K_4$. This model was used to generate simulated 2D titrations with a cooperativity index of either 10 (**D**) or 1 (**E**). (See data S6 to S8 for DynaFit scripts and full datasets.)

Downloaded from https://www.science.org at University of California Merced on October 09, 2021

of KaiB probe, demonstrating more efficient recruitment to the KaiC hexamer. Higher concentrations of SasA or fsKaiB resulted in competition with the probe, reducing its binding to the KaiC hexamer; an equivalence point was reached when the concentration of KaiC-EE matched that of the competitor. We observed a considerable overshoot of KaiB probe anisotropy values around this point, consistent with formation of a higher-molecular-weight complex consisting of both KaiB probe and SasA bound to the KaiC hexamer. Association of the KaiB probe to the WT KaiC-CI monomer was not significantly affected by the addition of 300 nM SasA or fsKaiB (fig. S19), nor did SasA interact directly with KaiB in the absence of KaiC, demonstrating that these competitors only enhance KaiB association in the context of the KaiC hexamer, as shown using phosphomimetics, which is consistent with our cooperativity model.

To quantitatively represent the heterotropic cooperativity observed in these two-dimensional (2D) titrations, a simplified two-site thermodynamic model was found by least-squares fitting to be sufficient to account for the data (Fig. 6C and fig. S19). In this model, we defined the heterotropic "cooperativity index" as the fold-increase in KaiB affinity given by the ratio of equilibrium constants K_1/K_3 (= K_2/K_4). Comparison of 2D titrations with SasA or fsKaiB to simulated data representing heterotropic cooperative binding (Fig. 6, A and B), to a model with competition and no cooperativity (Fig. 6, D and E), demonstrates that SasA and fsKaiB similarly influence cooperative recruitment of the KaiB probe on KaiC.

To explore the role of intermolecular KaiB-KaiB interactions in cooperative KaiB-KaiC binding, we characterized KaiB-R22A, a mutant originally identified in *Anabaena* (*54*) that reduces the apparent affinity of KaiB for KaiC although it is not located at the KaiB-KaiC interface (*36*). R22 has been implicated in KaiB cooperativity using native mass spectrometry (*52*) and is situated at the KaiB-KaiB interface in the KaiBC hexamer structure. We tested this mutant in our cooperativity assay and observed a small decrease in the cooperative recruitment of the KaiB probe relative to that of fsKaiB (fig. S19), demonstrating that intersubunit KaiB-KaiB interactions play a role in the cooperative recruitment process and opening the possibility that mutations at the SasA-KaiB interface could also disrupt cooperativity.

SasA-KaiB complementarity is required for proper circadian timing

To identify whether the enhancement of KaiBC association is important for the function of SasA in vivo, we set out to identify point mutations that would separate the cooperativity and output signaling functions of SasA. To this end, we first showed that the catalytically inactive SasA mutant H161A (*19*) is as effective as WT SasA in stimulating cooperative recruitment of KaiB to KaiC in vitro (fig. S19). Next, we constructed a structural model by overlaying crystal structures of $SasA_{trx}$-CI and KaiB-CI onto the lower-resolution structure of the full-length KaiBC hexamer complex (*36*) and used it to predict potential $SasA_{trx}$-KaiB interactions along the clockwise (CW) and counterclockwise (CCW) interfaces of the hybrid complex (Fig. 7A). Within this framework, we investigated a number of SasA substitutions near the CW and CCW interface (fig. S20) and estimated their ability to cooperatively recruit KaiB in simplified 2D titration assays comparing a single SasA concentration to the no-SasA control. The individual mutants H28A (CCW interface) or Q94A (CW interface) showed decreases in their cooperativity indices that were further decreased in the H28A-Q94A double mutant (Fig. 7B). It should be noted that the estimates of cooperativity in wild type were slightly

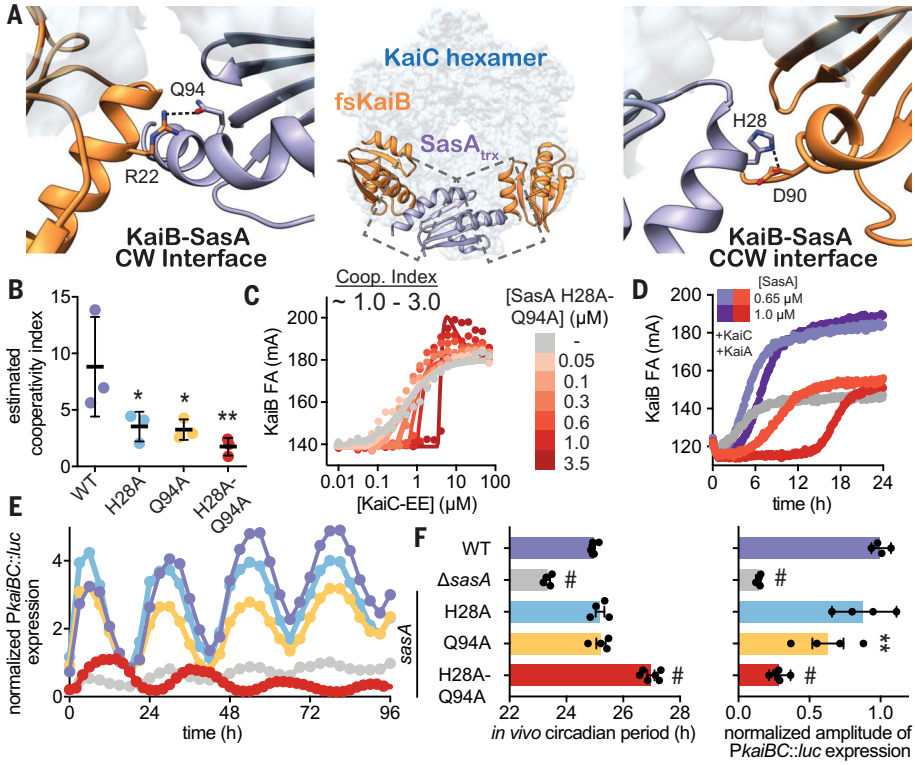

Fig. 7. SasA-KaiB interactions mediate cooperative recruitment of KaiB in vitro and sustain robust circadian rhythms in vivo. (**A**) Structural model of KaiB:SasA interactions on KaiC using KaiC-CI subcomplexes with fsKaiB (orange, PDB ID 5JWO) and $SasA_{trx}$ (purple, PDB ID 6X61) modeled onto adjacent subunits of KaiC (light blue) of the KaiBC heterododecamer (PDB ID 5JWQ). Key residues at clockwise (CW) and counterclockwise (CCW) interfaces are modeled as *S. elongatus* variants on the basis of the alignment in fig. S20. Polar contacts predicted by our hybrid structural model are indicated by dashed lines. (**B**) Cooperativity indices for SasA variants extracted from KaiC titrations done in the presence of 0.3 μM SasA (mean SD, n = 3). Statistical significance of differences between WT and mutant SasA variants was tested using one-way ANOVA with Dunnett's multiple comparisons as described in Fig. 3. (**C**) Representative 2D titration of fluorescently labeled KaiB with KaiC-EE in the absence (gray) or presence (light to dark red) of SasA-H28A-Q94A. (**D**) Time-dependent FA trajectories of 50 nM KaiB in the presence of 3.5 μM KaiC and 1.2 uM KaiA with 0.65 or 1.0 μM SasA WT (purple shades) or H28A-Q94A mutant (red shades). (**E**) Representative time course of bioluminescence driven by P*kaiBC* from *S. elongatus* cultures entrained under 12-hour light-dark cycles for 48 hours and subsequently allowed to free run in LL. (**F**) Raw luminescence curves were fit to a sine function to extract amplitude of P*kaiBC::luc* expression as well as free-running circadian period for each strain. WT control was included for each experiment, and the luminescence of each mutant was normalized to the amplitude of luminescence oscillation for the WT control in that run. Error bars depict SEM among replicate cultures (n = 4 to 6); when error bars are not visible, they were smaller than could be depicted. Symbols indicate significance determined from one-way ANOVA with Dunnett's multiple comparisons between mutant and WT *S. elongatus* with symbols to depict significance as summarized in Fig. 3 legend. Normal distribution was confirmed through quantile-quantile plots showing predicted versus actual residual values in addition to Anderson-Darling, D'Agostino-Pearson omnibus, and Shapiro-Wilk tests, which were all performed in GraphPad PRISM. Equal variance of the data was verified with Brown-Forsythe tests yielding P values above 0.05. Color scheme for data in (E) is consistent with and indicated on left vertical axis of (F).

Downloaded from https://www.science.org at University of California Merced on October 09, 2021

lower than those determined in the full 2D titrations (Fig. 6, A and C), likely owing to differences in experimental setup. While the H28A-Q94A double mutant did not strongly affect other SasA functions in vitro, such as KaiC association and the KaiC-dependent phosphotransfer to RpaA (fig. S21), it lacked the ability to stimulate KaiB binding in the 2D titration assay (compare Fig. 7C and Fig. 6E) demonstrating that both interfaces contribute to SasA heterotropic cooperativity.

To better understand these mutations in a more native context, we tested the ability of the H28A-Q94A variant to nucleate formation of the repressive complex using a partial oscillator experiment to directly measure the kinetics of KaiBC formation under limiting concentrations of KaiB with WT or H28A-Q94A SasA (Fig. 7D and fig. S21C). Notably, enhancement of KaiB recruitment was essentially nonexistent with the SasA H28A-Q94A mutant, instead showing a lengthened competitive phase that occurs even at physiological concentrations of SasA. When concentration of the double mutant was increased beyond physiological levels, the delay in KaiB association became even more exaggerated, suggesting that complementarity between the SasA-KaiB interfaces is critical for timely replacement of SasA with KaiB on the KaiC hexamer.

With this separation-of-function mutant in hand, we set out to test whether the SasA-induced cooperativity we observed for the expanded oscillator in vitro could influence circadian rhythms in vivo. We introduced the double mutation, as well as several single alanine substitutions, into SasA using markerless CRISPR-Cas12a and monitored bioluminescence from a P*kaiBC* luciferase reporter in constant light (LL) after synchronization in 12-hours light:12-hours dark cycles (Fig. 7E and fig. S22). Small effects on amplitude were seen with the individual H28 or Q94 alanine substitutions on their own, but when these were combined in the H28A-Q94A mutant, the amplitude of circadian rhythms decreased to an extent that was similar to the SasA knockout strain (Fig. 7F, Δ*sasA*), even though the mutant proteins were expressed to a similar level in vivo (fig. S22D), and the double mutant strain exhibited a ~2-hour-longer period (Fig. 7F and fig. S22). Taken together, these results provide a clear link between loss of complementarity at SasA-KaiB interfaces and the long-period phenotype observed in vivo, further supporting our conclusion that cooperative interactions between SasA and KaiB are crucial for proper circadian timing.

Discussion

This extended IVC is an autonomously oscillating system that remains phase coherent for several days without user intervention, allows real-time observation of rhythmic behaviors of several clock components in parallel, and rhythmically activates the interaction of a transcription factor with a promoter element on DNA. Complementing this assay with parallel measurements of phosphorylation and ATPase activities rounds out a movie of an intact cyanobacterial clock. As implemented here, the IVC has revealed a set of minimal components to execute clock-controlled gene expression, helped to dissect the mechanistic origins of a clock-disrupting mutant, and provided insight into mechanisms behind the narrow stoichiometric ratios that are tolerated in the in vitro oscillator (*45*). In particular, our data demonstrate that SasA, previously regarded solely as an output protein, plays a critical role in the enhancing the oscillator amplitude through heterocooperative regulation of KaiB association with KaiC. This newly developed IVC system offers an unparalleled opportunity to explore how the clock maintains consistency in vivo despite rhythmic changes in the concentration of clock components that result from the associated transcription-translation feedback (*11*, *55*) and protein turnover (*56*, *57*) and provides an experimental platform for integrating the oscillator with the upstream and downstream components with which it interacts. By reconstructing, and subsequently deconstructing, this elegant system, we have shown that a dichotomous view of timekeeping and signaling components provides an insufficient representation of the complexity and synergy that has evolved in this ancient circadian clock.

REFERENCES AND NOTES

1. J. C. Dunlap, J. J. Loros, P. J. DeCoursey, Eds., *Chronobiology: Biological Timekeeping* (Sinauer Associates, 2004).
2. M. A. Woelfle, Y. Ouyang, K. Phanvijhitsiri, C. H. Johnson, The adaptive value of circadian clocks: An experimental assessment in cyanobacteria. *Curr. Biol.* **14**, 1481–1486 (2004). doi: 10.1016/j.cub.2004.08.023; pmid: 15324665
3. T. Kondo *et al*., Circadian rhythms in prokaryotes: Luciferase as a reporter of circadian gene expression in cyanobacteria. *Proc. Natl. Acad. Sci. U.S.A.* **90**, 5672–5676 (1993). doi: 10.1073/pnas.90.12.5672; pmid: 8516317
4. M. Ishiura *et al*., Expression of a gene cluster *kaiABC* as a circadian feedback process in cyanobacteria. *Science* **281**, 1519–1523 (1998). doi: 10.1126/science.281.5382.1519; pmid: 9727980
5. J. Tomita, M. Nakajima, T. Kondo, H. Iwasaki, No transcription-translation feedback in circadian rhythm of KaiC phosphorylation. *Science* **307**, 251–254 (2005). doi: 10.1126/science.1102540; pmid: 15550625
6. M. Nakajima *et al*., Reconstitution of circadian oscillation of cyanobacterial KaiC phosphorylation in vitro. *Science* **308**, 414–415 (2005). doi: 10.1126/science.1108451; pmid: 15831759
7. M. J. Rust, J. S. Markson, W. S. Lane, D. S. Fisher, E. K. O'Shea, Ordered phosphorylation governs oscillation of a three-protein circadian clock. *Science* **318**, 809–812 (2007). doi: 10.1126/science.1148596; pmid: 17916691
8. T. Nishiwaki *et al*., A sequential program of dual phosphorylation of KaiC as a basis for circadian rhythm in cyanobacteria. *EMBO J.* **26**, 4029–4037 (2007). doi: 10.1038/sj.emboj.7601832; pmid: 17717528
9. H. Iwasaki, T. Nishiwaki, Y. Kitayama, M. Nakajima, T. Kondo, KaiA-stimulated KaiC phosphorylation in circadian timing loops in cyanobacteria. *Proc. Natl. Acad. Sci. U.S.A.* **99**, 15788–15793 (2002). doi: 10.1073/pnas.222467299; pmid: 12391300
10. S. B. Williams, I. Vakonakis, S. S. Golden, A. C. LiWang, Structure and function from the circadian clock protein KaiA of *Synechococcus elongatus*: A potential clock input mechanism. *Proc. Natl. Acad. Sci. U.S.A.* **99**, 15357–15362 (2002). doi: 10.1073/pnas.232517099; pmid: 12438647
11. Y. Kitayama, H. Iwasaki, T. Nishiwaki, T. Kondo, KaiB functions as an attenuator of KaiC phosphorylation in the cyanobacterial circadian clock system. *EMBO J.* **22**, 2127–2134 (2003). doi: 10.1093/emboj/cdg212; pmid: 12727879
12. Y. Xu, T. Mori, C. H. Johnson, Cyanobacterial circadian clockwork: Roles of KaiA, KaiB and the *kaiBC* promoter in regulating KaiC. *EMBO J.* **22**, 2117–2126 (2003). doi: 10.1093/emboj/cdg168; pmid: 12727878
13. Y.-G. Chang, R. Tseng, N.-W. Kuo, A. LiWang, Rhythmic ring-ring stacking drives the circadian oscillator clockwise. *Proc. Natl. Acad. Sci. U.S.A.* **109**, 16847–16851 (2012). doi: 10.1073/pnas.1211508109; pmid: 22967510
14. Y.-G. Chang, N.-W. Kuo, R. Tseng, A. LiWang, Flexibility of the C-terminal, or CII, ring of KaiC governs the rhythm of the circadian clock of cyanobacteria. *Proc. Natl. Acad. Sci. U.S.A.* **108**, 14431–14436 (2011). doi: 10.1073/pnas.1104221108; pmid: 21788479
15. J. Abe *et al*., Atomic-scale origins of slowness in the cyanobacterial circadian clock. *Science* **349**, 312–316 (2015). doi: 10.1126/science.1261040; pmid: 26113637
16. H. Iwasaki *et al*., A KaiC-interacting sensory histidine kinase, SasA, necessary to sustain robust circadian oscillation in cyanobacteria. *Cell* **101**, 223–233 (2000). doi: 10.1016/S0092-8674(00)80832-6; pmid: 10786837
17. O. Schmitz, M. Katayama, S. B. Williams, T. Kondo, S. S. Golden, CikA, a bacteriophytochrome that resets the cyanobacterial circadian clock. *Science* **289**, 765–768 (2000). doi: 10.1126/science.289.5480.765; pmid: 10926536
18. N. B. Ivleva, T. Gao, A. C. LiWang, S. S. Golden, Quinone sensing by the circadian input kinase of the cyanobacterial circadian clock. *Proc. Natl. Acad. Sci. U.S.A.* **103**, 17468–17473 (2006). doi: 10.1073/pnas.0606639103; pmid: 17088557
19. N. Takai *et al*., A KaiC-associating SasA-RpaA two-component regulatory system as a major circadian timing mediator in cyanobacteria. *Proc. Natl. Acad. Sci. U.S.A.* **103**, 12109–12114 (2006). doi: 10.1073/pnas.0602955103; pmid: 16882723
20. J. S. Markson, J. R. Piechura, A. M. Puszynska, E. K. O'Shea, Circadian control of global gene expression by the cyanobacterial master regulator RpaA. *Cell* **155**, 1396–1408 (2013). doi: 10.1016/j.cell.2013.11.005; pmid: 24315105
21. A. Gutu, E. K. O'Shea, Two antagonistic clock-regulated histidine kinases time the activation of circadian gene expression. *Mol. Cell* **50**, 288–294 (2013). doi: 10.1016/j.molcel.2013.02.022; pmid: 23541768
22. K. Ito-Miwa, Y. Furuike, S. Akiyama, T. Kondo, Tuning the circadian period of cyanobacteria up to 6.6 days by the single amino acid substitutions in KaiC. *Proc. Natl. Acad. Sci. U.S.A.* **117**, 20926–20931 (2020). doi: 10.1073/pnas.2005496117; pmid: 32747571
23. E. Leypunskiy *et al*., The cyanobacterial circadian clock follows midday in vivo and in vitro. *eLife* **6**, e23539 (2017). doi: 10.7554/eLife.23539; pmid: 28686160
24. G. K. Chow *et al*., Monitoring protein–protein interactions in the cyanobacterial circadian clock in real time via electron paramagnetic resonance spectroscopy. *Biochemistry* **59**, 2387–2400 (2020). doi: 10.1021/acs.biochem.0c00279; pmid: 32453554
25. J. Heisler, A. Chavan, Y.-G. Chang, A. LiWang, Real-time in vitro fluorescence anisotropy of the cyanobacterial circadian clock. *Methods Protoc.* **2**, 42 (2019). doi: 10.3390/mps2020042; pmid: 31164621
26. C. S. Theile *et al*., Site-specific N-terminal labeling of proteins using sortase-mediated reactions. *Nat. Protoc.* **8**, 1800–1807 (2013). doi: 10.1038/nprot.2013.102; pmid: 23989674
27. C. P. Guimaraes *et al*., Site-specific C-terminal and internal loop labeling of proteins using sortase-mediated reactions. *Nat. Protoc.* **8**, 1787–1799 (2013). doi: 10.1038/nprot.2013.101; pmid: 23989673
28. B. Guo *et al*., Monitoring ATP hydrolysis and ATPase inhibitor screening using ^{1}H NMR. *Chem. Commun.* **50**, 12037–12039 (2014). doi: 10.1039/C4CC04399E; pmid: 25170530
29. K. Terauchi *et al*., ATPase activity of KaiC determines the basic timing for circadian clock of cyanobacteria. *Proc. Natl. Acad. Sci. U.S.A.* **104**, 16377–16381 (2007). doi: 10.1073/pnas.0706292104; pmid: 17901204
30. R. M. Smith, S. B. Williams, Circadian rhythms in gene transcription imparted by chromosome compaction in the cyanobacterium *Synechococcus elongatus*. *Proc. Natl. Acad.*

Downloaded from https://www.science.org at University of California Merced on October 09, 2021

Sci. U.S.A. **103**, 8564–8569 (2006). doi: 10.1073/pnas.0508696103; pmid: 16707582
31. S. E. Cohen, S. S. Golden, Circadian rhythms in cyanobacteria. *Microbiol. Mol. Biol. Rev.* **79**, 373–385 (2015). doi: 10.1128/MMBR.00036-15; pmid: 26335718
32. H. Kageyama, T. Kondo, H. Iwasaki, Circadian formation of clock protein complexes by KaiA, KaiB, KaiC, and SasA in cyanobacteria. *J. Biol. Chem.* **278**, 2388–2395 (2003). doi: 10.1074/jbc.M208899200; pmid: 12441347
33. R. Tseng *et al*., Cooperative KaiA-KaiB-KaiC interactions affect KaiB/SasA competition in the circadian clock of cyanobacteria. *J. Mol. Biol.* **426**, 389–402 (2014). doi: 10.1016/j.jmb.2013.09.040; pmid: 24112939
34. P. B. Straughn *et al*., Modulation of response regulator CheY reaction kinetics by two variable residues that affect conformation. *J. Bacteriol.* **202**, e00089-20 (2020). doi: 10.1128/JB.00089-20; pmid: 32424010
35. A. H. West, A. M. Stock, Histidine kinases and response regulator proteins in two-component signaling systems. *Trends Biochem. Sci.* **26**, 369–376 (2001). doi: 10.1016/S0968-0004(01)01852-7; pmid: 11406410
36. R. Tseng *et al*., Structural basis of the day-night transition in a bacterial circadian clock. *Science* **355**, 1174–1180 (2017). doi: 10.1126/science.aag2516; pmid: 28302851
37. Y.-G. Chang *et al*., A protein fold switch joins the circadian oscillator to clock output in cyanobacteria. *Science* **349**, 324–328 (2015). doi: 10.1126/science.1260031; pmid: 26113641
38. N. B. Ivleva, M. R. Bramlett, P. A. Lindahl, S. S. Golden, LdpA: A component of the circadian clock senses redox state of the cell. *EMBO J.* **24**, 1202–1210 (2005). doi: 10.1038/sj.emboj.7600606; pmid: 15775978
39. Y. Taniguchi, N. Takai, M. Katayama, T. Kondo, T. Oyama, Three major output pathways from the KaiABC-based oscillator cooperate to generate robust circadian *kaiBC* expression in cyanobacteria. *Proc. Natl. Acad. Sci. U.S.A.* **107**, 3263–3268 (2010). doi: 10.1073/pnas.0909924107; pmid: 20133618
40. M. J. Rust, S. S. Golden, E. K. O'Shea, Light-driven changes in energy metabolism directly entrain the cyanobacterial circadian oscillator. *Science* **331**, 220–223 (2011). doi: 10.1126/science.1197243; pmid: 21233390
41. Y.-I. Kim, D. J. Vinyard, G. M. Ananyev, G. C. Dismukes, S. S. Golden, Oxidized quinones signal onset of darkness directly to the cyanobacterial circadian oscillator. *Proc. Natl. Acad. Sci. U.S.A.* **109**, 17765–17769 (2012). doi: 10.1073/pnas.1216401109; pmid: 23071342
42. M. L. Paddock, J. S. Boyd, D. M. Adin, S. S. Golden, Active output state of the *Synechococcus* Kai circadian oscillator. *Proc. Natl. Acad. Sci. U.S.A.* **110**, E3849–E3857 (2013). doi: 10.1073/pnas.1315170110; pmid: 24043774
43. J. S. Boyd, J. R. Bordowitz, A. C. Bree, S. S. Golden, An allele of the *crm* gene blocks cyanobacterial circadian rhythms. *Proc. Natl. Acad. Sci. U.S.A.* **110**, 13950–13955 (2013). doi: 10.1073/pnas.1312793110; pmid: 23918383
44. J. Ungerer, H. B. Pakrasi, Cpf1 is a versatile tool for CRISPR genome editing across diverse species of cyanobacteria. *Sci. Rep.* **6**, 39681 (2016). doi: 10.1038/srep39681; pmid: 28000776
45. M. Nakajima, H. Ito, T. Kondo, *In vitro* regulation of circadian phosphorylation rhythm of cyanobacterial clock protein KaiC by KaiA and KaiB. *FEBS Lett.* **584**, 898–902 (2010). doi: 10.1016/j.febslet.2010.01.016; pmid: 20079736
46. J. Chew, E. Leypunskiy, J. Lin, A. Murugan, M. J. Rust, High protein copy number is required to suppress stochasticity in the cyanobacterial circadian clock. *Nat. Commun.* **9**, 3004 (2018). doi: 10.1038/s41467-018-05109-4; pmid: 30068980
47. J. Lin, J. Chew, U. Chockanathan, M. J. Rust, Mixtures of opposing phosphorylations within hexamers precisely time feedback in the cyanobacterial circadian clock. *Proc. Natl. Acad. Sci. U.S.A.* **111**, E3937–E3945 (2014). doi: 10.1073/pnas.1408692111; pmid: 25197081
48. M. Kaur, A. Ng, P. Kim, C. Diekman, Y.-I. Kim, CikA modulates the effect of KaiA on the period of the circadian oscillation in KaiC phosphorylation. *J. Biol. Rhythms* **34**, 218–223 (2019). doi: 10.1177/0748730419828068; pmid: 30755127
49. R. Murakami *et al*., The roles of the dimeric and tetrameric structures of the clock protein KaiB in the generation of circadian oscillations in cyanobacteria. *J. Biol. Chem.* **287**, 29506–29515 (2012). doi: 10.1074/jbc.M112.349092; pmid: 22722936
50. J. Valencia S. *et al*., Phase-dependent generation and transmission of time information by the KaiABC circadian clock oscillator through SasA-KaiC interaction in cyanobacteria. *Genes Cells* **17**, 398–419 (2012). doi: 10.1111/j.1365-2443.2012.01597.x; pmid: 22512339
51. J. Snijder *et al*., Structures of the cyanobacterial circadian oscillator frozen in a fully assembled state. *Science* **355**, 1181–1184 (2017). doi: 10.1126/science.aag3218; pmid: 28302852
52. R. Murakami *et al*., Cooperative binding of KaiB to the KaiC hexamer ensures accurate circadian clock oscillation in cyanobacteria. *Int. J. Mol. Sci.* **20**, 4550 (2019). doi: 10.3390/ijms20184550; pmid: 31540310
53. J. Snijder *et al*., Insight into cyanobacterial circadian timing from structural details of the KaiB-KaiC interaction. *Proc. Natl. Acad. Sci. U.S.A.* **111**, 1379–1384 (2014). doi: 10.1073/pnas.1314326111; pmid: 24474762
54. R. G. Garces, N. Wu, W. Gillon, E. F. Pai, Anabaena circadian clock proteins KaiA and KaiB reveal a potential common binding site to their partner KaiC. *EMBO J.* **23**, 1688–1698 (2004). doi: 10.1038/sj.emboj.7600190; pmid: 15071498
55. Y. Xu, T. Mori, C. H. Johnson, Circadian clock-protein expression in cyanobacteria: Rhythms and phase setting. *EMBO J.* **19**, 3349–3357 (2000). doi: 10.1093/emboj/19.13.3349; pmid: 10880447
56. C. K. Holtman *et al*., High-throughput functional analysis of the *Synechococcus elongatus* PCC 7942 genome. *DNA Res.* **12**, 103–115 (2005). doi: 10.1093/dnares/12.2.103; pmid: 16303742
57. K. Imai, Y. Kitayama, T. Kondo, Elucidation of the role of Clp protease components in circadian rhythm by genetic deletion and overexpression in cyanobacteria. *J. Bacteriol.* **195**, 4517–4526 (2013). doi: 10.1128/JB.00300-13; pmid: 23913328

ACKNOWLEDGMENTS

We thank staff at the 23-ID-D beamline of the Advanced Photon Source, Argonne National Laboratory, for their help with data collection. The Advanced Photon Source (contract DE-AC02-06CH11357) is supported by the US Department of Energy. Molecular graphics and analyses performed with UCSF Chimera and ChimeraX, developed by the Resource for Biocomputing, Visualization, and Informatics at the University of California, San Francisco (UCSF), with support from National Institutes of Health P41-GM103311(Chimera) and R01-GM129325 and the Office of Cyber Infrastructure and Computational Biology, National Institute of Allergy and Infectious Diseases (ChimeraX). We thank G. Chow, Y.-G. Chang, M. Rust, L. Hong, S. Sukenik, and M. Zoghbi for helpful discussions. We also thank D. Rice and S. Grimaldi for maintaining the NMR facility and NMR cryoplatform, respectively, at UC Merced. **Funding:** This work was supported by US National Institutes of Health grants R01 GM107521 (to A.L.), R01 GM121507 (to C.L.P.), and R35 GM118290 (to S.S.G.), and NSF-CREST: Center for Cellular and Biomolecular Machines at the University of California, Merced (NSF-HRD-1547848). J.H. was supported by NSF-CREST CCBM HRD-1547848. J.G.P. was supported by NIH IMSD grant R25 GM058903-20. P.C. is supported by EMBO long-term fellowship 57-2019. **Author contributions:** Conceptualization: A.G.C., J.A.S., J.H., S.S.G., C.L.P., and A.L. Methodology: A.G.C., J.H., J.A.S., C.S., D.C.E., M.F., and C.R.B. Investigation: A.G.C., J.A.S., J.H., C.S., D.C.E., M.F., J.G.P., R.K.S., and S.T. Validation: A.G.C., J.A.S., J.H., C.S., D.C.E., M.F., and S.T. Formal analysis: A.G.C., J.H., J.A.S., C.R.B., P.C., C.S., D.C.E., and M.F. Resources: S.S.G., C.L.P., and A.L. Data curation: A.G.C., J.H., J.A.S., and C.S. Writing – original draft: A.G.C., J.H., J.A.S., C.L.P., and A.L. Writing – review and editing: A.G.C., J.A.S., J.H., D.C.E., C.R.B., S.S.G., C.L.P., and A.L. Funding acquisition: J.H., J.G.P., P.C., S.S.G., C.L.P., and A.L. Supervision: S.S.G., C.L.P., and A.L. **Competing interests:** The authors declare no competing interests. **Data and materials availability:** All data are available in the main text or the supplementary materials.

SUPPLEMENTARY MATERIALS

science.org/doi/10.1126/science.abd4453
Materials and Methods
Figs. S1 to S22
Tables S1 to S12
References (*58*–*82*)
MDAR Reproducibility Checklist
Data S1 to S8

View/request a protocol for this paper from *Bio-protocol*.

21 June 2020; accepted 30 August 2021
10.1126/science.abd4453

Downloaded from https://www.science.org at University of California Merced on October 09, 2021

Science

Reconstitution of an intact clock reveals mechanisms of circadian timekeeping

Archana G. ChavanJeffrey A. SwanJoel HeislerCigdem SancarDustin C. ErnstMingxu FangJoseph G. PalaciosRebecca K. SpanglerClive R. BagshawSarvind TripathiPriya CrosbySusan S. GoldenCarrie L. PartchAndy LiWang

Science, 374 (6564), eabd4453.

A biological clock in a test tube

The biological clock of cyanobacteria, which remarkably requires just three proteins, has been reconstituted in vitro in a system that allows detailed study of its inputs and outputs, bringing new understanding of how environmental signals can influence a biological oscillator and how the clock controls cellular events such as gene transcription. Chavan *et al*. extended the known in vitro function of the core clock components to include output signals to transcriptional regulation and allow monitoring through fluorescence measurements in real time. The authors combined crystallography, mutagenesis, and quantitative modeling to further explore the clock mechanism, which may enable future synthetic biology applications. —LBR

View the article online
https://www.science.org/doi/10.1126/science.abd4453
Permissions
https://www.science.org/help/reprints-and-permissions

Downloaded from https://www.science.org at University of California Merced on October 09, 2021

Use of think article is subject to the Terms of service

Science (ISSN) is published by the American Association for the Advancement of Science. 1200 New York Avenue NW, Washington, DC 20005. The title *Science* is a registered trademark of AAAS.
Copyright © 2021 The Authors, some rights reserved; exclusive licensee American Association for the Advancement of Science. No claim to original U.S. Government Works

Science
AAAS

Supplementary Materials for

Reconstitution of an intact clock reveals mechanisms of circadian timekeeping

Archana G. Chavan *et al.*

Corresponding authors: Carrie L. Partch, cpartch@ucsc.edu; Andy LiWang, aliwang@ucmerced.edu

Science **374**, eabd4453 (2021)
DOI: 10.1126/science.abd4453

The PDF file includes:

Other Supplementary Material for this manuscript includes the following:

Materials and Methods

Cloning, expression and purification of proteins:

PCR-mediated mutagenesis was performed on the pET-28b vector utilizing Nde I/Hind III restriction sites as described previously (*58*) to modify clock genes from *Synechococcus elongatus* to produce 6x-His-SUMO fusion proteins in *Escherichia coli* BL21(DE3) (Agilent). All constructs are listed in **Table S1**. Point mutations were introduced using long-range PCR with overlapping primers (*14*). A single colony from freshly transformed cells was used for inoculation of a starter culture grown in LB medium supplemented with 50 µg/mL kanamycin sulphate at 37 ºC, 220 rpm. After 6.5 h a 5 mL starter culture was transferred to 1 L M9 medium supplemented with 0.2% D-glucose, 2 mM $MgSO_4$, 0.1 mM $CaCl_2$, and 50 µg/mL kanamycin sulfate. Cells were grown to $OD_{600} \approx 0.6$ at 37 ºC before inducing expression by addition of 0.2 mM isopropyl β-d-1-thiogalactopyranoside (IPTG) and incubating cells at 30 ºC for 12 h, except for CikA expression for which cells were incubated at 20 ºC for 22 h.

Cells were harvested and lysed using an Avestin C3 Emulsiflex homogenizer (Avestin Inc, Canada). Cell lysate was clarified by high-speed centrifugation before affinity purification on Ni-NTA resin (QIAGEN) in polypropylene gravity columns using the buffers specified in Table S1. All purification steps were carried out at 4 ºC. For cleavage of the 6x-His-SUMO fusion protein, 6x-His-ULP1 protease was added to final concentration of 3 µM and incubated at 4 ºC for 15 h. Reductant tris(2-carboxyethyl)-phosphine (TCEP) was added to SasA and CikA samples during ULP1 cleavage (concentrations given in **Table S2**). 6x-His-SUMO was removed by loading the cleaved protein on a Ni-NTA column for a second time. The flow-through was concentrated using 10 kDa molecular weight cut-off (MWCO) membrane filters in an Amicon™ (Millipore Sigma) stir-celled concentrator at 4 ºC before purifying by gel-filtration chromatography. SasA used for two-dimensional titration experiments was purified as His-Gβ1-tagged full-length SasA constructs over Ni-NTA resin using the standard protocol described previously (*14*), followed by overnight cleavage at 4°C with TEV protease with final concentration of 0.1 mg/mL. SasA was subsequently resolved from the His-Gβ1 tag on a Sephadex 200 size-exclusion column (GE Healthcare) equilibrated with 20 mM Tris, 150 mM NaCl pH 7.4.

Fluorescent labeling of proteins:

N-terminal sortase-mediated ligations were performed for full-length protein constructs used in IVC that had been modified to carry an N-terminal glycyl residue (see **Table S3**). The fluorophore-containing peptides 5-carboxyfluorescein (5-FAM)-LPETGG and C-(Cy3)-LPETGG were purchased from GenScript (New Jersey). For C-terminal ligations, target proteins were fused to sortase-A recognition peptide LPETGG at the C-terminus. The peptide GGGYCN was expressed and purified in-house as a 6x-His-SUMO-fusion protein. The cysteinyl residue on the purified fusion protein was labeled with the fluorophore 6-iodoacetamidofluorescein (6-IAF) (Invitrogen) as described previously (*25*). The labeled peptide was cut from the SUMO-fusion protein using ULP1 and passed through 10 kDa MWCO membrane in stirred cell concentrator. The flow-through containing labeled peptide was further purified by C4 reverse-phase column chromatography. The peptide was eluted with a linear acetonitrile gradient and then lyophilized. Dried peptide was dissolved in sortase buffer before use. Concentration was determined by UV absorbance by the 6-IAF fluorophore at 493 nm. Each target protein was buffer exchanged in sortase buffer (20 mM Tris, 150 mM NaCl, pH 7.5) before ligation. For ligation, 50 µM target protein was incubated with 250 µM fluorophore peptide, 5 µM sortase-A, and 10 mM $CaCl_2$ in the dark at 4 ºC for 12-16 h. Sortase-A was separated from reaction mixtures by Ni-NTA chromatography using prepacked 5 mL HiTrap-Ni-NTA columns (GE Healthcare) on an AKTA FPLC using a step gradient of imidazole. Labeled protein fractions were concentrated and purified further by gel-filtration chromatography using a Superose-6-Increase-10/300 GL analytical grade column (GE Healthcare). Table S2 lists the fluorophore peptides used for labeling each protein construct. Fluorescence labeling of fsKaiB, $SasA_{trx}$, and $CikA_{psr}$ constructs was done with 6-iodoacetamidofluorescein (6-IAF, Invitrogen) as described previously (*37*).

Reconstitution of clock reactions for fluorescence anisotropy measurements:

For monitoring multiple probes simultaneously, a master mix of oscillator reactions was prepared in 20 mM Tris, 150 mM NaCl, 5 mM $MgCl_2$, 1 mM ATP, and pH 8.0 buffer by mixing unlabeled proteins at the final concentrations shown in **Table S4,** except for KaiC and fluorescently labeled probes. IVC reactions were initiated by adding a solution of KaiC and ATP to the master mix. Aliquots (95 µL) of reaction master mix were pipetted into black, non-binding

384-well microplates (Greiner BioOne). Finally, 5-µL aliquots of fluorophore-labeled protein (50 nM final concentration) or DNA (100 nM final concentration) were added to separate wells. The plate was sealed using clear, adhesive film (MicroAmp^{TM}). The plate was transferred to a CLARIOstar multimode microplate reader (BMG Labtech), pre-equilibrated at 30 ºC. The plate was incubated for 30 minutes prior to starting measurements to allow equilibration of all samples. Detector gain for parallel and perpendicular channels was adjusted on a 50 nM or 100 nM fluorescent probe mixed in buffer, where the target polarization was set to 10% of the maximum theoretical polarization of fluorescein (350 milli-polarization units). Fluorescence polarization was measured in kinetic mode, every 15 minutes for 800 cycles. Fluorescence polarization (FP) was converted to fluorescence anisotropy (FA) in CLARIOstar MARS software before analysis. All the anisotropy values are reported in millianisotropy (mA) units.

Fluorescence anisotropy oscillator data in Figs. 3 and 4 and Figs. S15-S20 were collected *in vitro* on either a CLARIOstar (BMG) or Spark 10M (TECAN) microplate reader. The fluorescein channel was used for all data collection ($\lambda_{excitation}$, 482 ± 8 nm; $\lambda_{emission}$, 530 ± 20 nm). Fluorescence anisotropy was monitored from each well in the 384-well plate and recorded every 15 minutes, with time zero representing 3-5 minutes following the addition of KaiC to oscillation reactions. See **Table S4** for specific experimental conditions for each run.

Phosphorylation assays for KaiC and RpaA

For phosphorylation measurements, 250 µL samples from identical clock reactions were incubated in parallel with the FA experiments and special attention was taken to ensure that phosphorylation reactions were initiated identically to FA reactions by the addition of a solution of KaiC and ATP to a master mix. For detection of RpaA phospho-states, fluorophore-labeled RpaA (50% of total concentration) was used. Samples were incubated at 30 ºC in a benchtop water bath. Aliquots (8 µL) were removed every 4 h by manual pipetting over a period of 72 h. Each aliquot was immediately flash frozen by dipping the tubes in liquid nitrogen and storing at -80 ºC until all the aliquots were collected. For phosphorylation analysis, time points were first run on Zn^{2+}-Phos-tag^{TM} gels as described below and then the same set of aliquots was run on 7.5% SDS-PAGE for analysis of KaiC~P states.

Sample preparation and analysis on Phos-tagTM gels: Frozen protein aliquots were thawed on ice for 15 minutes and mixed with 8 µL of chilled 2x-SDS-PAGE loading buffer. Samples were spun at 1500 rpm for 30 seconds and transferred quickly to ice. In each lane 4 µL samples were loaded on precast 50 µM-Zn^{2+}-Phos-tag^{TM} -12.5% SDS-PAGE gels (Wako Chemicals, Japan). Phosphorylated RpaA was separated by electrophoresis at constant voltage (140 V) for 2 h in freshly prepared 1x running buffer (100 mM Tris, 100 mM MOPS, 0.1% SDS and 5 mM sodium bisulfite, pH 7.8). The electrophoresis apparatus was kept in an ice bath during electrophoresis and running buffer was chilled to 4 ºC before use. Fluorescent bands of RpaA were visualized under UV transillumination (E-Gel Imager, Thermo fisher) immediately after electrophoresis was completed and before staining the gels with Coomassie blue protein gel stain.

SDS-PAGE for KaiC phosphorylation: Aliquots prepared for Phos-tag^{TM} gels were saved at -20 ºC until analysis. Samples were boiled at 95 ºC for 5 min and spun down at 15000 rpm for 30 seconds before loading on 7.5% SDS-PAGE gels. Samples (4 µL) were loaded in each well and two-step electrophoresis was performed at 60 V for 30 min followed by at 140 V for 1 h 40 min. The electrophoresis apparatus was kept in an ice bath and pre-chilled running buffer was used. Gels were stained with InstantBlue® protein gel stain (Expedeon Inc., Novus Biologicals, Centennial Co.) for at least 1 h followed by de-staining in D.I. water for 30 minutes. Gels were imaged by E-gel Imager (Invitrogen, Thermo Fisher Scientific). Densitometry of gel images was performed using NIH ImageJ software (*59*).

ATPase activity measured by 1H-NMR

A solution of 1.2 µM KaiA, 3.5 µM KaiB, 3.5 µM KaiC, 95% H_2O, 5% D_2O, and 10 µM DSS was prepared in a reaction buffer containing 20 mM Tris, 100 mM NaCl, 1 mM ATP, 5 mM $MgCl_2$, pH 8. The oscillator reaction was initiated by adding a solution of KaiC and ATP to a solution of KaiA and KaiB. One-dimensional proton NMR spectra were measured at 30 ºC, every hour for 5 days. The ATP and ADP peaks were fit using an interpolation function in Wolfram Mathematica. Peak intensities were plotted as function of time and fit to a straight line

from which overall ATPase activity was determined. Oscillations of ATP and ADP resonances about the line provided the determination of ATPase rhythms (see Fig. S6 for details).

Data fitting for phase and period analysis

First 12 h of raw data were removed before analysis because during this time samples are approaching stable limit cycles. Anisotropy and phosphorylation data were baseline-corrected using a quadratic function and normalized to ±1 before fitting to a damped single cosine function:

$$Y = a\ cos[2\pi\left(\frac{t}{p}\right) - \phi]e^{-kt}$$

where, a = amplitude, p = period, $\phi = phase\ angle$, k = decay constant.

Fluorescence data quantification and statistical analyses in titration experiments: Fluorescence anisotropy readings from clock reactions were collected in MARS Data Analysis Software or SparkControl Software for experiments run on the BMG CLARIOstar Plus or TECAN Spark 10M, respectively. All data were analyzed in the online BioDare suite by FFT-NLLS (*60*, *61*) (https://biodare2.ed.ac.uk/welcome). Prior to analysis, fluorescence anisotropy rhythms were baseline detrended and normalized to [-1, 1] with mean of zero. The first 12-h of data were disregarded for quantification of period, amplitude, and phase. Period (**Table S7**) and amplitude (**Table S8**) analysis in **Fig. 3, 4 and S13,** and **S20** were assessed by ordinary one-way ANOVA with Dunnett's multiple comparison tests in Prism 8 (Graph Pad). The significance values and the number of independent experiments for each experimental group are reported in the corresponding figure legends.

Comparisons of the effects of added SasA or CikA on period (**Table S7**) and amplitude (**Table S8**) under different concentrations of the core clock proteins KaiA and KaiB presented in **Table S5** were determined by ordinary two-way ANOVA with Dunnett's multiple comparison tests in Prism 8 (GraphPad). Normalized fluorescence anisotropy rhythms were plotted in conjunction with nonlinear regression least squares cosinor fit in Prism 8 in **Fig. 4**, while raw fluorescence anisotropy data were plotted with Origin Student 2019b (Origin Lab) in **Fig. 3, 4, S13,** and **S20**.

Raw anisotropy data were baseline corrected using an unbound labeled-KaiB reaction well as a reference in each independent experiment.

The damping constant, k, was determined in Prism 8 (GraphPad) using a nonlinear least square regression cosinor fit:

$$y = m * x + amplitude * e^{-kx} * cos\left[\left(2\pi * \frac{x}{period}\right) + phase\right]$$

where y is the signal, x the corresponding time, amplitude is the height of the peak of the waveform above the trend line, k is the decay constant (such that 1/k is the half-life), period is the time taken for a complete cycle to occur and phase is the shift in x relative to a cosinor wave.

Strains and culture conditions for *in vivo* experiments

Synechococcus elongatus PCC 7942 and its derivative strains (Table S12) were maintained on BG-11 medium containing antibiotics as needed for selection (*62*). Growth on plates or in liquid medium was carried out at 30 ºC under 150 µmol m^{-2} s^{-1} light. *E. coli* DH5α used for cloning was grown on LB with the appropriate antibiotics at 37 ºC.

Construction of rpaA-R121Q strain: Introduction of point mutations into the *S. elongatus* chromosome was accomplished using a previously described CRISPR-editing approach (*44*). The pSL2680 (Km^R) plasmid used for CRISPR-Cas12a (formerly Cpf1) editing was purchased from Addgene (Plasmid #85581). Primers rpaA_gRNA_F and rpaA_gRNA_R were annealed together and ligated into AarI-cut pSL2680 to serve as the *rpaA-R121Q* gRNA template. The resulting construct was purified and digested with KpnI to facilitate insertion of the *rpaA-R121Q* homology directed repair (HDR) template. The HDR template was generated by amplifying overlapping upstream and downstream fragments using primers rpaA_HDR-UP_F and rpaA_HDR-UP_R (AMC1722 genomic DNA as template) and rpaA_HDR-DWN_F and rpaA_HDR-DWN_R (AMC541 genomic DNA as template), respectively. The upstream and downstream HDR fragments were assembled into KpnI-cut pSL2680+gRNA using the GeneArt Seamless Assembly Kit (Thermo Fisher Scientific), forming pDE32. Plasmid pDE32 was electroporated into *E. coli* DH10B containing a helper plasmid pRL623 (chloramphenicol resistance, Cm^R) and conjugal plasmid pRL443 (ampicillin resistance, Ap^R) (*63*). The resulting

strain was grown overnight in LB medium containing antibiotics (Ap, kanamycin Km, and Cm), washed 3x with fresh LB, and mixed in a 1:2 ratio with an *S. elongatus* reporter-strain aliquot. The cell mixture was plated onto BG-11 agar with added LB (5% vol/vol), incubated under 100 µmol m^{-2} s^{-1} light for 36 h, then underlaid with Km (10 µg/ml final concentration) to select for *S. elongatus* cells that contain pDE32. Colonies that emerged after 6-8 days were passaged three times on BG-11 agar containing Km to allow editing to occur. Successful editing of chromosomal *rpaA* was verified by sequencing. Plasmid pDE32 was cured from the edited strain by inoculating cells into non-selective BG-11 medium, growing the culture to OD_{750} = 0.6, then dilution plating on non-selective BG-11 plates. Fifty colonies were picked and replica patched to selective (Km) and non-selective medium to identify and isolate clones that had lost pDE32.

Generation of SasA mutants in S. elongatus: Markerless point mutations were introduced in *sasA* of *Synechococcus elongatus* PCC 7942 by CRISPR/Cas12a engineering as previously described (*44*). Plasmids and the primers used in vector construction and sequence verification are listed in **Table S11 and S12**. Briefly, oligos with complementarity to the guide RNA (gRNA) recognition site were annealed and cloned into AarI-cut pSL2680 (Addgene Plasmid #85581). Clones of pSL2680 that carry the appropriate gRNA insert were isolated and plasmid sequences were verified. Upstream and downstream homologous repair templates that encode the point mutation(s) of interest were amplified by PCR and assembled (GeneArt Seamless Assembly, Thermo Fisher) into KpnI-cut constructs that contain the respective gRNAs. Recovered plasmids were checked for accuracy by Sanger sequencing prior to editing in *S. elongatus*.

The RSF1010-based editing constructs were electroporated into *E. coli* AM1359 that contain conjugal helper plasmids (pRL623 and pRL443) as previously described (*64–68*). The resulting *E. coli* strains were grown overnight in LB containing ampicillin (100 µg/ml), chloramphenicol (17 µg/ml) and kanamycin (50 µg/ml). Cells from a 1 ml aliquot were washed three times with fresh LB and resuspended in a final volume of 100 µl LB, then mixed with 100 µl of an *S. elongatus* clock-reporter strain (AMC541) concentrated down from 2 ml of a dense culture (OD_{750} = ~0.6). The mixed culture was plated to solid BG-11 medium containing 5% LB (v/v) and incubated at 30˚C under 30 µmol photons m^{-2} s^{-1} (µE) illumination for 24 hours. Plates were

then underlaid with kanamycin (5 µg/ml final concentration) to select for the editing plasmid. *S. elongatus* colonies that emerged after 8-10 days at 30˚C and 100 µE light were serially patched three times to BG-11 containing kanamycin to maintain the editing plasmid long enough to complete segregation of the mutant allele in all copies of the chromosome. After editing, *sasA* was amplified by colony PCR using primers that anneal outside of the homologous repair region and the resulting PCR product was submitted for Sanger sequencing to confirm segregation of the point mutation(s) of interest.

Bioluminescence monitoring of S. elongatus circadian rhythms: Bioluminescence was monitored using a P*kaiBC*::*luc* firefly luciferase fusion reporter inserted into a neutral site of the *S. elongatus* chromosome as previously described (*62*). Strains to be monitored were grown in liquid culture to OD_{750} = 0.4-0.7, diluted to OD_{750} = 0.2, and added as 20 µl aliquots to 280 µl of BG-11 agar containing 3.5 mM firefly luciferin arrayed in 96-well plates. Plates were covered with a gas-permeable seal and cells were entrained under 12-h light-dark cycles (80 µmol m^{-2} s^{-1} light) to synchronize clock phases. After 48 h of entrainment, cells were released into continuous light (30 µmol m^{-2} s^{-1}) and bioluminescence was monitored every 2 h using a Tecan Infinite Pro M200 Bioluminescence Plate Reader. Mutant *sasA* strains, along with positive and negative clock-output controls, were grown in BG-11 medium, diluted to OD_{750} = 0.2 and arrayed in 96-well plates containing solid BG-11 medium and 10 µl of 5 mM D-luciferin. Plates were covered by a gas permeable seal and incubated in a light-dark chamber at 30˚C for 48 hours, with 12 h intervals of 120 µE light and darkness. Following release into constant light at the end of 48 hours, plates were transferred to a lighted stacker (40 µE light) attached to a Tecan Infinite M200 Pro and bioluminescence was monitored every 2-3 hours. The raw bioluminescence data were plotted as a function of time (GraphPad Prism 8) and processed using BioDare2 to determine period and amplitude for each set of replicates (*61*). All strains used in this study are listed in **Table S11**.

Immunoblotting: For detection of RpaA phosphorylation flask-grown cells were collected (15 ml) at ZT 0 and ZT 12 from liquid cultures (OD_{750} = 0.6-0.7) incubated under 12-h light-dark cycles (40 µmol m^{-2} s^{-1}). Cells were pelleted, washed once with cold 10 mM sodium chloride

solution and frozen at -80 ºC. Cell pellets were thawed on ice and resuspended in tris-buffered saline (pH 7.4) containing 1 mM phenylmethylsulfonyl fluoride, then disrupted by bead beating at 4 ºC (30 s of beating, followed by 2 min on ice for 10 cycles). Following centrifugation (20,000 x *g* for 10 min), protein concentrations were determined by the Bradford assay and a total of 10 µg of protein was loaded per well. Phos-tag^{TM} reagent (20 µM) (Wako Chemicals, Japan) and manganese chloride (100 µM) were added to standard SDS-PAGE gels (12.5 %) to allow detection of phosphorylated RpaA. Electrophoresis was conducted on ice using pre-chilled running buffer to limit hydrolysis of the heat-labile phospho-aspartate. Current was maintained at 25 mA until the bromophenol blue dye reached the bottom edge of the gel. The gel was then incubated for 10 min in transfer buffer containing 10 mM EDTA, followed by a 10 min incubation in transfer buffer without EDTA prior to semi-dry transfer to a PVDF membrane using a Trans-Blot Turbo System (BioRad). Detection of RpaA was achieved using RpaA-antiserum (gift from E. O'Shea, HHMI–Janelia, Ashburn, VA) at a dilution of 1:2000 as described previously (*69, 70*). Secondary antibody (goat anti-rabbit IgG; 401315, Calbiochem) was used at a dilution of 1:100,000 and chemiluminescent signal was produced using the SuperSignal West Femto Maximum Sensitivity Substrate (Thermo Fisher Scientific).

For detection of total SasA levels protein extraction was performed as described above. Bio-Rad Any kD™ Mini-PROTEAN® TGX™ Precast Protein Gels (cat #4569036) were used to perform SDS-PAGE with 10 µg of protein loaded per well. Detection of SasA was achieved using SasA-antiserum (Aves Lab) at a dilution of 1:4000. Secondary antibody (goat anti-chicken IgY; ab96947, Abcam) was used at a dilution of 1:5000 and chemiluminescent signal was detected by using the SuperSignal West Femto Maximum Sensitivity Substrate (Thermo Fisher Scientific) and imaging with BioRad ChemiDoc system.

Crystallization of monomeric T. elongatus C1 domain in complex with T. elongatus SasAtrx

A monomeric mutant of *T. elongatus* KaiC-CI domain (see **Table S1** for details) was incubated at 250 µM with an excess of *T. elongatus* $SasA_{trx}$ (460 µM) overnight in 20 mM Tris pH 7.0, 150 mM NaCl, 5 mM DTT, 1 mM $MgCl_2$ and 1 mM ATP at room temperature. The complex was subsequently purified by size-exclusion chromatography on a Sephadex 70 column (GE

Healthcare) equilibrated in the same buffer, but with $MgCl_2$ and ATP concentrations reduced to 0.5 mM. The complex was mixed in a 1:1 ratio to a final concentration of 10.8 mg/mL with the crystallization buffer containing 1.26 M NaH_2PO4, 0.54 M K_2HPO_4 (pH unadjusted, total PO_4 concentration 1.8 M), 0.1 M Glycine (added from a 1 M solution adjusted to pH 10.5) and 0.2 M $Li_2(SO_4)_2$. Crystals formed over 10 days at 22 °C using the hanging drop method. The flat, plate-like crystals were then frozen in liquid nitrogen after soaking in cryoprotectant composed of the crystallization buffer plus 20% (v/v) glycerol.

Structure determination and refinement: Single crystal diffraction data were collected with a wavelength of 1 Å on the 23-ID-D X-ray source at the Advanced Photon Source at the Argonne National Laboratory. Data were processed and scaled using iMOSFLM (*71*) and Aimless (*72*). Phases were solved by molecular replacement with the structure of *T. elongatus* KaiC-CI monomer in complex with fsKaiB (PDB 5JWO) using Phaser (*73*). Refinement and model building were performed using Phenix (*74*) and Coot (*75*). See **Table S6** for crystal and refinement statistics. Structural figures were made using UCSF Chimera (*76*, *77*) and ChimeraX (*78*).

Equilibrium binding assays: Binding titrations were performed in 20 mM Tris pH 7.4, 150 mM NaCl, 1 mM ATP, 1 mM $MgCl_2$ and 0.1 % (v/v) Tween-20. Fluorescein-labeled KaiB or $SasA_{trx}$ probes were present at 50 nM, while the titrant was diluted serially in 1/3-fold increments. Serial dilutions were performed in a 384-well plate before sealing with tape and incubating at room temperature overnight (9-15 h). Fluorescence polarization anisotropy measurements were subsequently collected on a Synergy2 plate reader (BioTek). Replicate measurements were collected and averaged for each well (20). For 2D titration assays looking at the effect of an additive on KaiB binding to KaiC, fsKaiB or SasA additives were included in both KaiC and diluent buffer to maintain a constant concentration. Diluent was added to the 384-well plate using a single channel pipettor, and additives were mixed into the KaiC stock last and diluted within 10 minutes. See thermodynamic modeling of binding equilibria below for more information.

Thermodynamic modeling of binding equilibria: The fluorescence anisotropy titrations outlined above involve cooperative and competitive reactions and span a wide range of concentrations,

such that free ligand concentrations cannot be approximated by the total added concentration. Consequently, these data cannot be analyzed by fitting to standard analytical equations (*79*). Fitting the data to the profiles simulated by a model avoids this problem but introduces others in terms of the complexity of the model that is required for the fit. Initially, we attempted to fit to a general hexameric model for KaiC but found there were too many parameters to reach convergence. When simplified to a dimer model, the fits were reasonably robust and showed no systematic deviations. Nevertheless, such a simplified model required positive heterotropic or homotropic cooperativity between KaiB and additives such as SasA and fsKaiB, respectively, as well as competition between these additives. Thus, a dimer model captures the essence of the interaction, although how this relates in detail to cooperativity within the KaiC hexamer remains in question.

Least-squares fitting analysis to models was performed using DynaFit (BioKin) (*80*). Scripts used for analysis are available in supplemental data (**Data 1** and **2**). Statistical analysis was performed using the Monte Carlo routine. Cooperativity indices (described by $K_1/K_3 = K_2/K_4$, see **Data S3**) were calculated for each simulation (n = 1000) and median and 95% confidence intervals taken as ranks 500, 25 and 975 (respectively) in the n = 1000 simulation. Where replicate measurements are reported, the values of median or 95% confidence boundaries were averaged amongst the replicates.

In order to reduce the number of parameters of the fit, the binding of KaiB alone was initially modeled without any homotropic cooperativity by assigning $K_5 = 4*K_1$, as is appropriate for the macroscopic equilibrium constants for two-site independent binding. When K_5 was floated, a slightly improved fit was obtained with a returned $K_5 < K_1$, indicative of homotropic cooperativity, but K_5 was not robustly defined. The value of the heterotropic cooperativity index in the presence of additives increased when K_5 was floated, however, we report fits where K_5 was defined as $4*K_1$ for simplicity, which gives a minimal estimate of the heterotropic cooperativity index. The input and output files from the least-squares fitting and Monte Carlo analysis are available as **Data S3**. Input KaiC dimer concentrations are given in Data S3, while KaiC concentrations given in terms of total monomer elsewhere.

Triplicate 2D titrations were collected with SasA to optimize the analysis and showed some variability that was ameliorated by floating additive concentrations at the 3 highest additive concentrations. The averages from these fits were used for SasA and KaiB variant 2D titration datasets when analyzing 300 nM data, where additive concentrations were also allowed to float. Little variation was seen in the experimental anisotropy values determined for fluorescently labeled KaiB alone or the final peak values for the KaiB-KaiC complex, though the average peak experimental anisotropy values of putative ternary complexes seeded by heterocooperativity differed modestly between the SasA and fsKaiB variants (KaiB peak anisotropy = 0.211 for SasA or 0.205 for fsKaiB).

Size-exclusion chromatography-multiangle light-scattering (SEC-MALS) assays: SEC-MALS assays were performed at room temperature using a silica-based size-exclusion column (particle size 5 μm, pore size 500 Angstrom, 4.6 mm ID, Cat. No. WTC-050N5, Wyatt Technologies) to resolve the oligomeric state of SasA. 20 μL injections of full-length SasA at 1.5 mg/mL were made using an Agilent G1311A quaternary pump and manual injector (Rheodyne), run over the silica-based column, and analyzed by a T-rEX refractometer and miniDAWN TREOS II static multiangle light scattering instrument (Wyatt Technologies) directly after the column. Analysis of absolute molecular weight was carried out using Astra 6.0 software (Wyatt Technologies).

^{32}P phosphotransfer assay

Assays were performed in the presence of **γ**-^{32}P ATP as originally described (*19*). These experiments were conducted with 5 μM KaiC-EE, 3.5 μM RpaA, and 2.5 μM SasA variant in 0.1 mM ATP. To do this 100 μM KaiC in 1.0 mM ATP was diluted with 20 mM Tris pH 7.4, 150 mM NaCl, 1 mM $MgCl_2$, 1 mM TCEP. 4 μL of undiluted **γ**-^{32}P ATP (EasyTides).
SasA-WT and SasA-DM were compared in this assay by quenching the reactions at discrete timepoints using an equivalent volume of 6x SDS-PAGE loading buffer. ^{32}P labeled protein was separated on an anyK_D™ pre-cast SDS-PAGE gel (BioRad). Gels were dried and exposed overnight for visualization on a Typhoon phosphorimager, and subsequent quantification by densitometry. Slopes of the resulting trajectories were compared in triplicate between wild-type SasA and SasA-H28A-Q94A to determine the % activity the double mutant. A control was also

included where no RpaA was added to quantify the efficiency of initial histidine phosphorylation to the SasA variants, and triplicate densitometries were compared at a single timepoint.

Supplementary Data and Figures

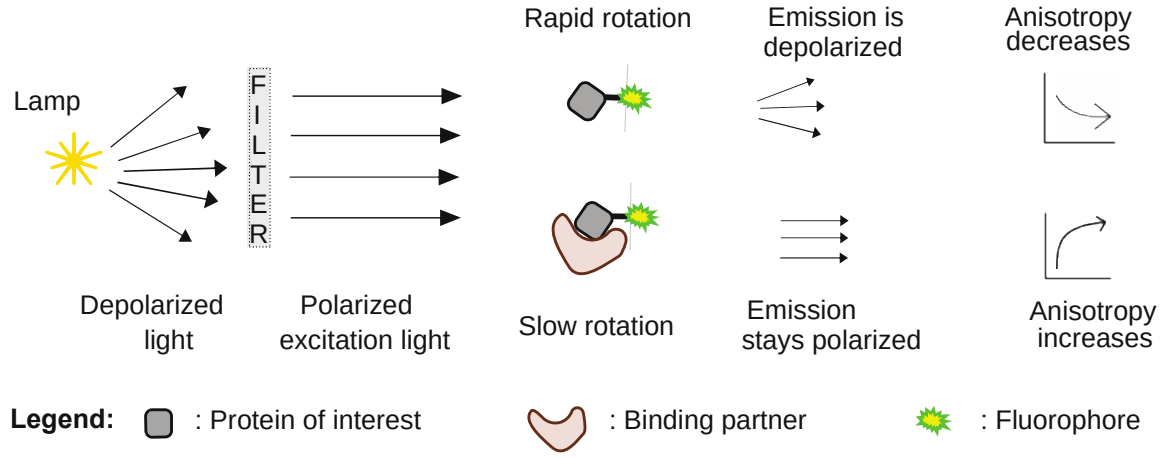

Figure S1: A schematic of fluorescence anisotropy (FA) assay used for real-time monitoring of rhythmic protein-protein interactions in IVC.

Fluorescence anisotropy occurs through excitation of a fluorescently labeled protein of interest. When the protein of interest is not part of a high molecular weight complex, its rotational correlation time is generally shorter than the fluorescence lifetime of the fluorophore, resulting in depolarized emission which can be quantified as lower anisotropy. Upon binding to its partner, the rotational correlation time of the labeled protein of interest increases, resulting in more polarized emission and a higher anisotropy value.

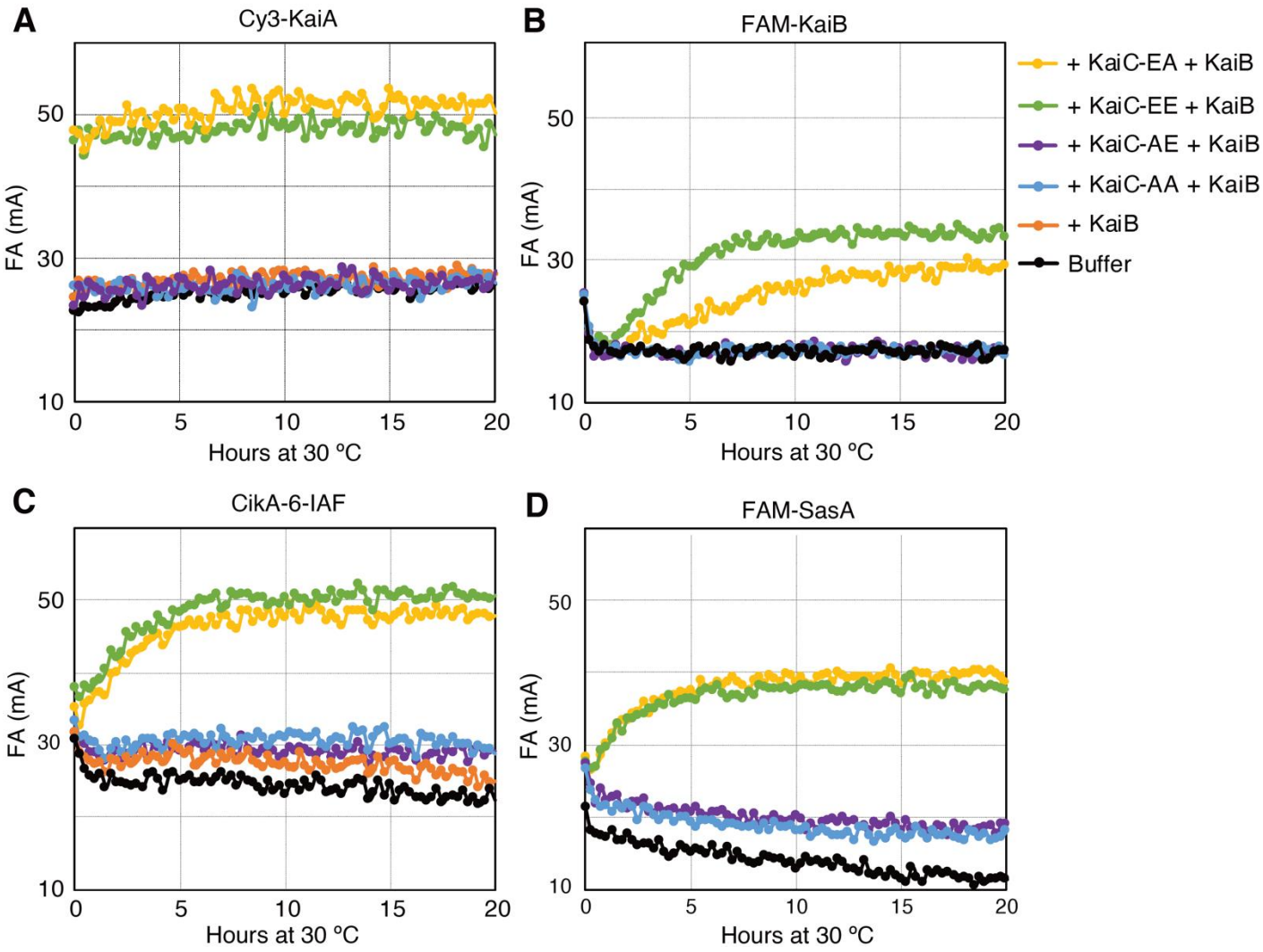

Figure S2. Fluorescence anisotropy of KaiA, KaiB, CikA, and SasA in partial clock reactions.

Control experiments of fluorescence anisotropies (FA) of labeled clock proteins at 50 nM were incubated with 3.5 µM KaiB (orange), or a mixture of 3.5 µM KaiB with a separate 3.5 µM KaiC phosphomimetics. Anisotropies of each labeled protein mixed with buffer are shown in black. The four phospho-states of KaiC can be mimicked by mutating S431 and T432 to either Ala or Glu (*8*). These phosphostates are indicated as KaiC-AA (S431A, T432A, blue), KaiC-AE (S431A, T432E, violet), KaiC-EE (S431E, T432E, green) and KaiC-EA (S431E, T432A, yellow). KaiC-EE and KaiC-EA respectively approximate the dusk pS,pT and nighttime pS,T states of KaiC. **(A)** Cy3-KaiA: G-KaiA was labeled at the N-terminus with C(-Cy3)-LPETGG **(B)** FAM-KaiB: G-KaiB was labeled at the N-terminus with 5-FAM-LPETGG **(C)** CikA-6-IAF: CikA-LPETG was labeled at the C-terminus with GGGYC-(6-IAF)N, shows binding to KaiB

only in presence of KaiC-EA/EE and **(D)** FAM-SasA: G-SasA was labeled at the N-terminus with 5-FAM-LPETGG and shows increased anisotropy in presence of KaiC-EE/EA. (**A and C**) shows that KaiA and CikA anisotropies report their binding to KaiB in presence of KaiC-EE or KaiC-EA, suggesting nighttime ternary complex formation and is consistent with the peak anisotropies observed for KaiA and CikA in IVC that peaks with KaiB anisotropy (**Fig. 2**). (**B** and **D**) Shows that SasA and KaiB both bind to hyperphosphorylated KaiC (KaiC-EE/EA) at dusk. Difference in binding kinetics of SasA and KaiB is also consistent with phase difference observed in IVC (**Fig 1**).

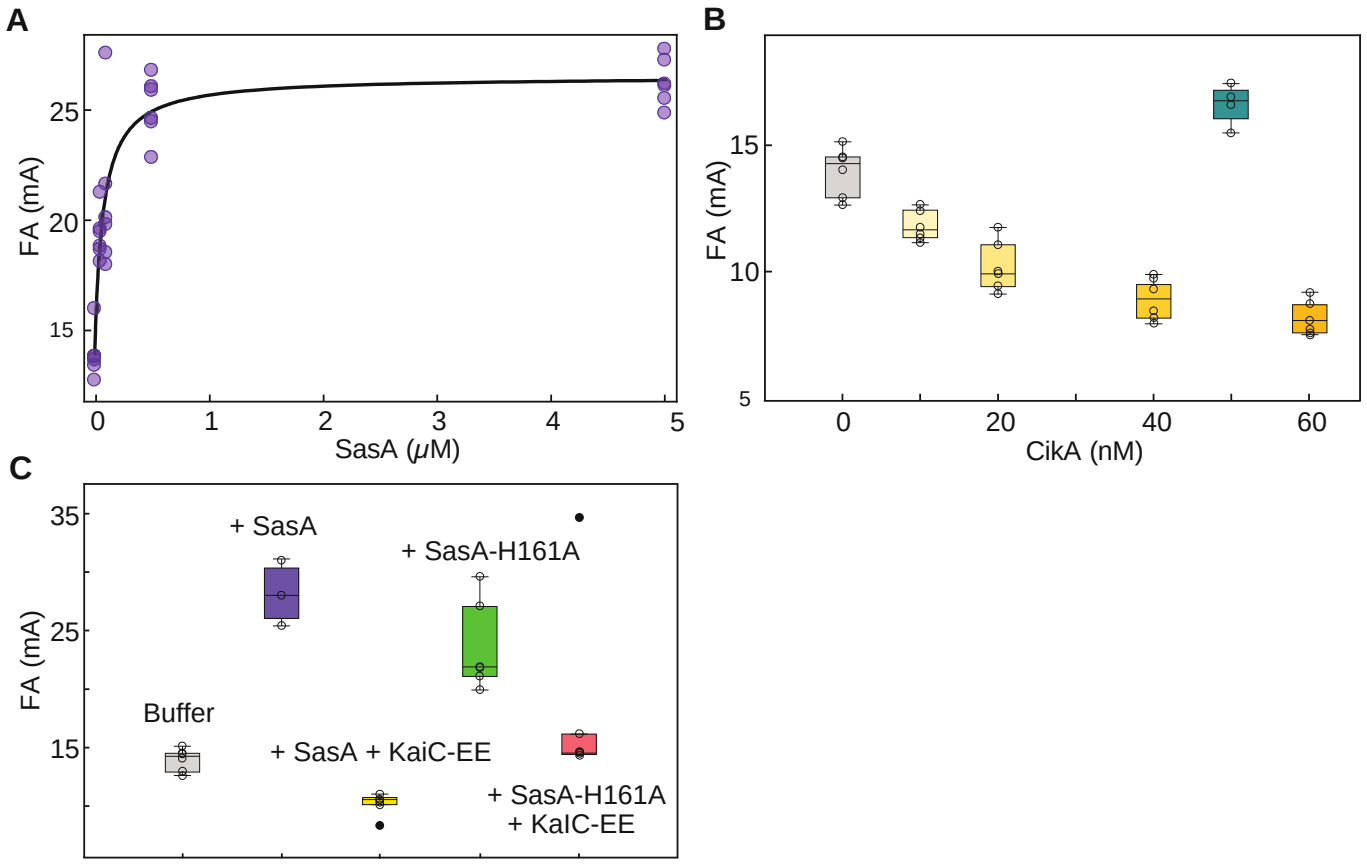

Figure S3. Fluorescence anisotropy of RpaA in the presence of SasA and CikA.
FAM-labeled RpaA (50 nM) was incubated at 30 ºC with various amounts of **(A)** SasA or **(B)** CikA. Reported fluorescence anisotropies were measured when the reactions reached steady state. **(A)** Fluorescence anisotropies of 50 nM FAM-labeled RpaA from six replicates are plotted as a function of SasA concentration (purple circles) and data for each replicate were separately fit to the following equation (*81*):

$$FA = FA_i + (FA_{max} - FA_i)\left(\frac{[SasA]}{[SasA]+K_D}\right)$$

where, FA = fluorescence anisotropy of RpaA,

FA_i = initial fluorescence anisotropy of RpaA,

FA_{max} = maximum fluorescence anisotropy of RpaA,

[SasA] = concentration of SasA (μM),

K_D = apparent dissociation constant (μM).

(A) Fitting the six data sets separately, the average apparent dissociation constant (K_D) is 0.07 ± 0.02 μM. **(B)** Box and whisker plots for RpaA fluorescence anisotropies measured from six

replicates as a function of CikA concentration (light to dark yellow), and also when separately incubated with 50 nM of CikA-H393A (teal, 4 replicates). RpaA alone is shown in gray. **(C)** Box and whisker plots for fluorescence anisotropies from six replicates of RpaA alone (gray), when incubated with 0.65 µM SasA (purple, 3 replicates), 0.65 µM SasA-H161A (green), 0.65 µM SasA + 3.5 µM KaiC-EE (yellow), or 0.65 µM SasA-H161A + 3.5 µM KaiC-EE (pink). The whisker fences denote minimum and maximum values in the data sets, excluding outliers, while the bottom and top of a box represent the first and third quartiles, respectively. A horizontal black line inside the box denotes the median. Individual data points are shown with open circles and outliers are shown as filled black circles. RpaA anisotropy decreases in presence of SasA+KaiC-EE or CikA, suggesting that phosphorylation of RpaA results in decrease in RpaA anisotropy. Kinase-dead mutants of SasA (H161A) and of CikA (H393A) serve as negative controls to show that RpaA anisotropy remains high in absence of phosphorylation.

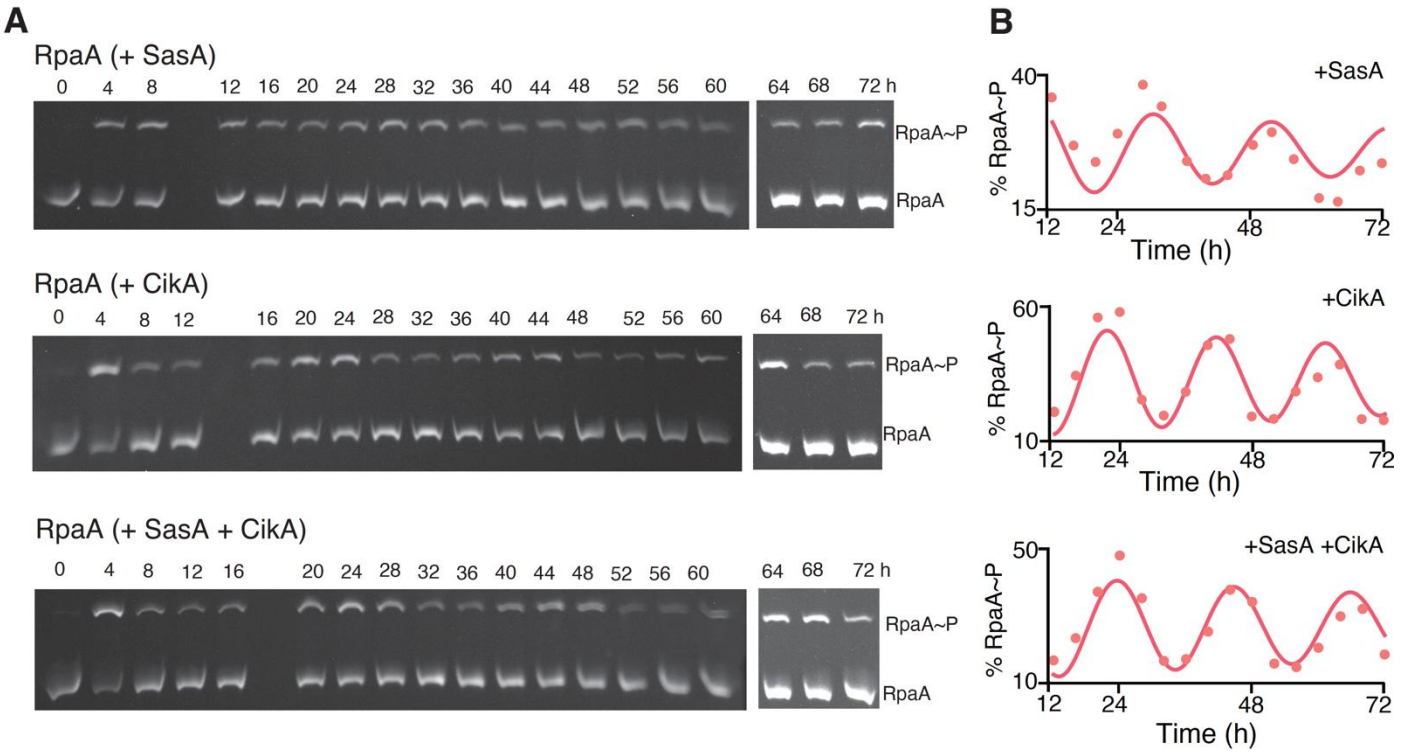

Figure S4. Phos-tag™ SDS-PAGE for WT RpaA phosphorylation *in vitro.*

(A) Aliquots of reconstituted clock reactions containing KaiA, KaiB, KaiC, RpaA, DNA, and either SasA, CikA, or both were sampled every 4 h manually, subjected to 12.5% Zn^{2+} Phos-tag™ SDS-PAGE, and visualized by UV-transillumination (see Materials and Methods for details). (**B**) Densitometry of the gels was performed by ImageJ (NIH) and band intensities were used to determine the level of RpaA phosphorylation at each time point using the equation

$$\%RpaA\sim P = 100\% * RpaA\sim P / (RpaA + RpaA\sim P)$$

Top, middle, and bottom panels are from IVC reactions that used SasA, CikA, and SasA + CikA.

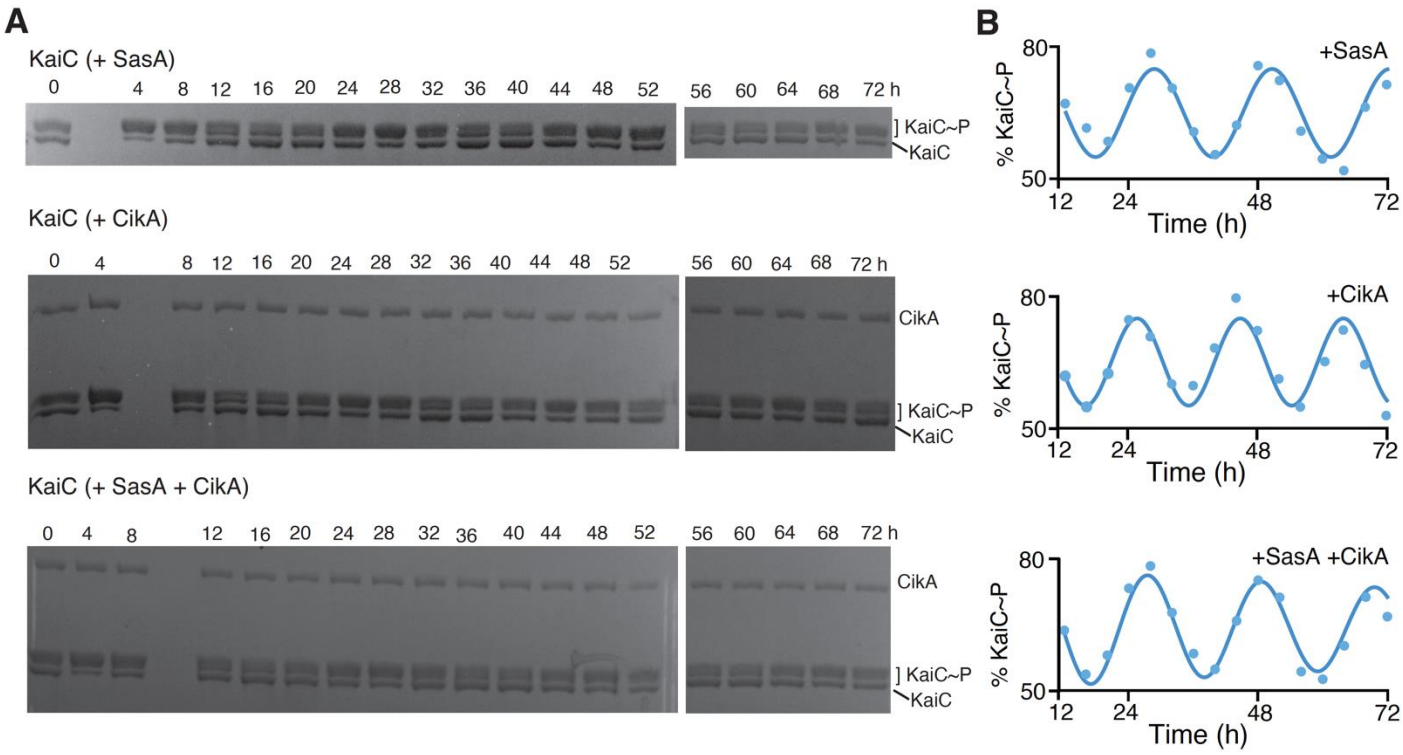

Figure S5. SDS-PAGE of KaiC phosphorylation *in vitro.*

KaiC~P was measured in IVC reactions containing KaiA, KaiB, KaiC, RpaA, DNA, and either SasA (top), CikA (middle), or both SasA and CikA (bottom). (**A**) Aliquots were collected every 4 h, subjected to 7.5% SDS-PAGE, and stained with Instant Blue (Expedion) dye. The gels were analyzed by ImageJ software (NIH), where the sum of intensities of the top three bands were used to calculate the level of phosphorylated KaiC (KaiC~P). The bottom band is of unphosphorylated KaiC. (**B**) %KaiC~P = KaiC~P/total KaiC is plotted as function of time where top, middle, and bottom panels are from IVC reactions that used SasA, CikA, and SasA + CikA.

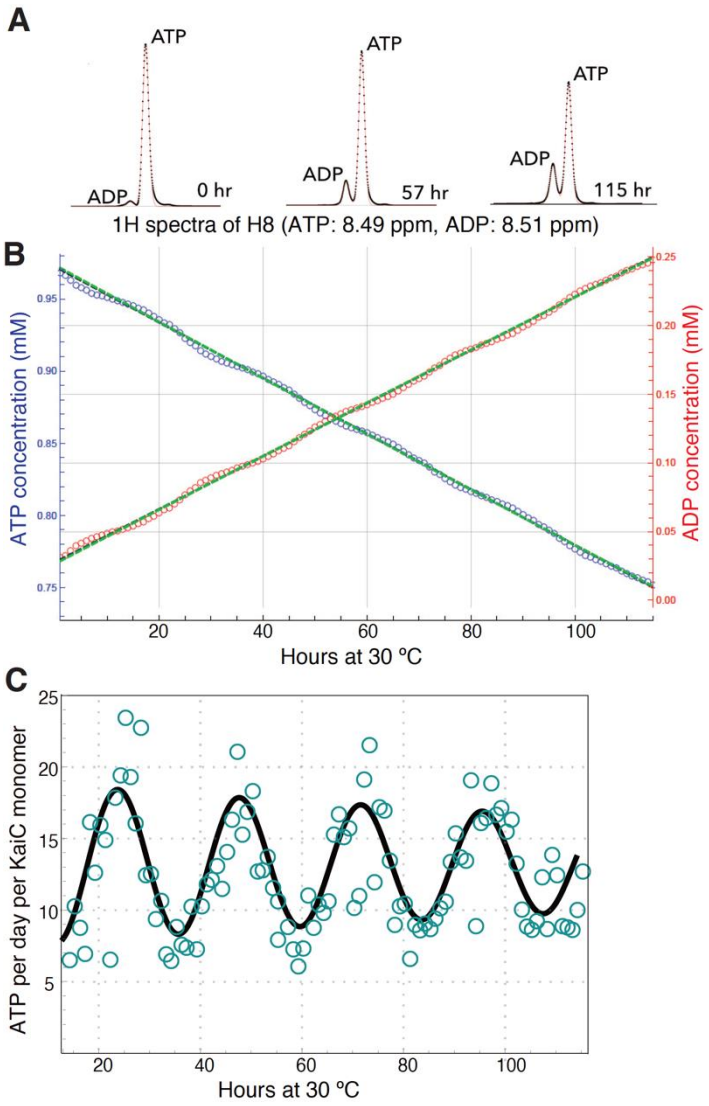

Figure S6. 1H NMR of ATP and ADP in a KaiABC oscillator reaction.
(A) H8 protons on the adenosine rings of ATP and ADP with chemical shifts of 8.49 ppm and 8.51 ppm, respectively, were monitored by ^{1}H NMR as a function of reaction time. One-dimensional spectra were collected every hour and changes in peak intensities were measured. **(B)** Based on total nucleotide concentration of 1 mM, integrated peak intensities of ATP (blue) and ADP (red) at each time point were converted to concentrations in mM. The green lines are linear fits through the data. **(C)** ATPase activity is shown by teal circles and a cosine fit is shown in black. ATPase activity oscillated between 8-18 ATPs per day per KaiC monomer. During the first 12 hours, the sample was approaching a stable limit cycle and thus this data was not used in the fit. In a second measurement oscillations were between 7-13 ATPs per day per KaiC monomer.

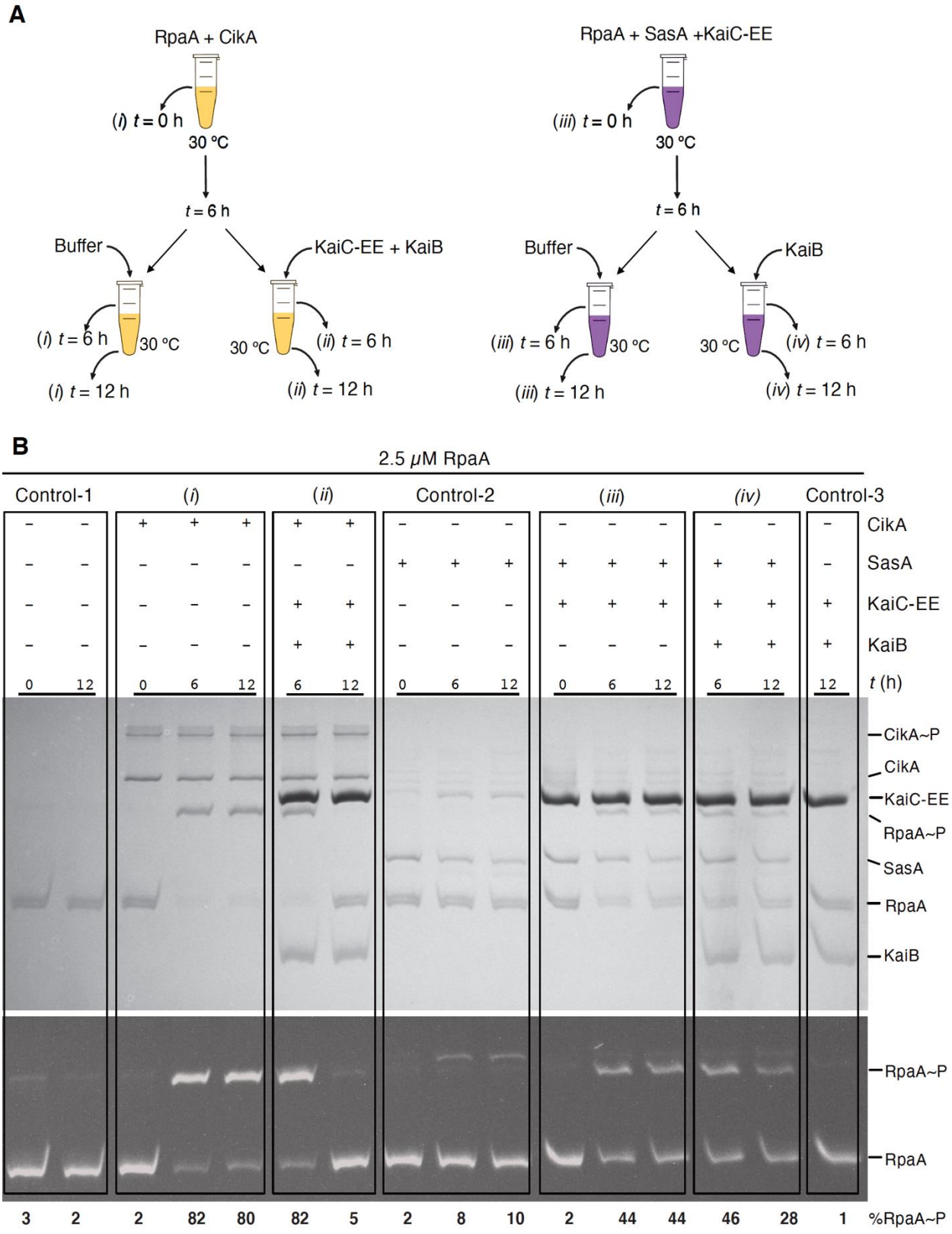
A
RpaA + CikA
(i) t = 0 h
30 °C
t = 6 h
Buffer
KaiC-EE + KaiB
(i) t = 6 h
30 °C
(i) t = 12 h
30 °C
(ii) t = 6 h
(ii) t = 12 h
RpaA + SasA +KaiC-EE
(iii) t = 0 h
30 °C
t = 6 h
Buffer
KaiB
(iii) t = 6 h
30 °C
(iii) t = 12 h
30 °C
(iv) t = 6 h
(iv) t = 12 h
B
2.5 μM RpaA
Control-1
(i)
(ii)
Control-2
(iii)
(iv)
Control-3
CikA
SasA
KaiC-EE
KaiB
t (h)
CikA~P
CikA
KaiC-EE
RpaA~P
SasA
RpaA
KaiB
RpaA~P
RpaA
3 2 2 82 80 82 5 2 8 10 2 44 44 46 28 1 %RpaA~P

Figure S7. Enzymatic activities of SasA and CikA in partial clock reactions.
(A) Schematics for RpaA phosphorylation assay in the presence of CikA (left panel) and SasA + KaiC-EE (right panel). 2.5 µM FAM-RpaA was incubated with either 0.65 µM CikA or a mixture of 0.65 µM SasA and 3.5 µM KaiC-EE at 30 ºC in a buffer containing 1 mM ATP and 5 mM $MgCl_2$, pH 8. In the left panel an aliquot was removed immediately after RpaA and CikA were mixed (t = 0 h). The reaction was incubated at 30 ºC for 6 h then divided into two equal portions, one portion received an equal volume of buffer and other received a pre-incubated mixture of KaiB + KaiC-EE (3.5 µM each). Aliquots were taken from both tubes immediately after mixing (t = 6 h). Incubation continued at 30 ºC for an additional 6 h at the end of which aliquots were removed from each tube (t = 12 h). In the right panel, FAM-RpaA was mixed with SasA and KaiC-EE. An aliquot was removed immediately after mixing (t = 0 h). After incubating for 6 h at 30 ºC the sample was divided into two separate tubes. One tube received buffer and other tube received 3.5 µM KaiB after which aliquots were immediately taken (t = 6 h). Both samples were further incubated for 6 h at 30 ºC at the end of which aliquots were removed from each tube (t = 12 h). Time points for control reactions containing FAM-RpaA (Control-1), FAM-RpaA + SasA (Control-2) or FAM-RpaA + KaiC-EE + KaiB (Control-3) were also collected. **(B)** Aliquots were loaded onto 12.5% Zn^{2+}-Phos-tag^{TM} SDS-PAGE for separation of RpaA phosphoforms. Coomassie blue-stained gel is in the top panel. Fluorescently labeled RpaA (FAM-RpaA) bands were visualized under UV transillumination (bottom panel). %RpaA~P was determined by densitometry.

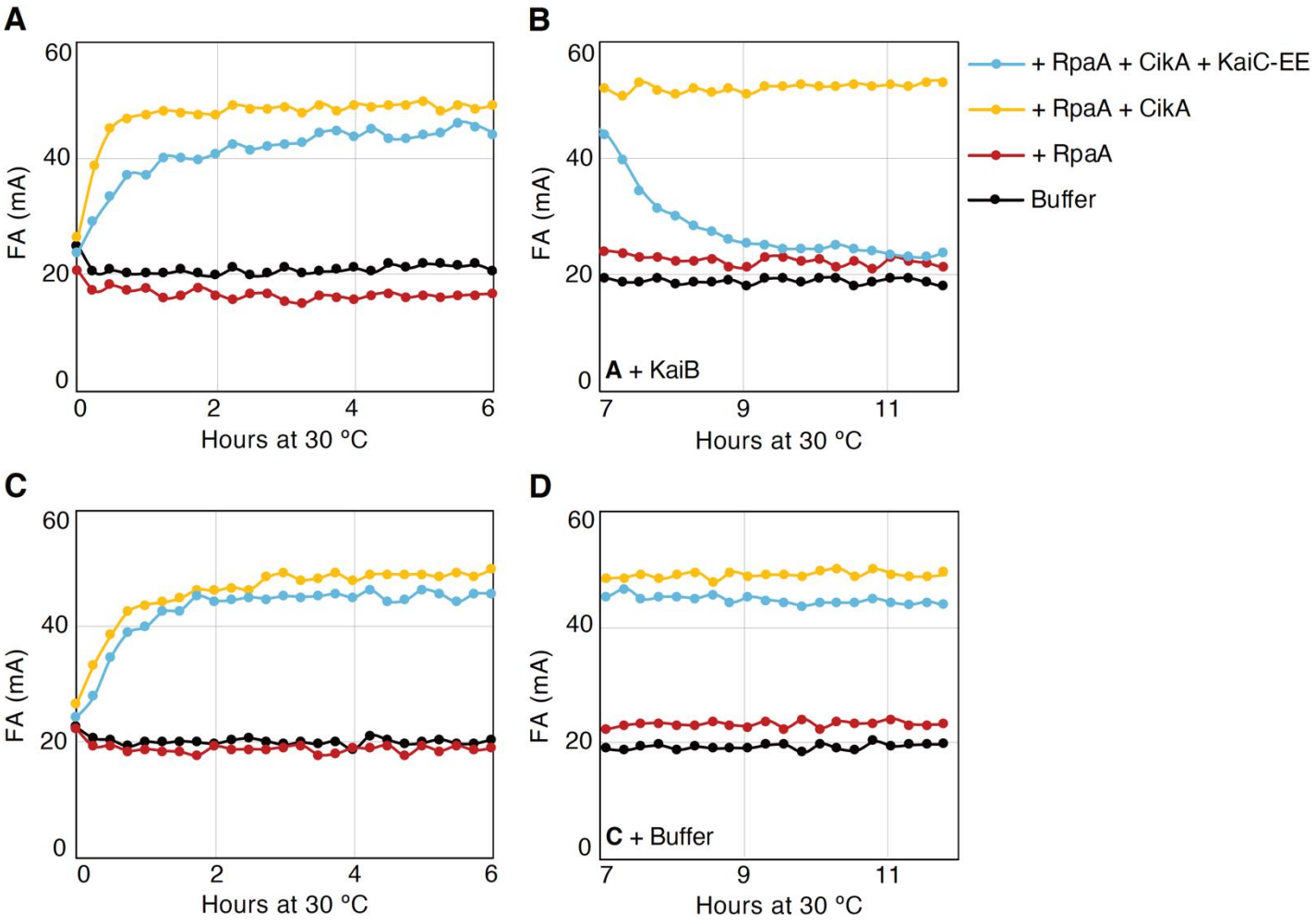

Figure S8. Kinase and phosphatase activity of CikA assessed by DNA binding in vitro. Fluorescence anisotropies of 100 nM Cy3-labeled P*kaiBC* DNA was measured in buffer containing 1 mM ATP and 5 mM $MgCl_2$, pH 8. (**A**) P*kaiBC* alone (black), P*kaiBC* + RpaA (red), P*kaiBC* + RpaA+ CikA (yellow), and P*kaiBC* + RpaA+ CikA + KaiC-EE (light blue). (**B**) KaiB was added to samples in (A). (**C**) Replicate of (A). (**D**) Buffer was added to samples in (C). After addition of KaiB or buffer at t = 6 h, samples were incubated for 1 h before measuring anisotropies for another 5 h. Sample concentrations were 2.5 µM RpaA, 0.65 µM CikA, 3.5 µM KaiB, and 3.5 µM KaiC-EE.

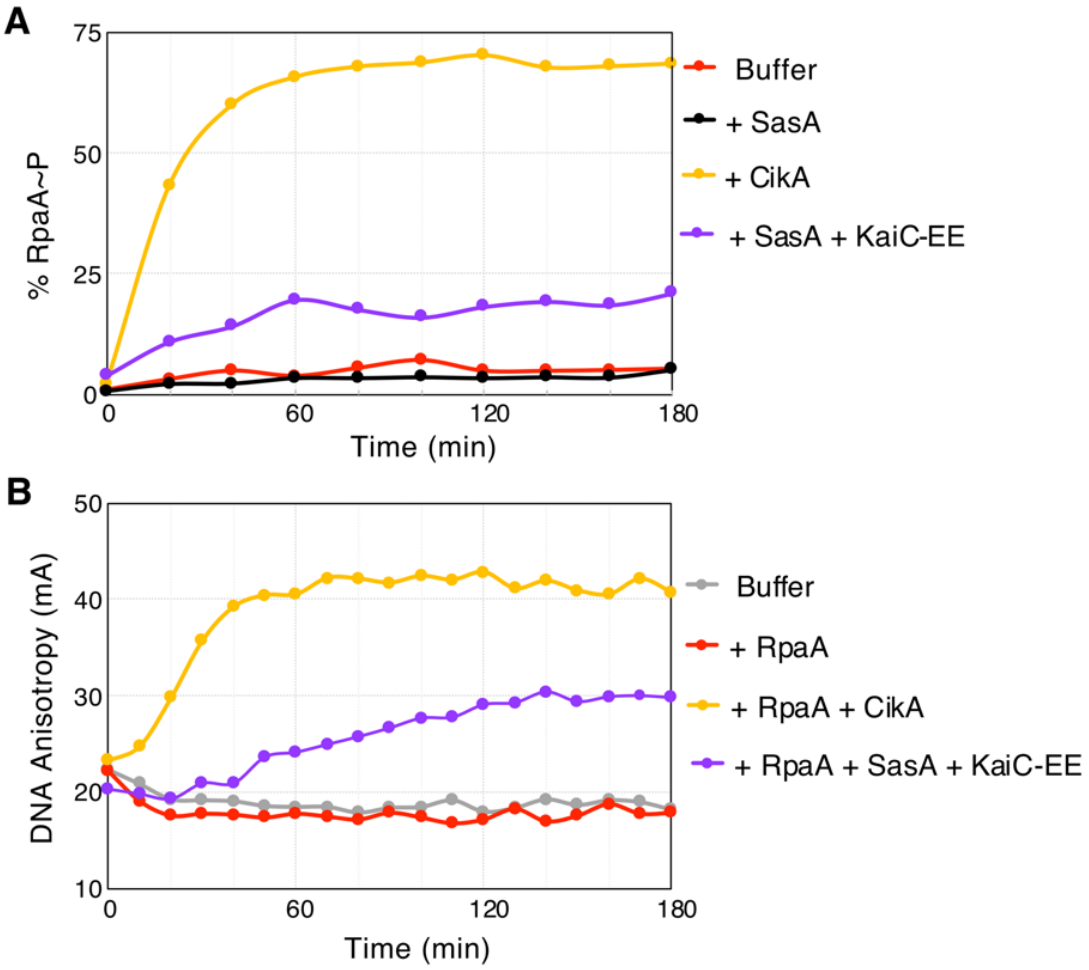

Figure S9. Differential kinetics of SasA and CikA activities produce phase offset in RpaA~P and DNA rhythms.

(**A**) Rates of RpaA phosphorylation measured in just buffer (red) and in the presence of SasA (black), CikA (yellow), and SasA+KaiC-EE (purple). (**B**) Fluorescence anisotropy of Cy3-labeled *PkaiBC* DNA measured in just buffer (grey) and in the presence of RpaA (red), RpaA+CikA (yellow), and RpaA+SasA+KaiC-EE (purple). Concentrations of proteins used are: RpaA: 2.5 μM, CikA: 0.65 μM, SasA: 0.65 μM, KaiC-EE: 3.5 μM and Cy3-*PkaiBC*: 100 nM.

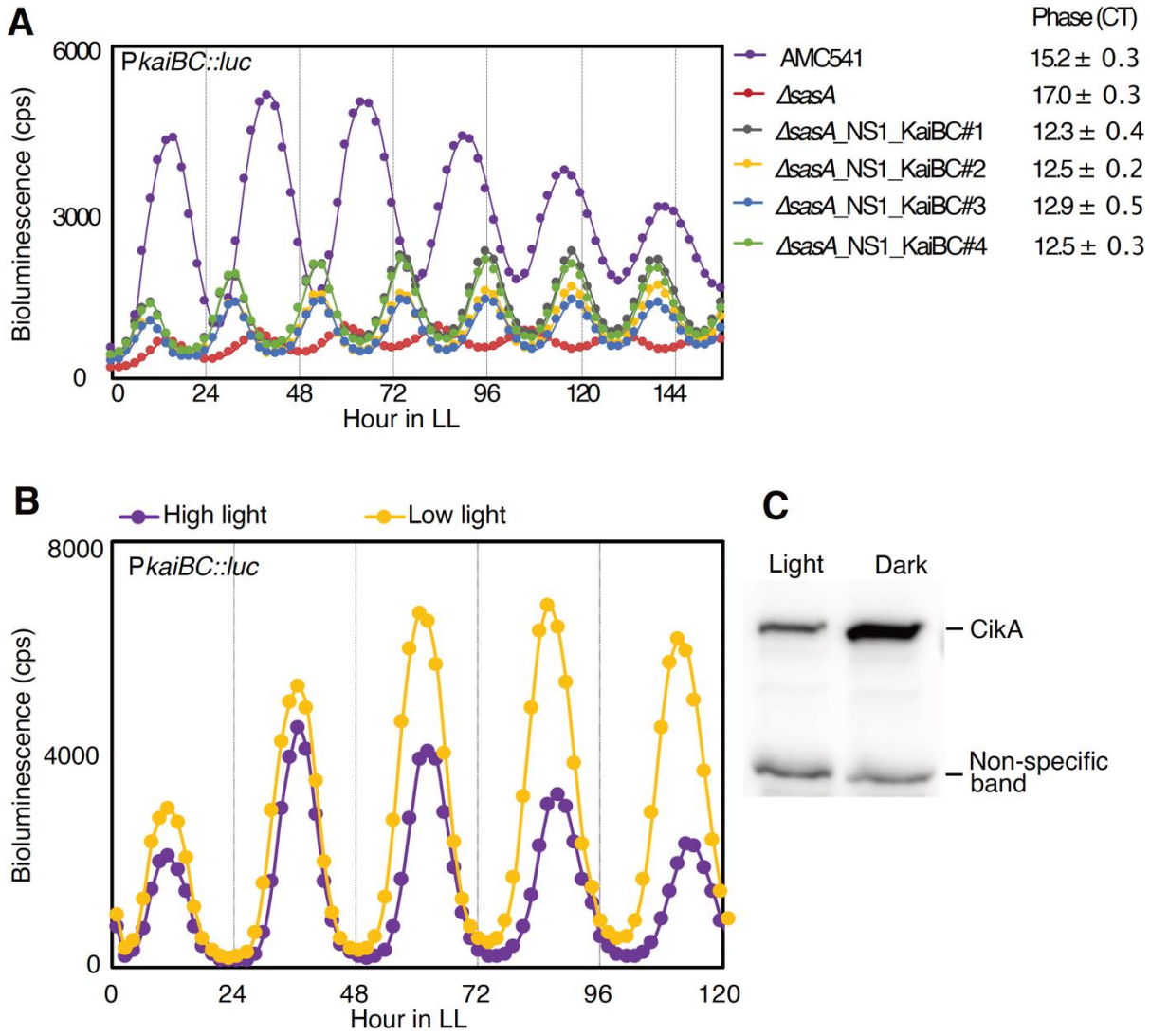

Figure S10. Bioluminescence rhythms of P*kaiBC* in a Δ*sasA* background.

(A) Expression from P*kaiBC* monitored as bioluminescence from a P*kaiBC*::*luc* firefly luciferase reporter. Bioluminescence is nearly arrhythmic in a Δ*sasA* mutant (red) as compared to WT strain (AMC541, purple). When *kaiBC* was driven by an *E. coli* promoter, P*trc* (*20*), in a Δ*sasA* background to restore wild-type levels of KaiBC, rhythms were restored with ~3-h phase advance as compared to WT (traces from 4 replicates shown). **(B)** Rhythms of bioluminescence generated by P*kaiBC::luc* expression were monitored for entrained wild type (AMC541) in high light (purple) or low light (yellow) conditions. **(C)** CikA levels in AMC06 were probed using anti-CikA serum in cells grown in light or dark. Culture from one flask was split and kept under light or dark conditions for 6 h before harvesting. A more detailed analysis on CikA level under light/dark conditions can be found in Ivleva et al. (38).

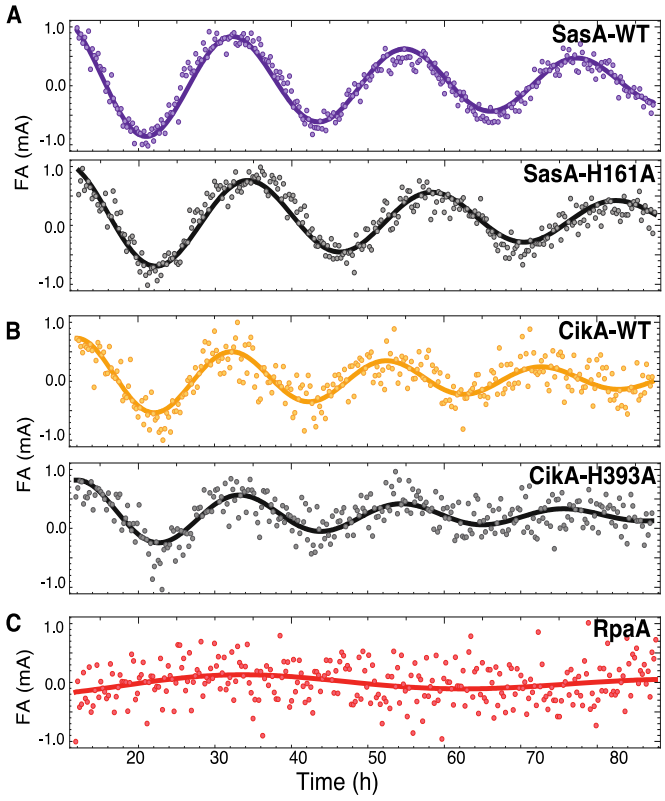

Figure S11: Fluorescence anisotropy rhythms of SasA and CikA kinase dead mutants in an IVC.

(A) Fluorescence anisotropy of SasA-WT (purple) and SasA-H161A (black) probes in an IVC containing KaiA, KaiB, and KaiC and unlabeled WT or mutant SasA. **(B)** Fluorescence anisotropy of CikA-WT (yellow) and CikA-H393A (black) probes in an IVC containing KaiA, KaiB, and KaiC and unlabeled WT or mutant CikA. Rhythmicity in fluorescence anisotropy for both WT and mutants of SasA and CikA suggesting their interaction with the core clock are unaffected by the mutations. RpaA~P and DNA fluorescence anisotropy showed no rhythmicity in IVC containing SasA-H161A or CikA-H393A mutants, suggesting phosphorylation dependent interaction of RpaA and DNA. **(C)** Fluorescence anisotropy of labeled RpaA (red) in core oscillator reaction containing KaiA, KaiB and KaiC, but no SasA or CikA, has no rhythmicity of interaction with core clock proteins.

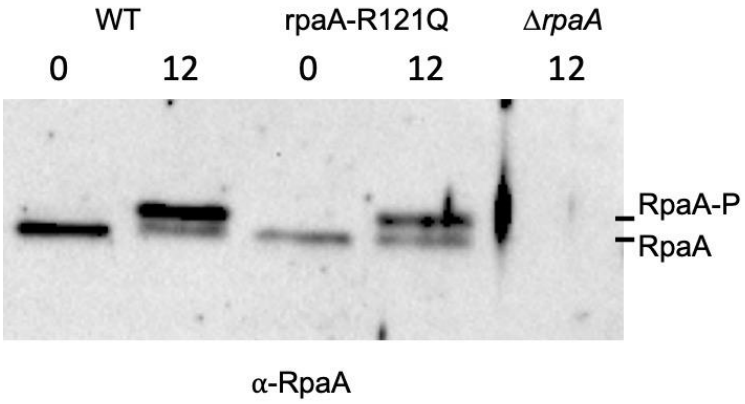

Figure S12. RpaA-R121Q mutant shows WT-like phosphorylation pattern *in vivo.*

Phos-tag™ immunoblots reveal the level of RpaA phosphorylation in entrained wild-type, and *rpaA-R121Q* cells at ZT = 0 (dawn) and ZT = 12 (dusk). A sample from a Δ*rpaA* strain is included as a negative control. Each lane contains 10 µg of total protein.

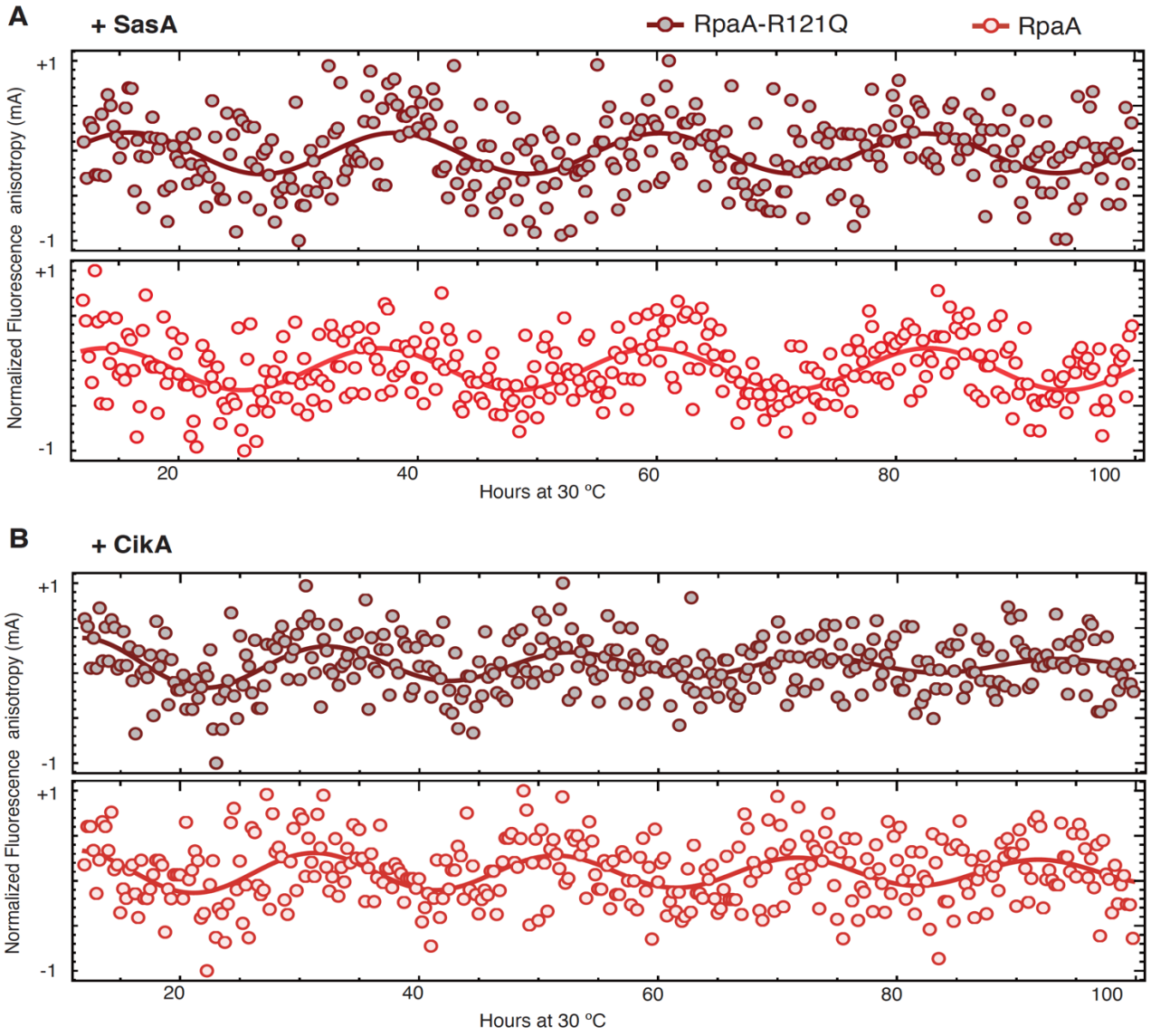

Figure S13. RpaA and RpaA-R121Q fluorescence anisotropy in IVC.
Fluorescence anisotropy rhythms of labeled FAM-RpaA (red) and FAM-RpaA-R121Q (brown), measured in IVC containing KaiA, KaiB, KaiC and 0.65 μM of either (**A**) SasA or (**B**) CikA.

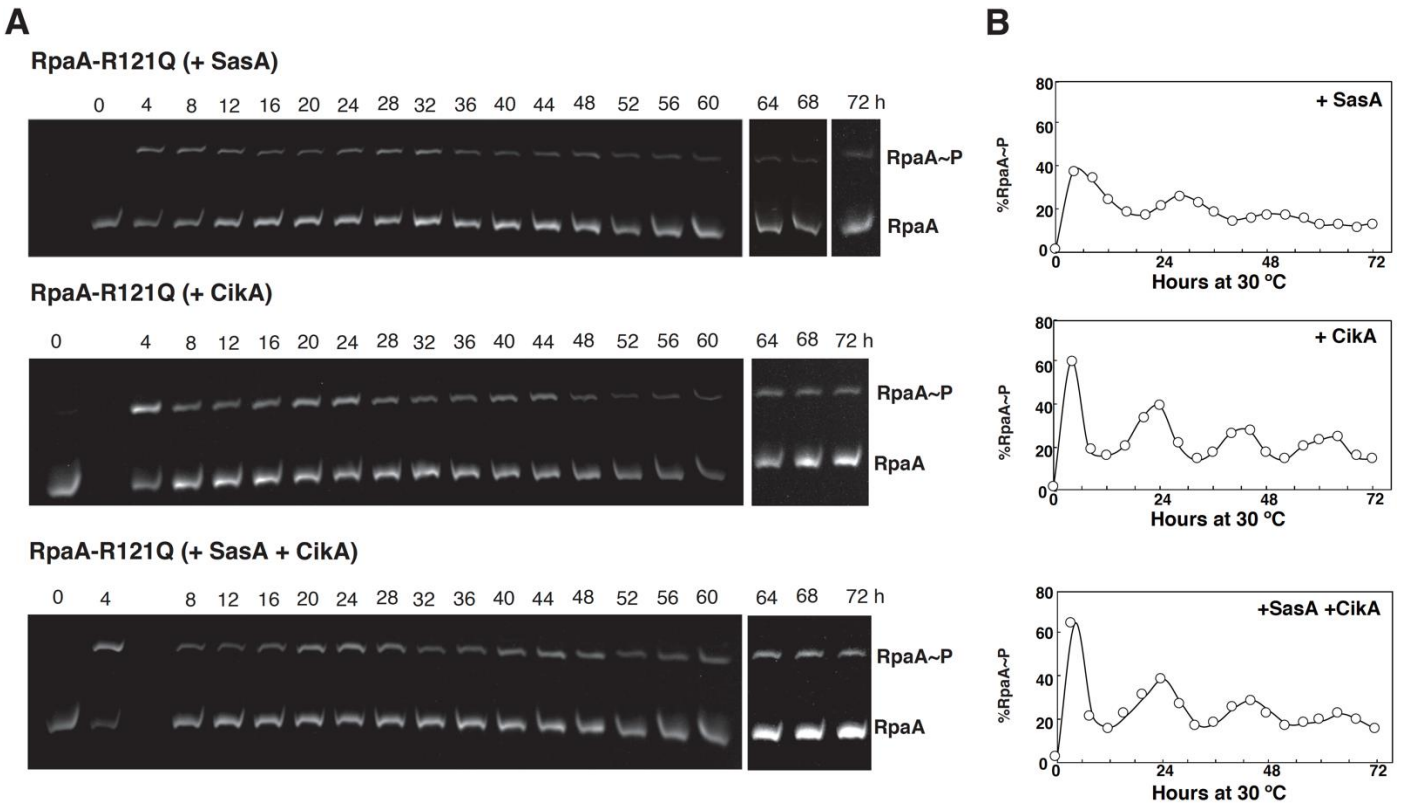

Figure S14. Phos-tagTM SDS-PAGE of RpaA-R121Q phosphorylation in vitro.
(**A**) Aliquots of reconstituted clock reactions containing KaiA, KaiB, KaiC, RpaA-R121Q, DNA, and either SasA (top), CikA (middle), or both (bottom) were sampled every 4 h manually, subjected to 12.5% Zn^{2+} Phos-tag^{TM} SDS-PAGE, and visualized by UV-transillumination (see Materials and Methods for details). (**B**) Densitometry of the gels was performed by ImageJ (NIH) and %RpaA~P = 100% * RpaA~P / (RpaA + RpaA~P) is plotted as function of time.

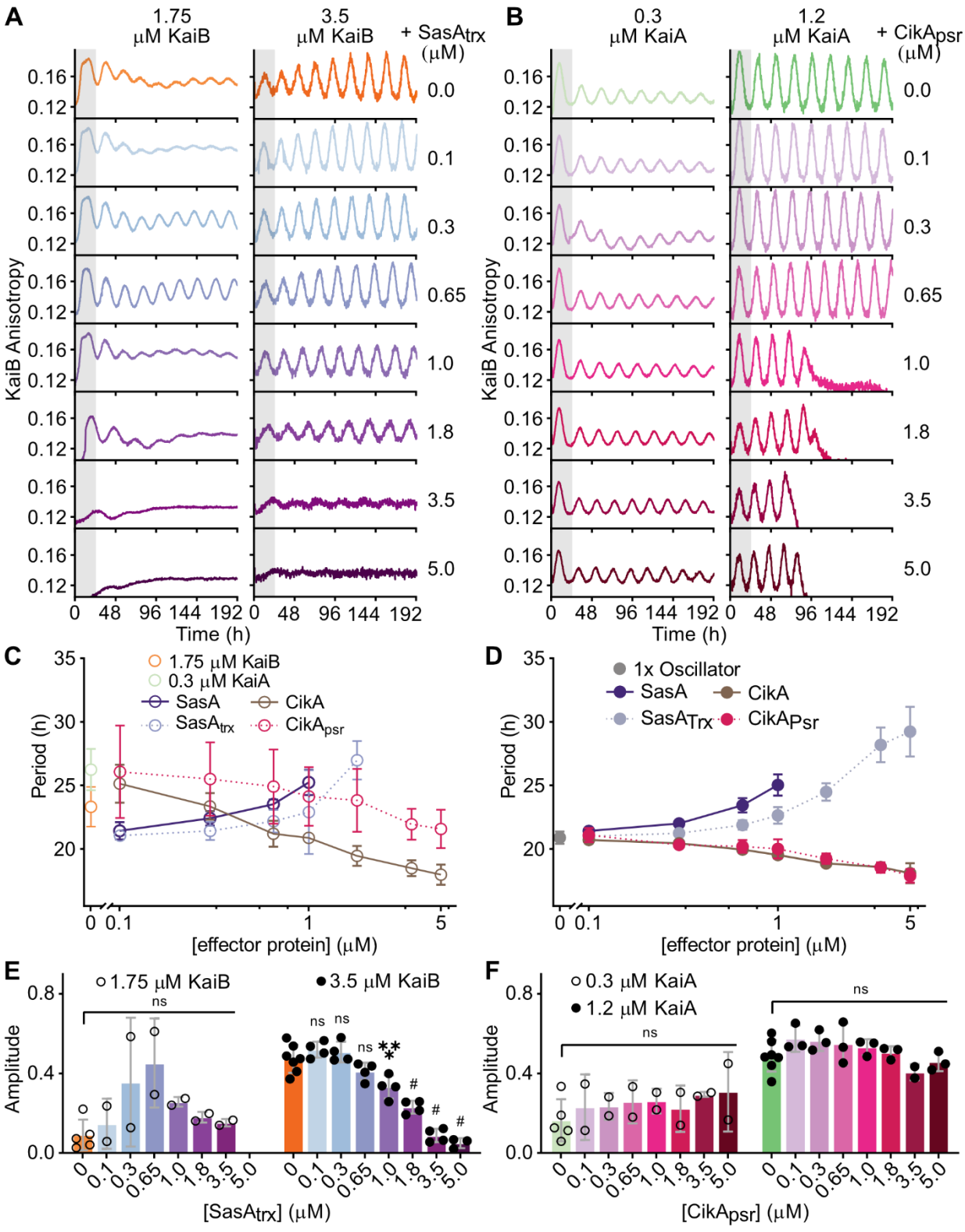
A
1.75 μM KaiB
3.5 μM KaiB
+ SasAtrx (μM)
0.0
0.1
0.3
0.65
1.0
1.8
3.5
5.0
KaiB Anisotropy
Time (h)
B
0.3 μM KaiA
1.2 μM KaiA
+ CikApsr (μM)
C
1.75 μM KaiB
0.3 μM KaiA
SasA
SasAtrx
CikA
CikApsr
Period (h)
[effector protein] (μM)
D
1x Oscillator
SasA
CikA
SasATrx
CikAPsr
E
1.75 μM KaiB
3.5 μM KaiB
Amplitude
[SasAtrx] (μM)
F
0.3 μM KaiA
1.2 μM KaiA
[CikApsr] (μM)
ns

Figure S15. Domain truncation studies on SasA and CikA oscillator effects.
(A-B) Fluorescence assays under conditions of 3.5 μM KaiC, 50 nM fluorescently labeled KaiB as a probe, and either (panel **A**) standard 1.2 μM KaiA with 1.75 μM or 3.5 μM KaiB, or (panel **B**) standard 3.5 μM KaiB with 0.3 μM or 1.2 μM KaiA as indicated with titrations of truncated domain (panel **A**) $SasA_{trx}$ or (panel **B**) $CikA_{psr}$ from 0.1 – 5.0 μM. Representative assay from n ≥ 2 shown; the first 24-h period after release into constant conditions is marked in gray. (**C-D**) Period values for fluorescence assays prepared with deficient (panel **C**) 1.75 μM KaiB and (panel **D**) 0.3 μM KaiA (open circles) or standard oscillator concentrations (panel **C**) 3.5 μM KaiB and (panel **D**) 1.2 μM KaiA (closed circles) in the absence and presence of full-length (solid connecting lines) and truncated additive proteins (dotted connecting lines). Period and amplitude data are representative of one or more independent experiments with duplicate samples, presented as the mean ± SD. (**E-F)** Amplitude for fluorescence assays prepared under different core KaiB and KaiA concentrations of (panel **E**) deficient (open circles) or (panel **F**) standard (closed circles) in the absence or presence of truncated additive proteins. Data are shown as mean ± SD (n ≥ 2 with duplicate samples). Analysis of variance (ANOVA) was used to compare amplitudes of fluorescence anisotropies under the two KaiB and KaiA concentrations in the absence of truncated domains $SasA_{trx}$ and $CikA_{psr}$, respectively, versus the indicated concentrations of those additive proteins: ns, not significant; *, $P < 0.05$; **, $P < 0.01$; ***, $P < 0.001$; #, $P < 0.0001$.

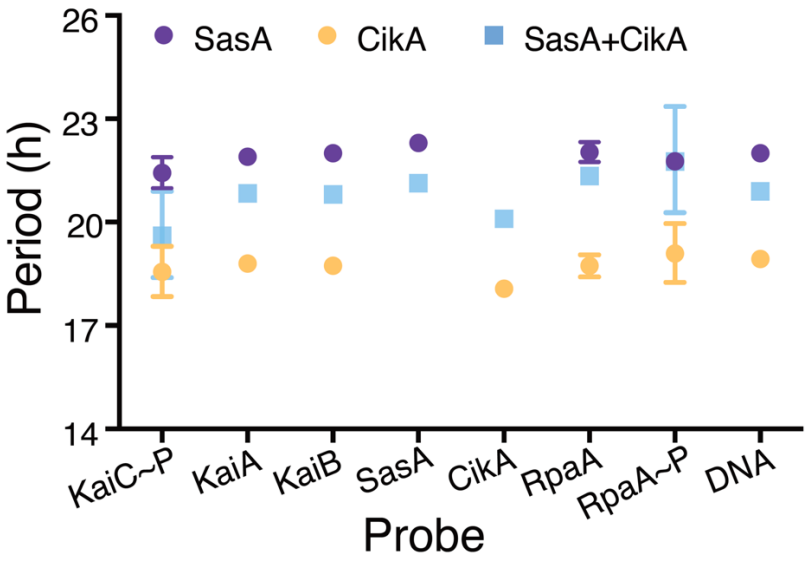

Figure S16. Counterbalancing effect of SasA and CikA on the period of the IVC.
Periods were calculated for each probe in IVC reactions containing SasA (purple), CikA (yellow) or both (blue). Each data point represents the mean from three independent measurements and vertical bars indicate the standard error. The SasA + CikA IVC produced the oscillations with a period of 20.9 ± 0.4 h. The SasA-only IVC showed a slight period lengthening, producing oscillations with a period of 21.9 ± 0.2 h, while the CikA-only IVC had a shorter period of 18.7 ± 0.3 h. These observations indicate that the period of clock is counterbalanced by the signal transduction proteins SasA and CikA.

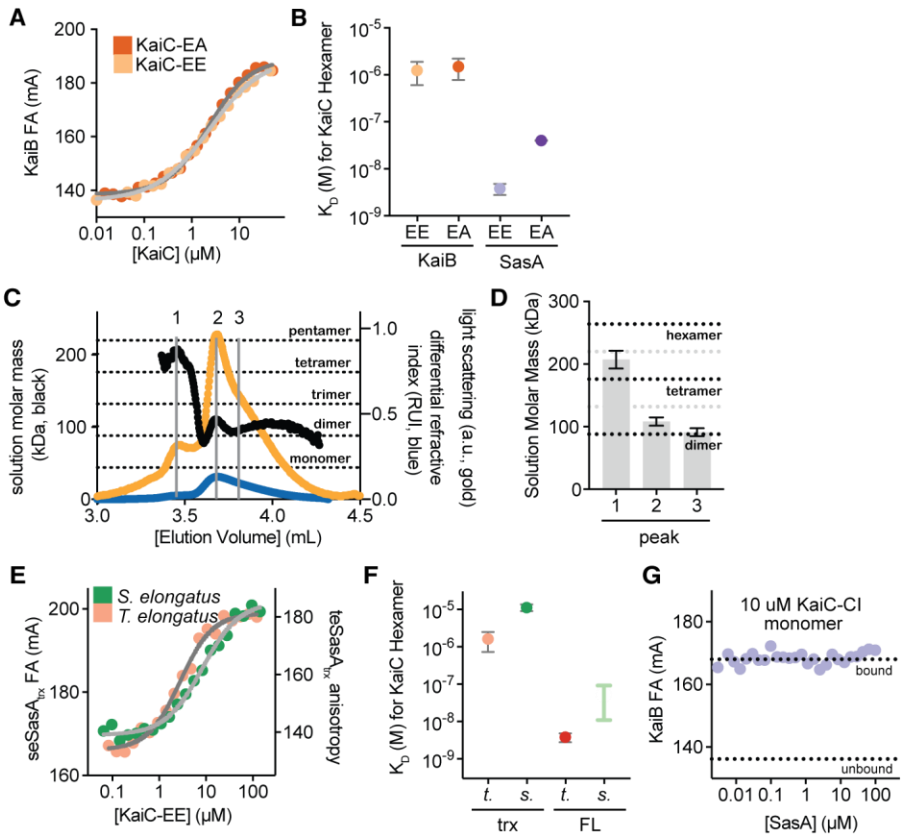

Figure S17. Biochemical properties of the SasA-KaiC interaction.

(A) KaiB binds to KaiC-EE and KaiC-EA with similar affinity. Representative equilibrium binding assays of 50 nM fluorescently labeled KaiB from *S. elongatus* in the presence of increasing concentrations of *S. elongatus* KaiC-EA (dark orange) and KaiC-EE (light orange). Data were fit to a Langmuir binding isotherm (EA, dark gray; EE, light gray). (**B**) SasA binds KaiC more tightly than does KaiB, with a preference for the pS/pT phosphomimetic, KaiC-EE. Calculated equilibrium dissociation constants (K_D) from binding data in panel **A** (mean ± SD, n = 3; light and dark orange) are compared to affinities from Valencia et al. (*50*) (mean ± SD, K_D measured by SPR; light and dark purple) for full-length SasA from *T. elongatus*. (**C**) Full-length SasA exists primarily a dimer in solution. Traces from a representative size-exclusion chromatography coupled to multiangle light scattering (SEC-MALS) run for full-length SasA from *S. elongatus*. Differential refractive index (blue) is depicted with light scattering (gold) and absolute mass estimation (kDa, black line). (**D**) Quantitative mass analysis of peaks indicated at the top of panel **C** (peaks 1-3) analyzed from triplicate SEC-MALS runs are consistent with a dimer-tetramer equilibrium (mean mass in kDa ± SD). Calculated masses for dimer, tetramer and hexamer are represented by black dotted lines. (**E**) The $SasA_{trx}$ domain of *T. elongatus* binds

with higher affinity than the *S. elongatus* $SasA_{trx}$ domain to the respective KaiC-EE variant from each organism. Equilibrium binding assays of fluorescently labeled $SasA_{trx}$ from *S. elongatus* (dark green) or *T.* (pink) *elongatus*. Data were fit as in panel **A**. (**F**) Full-length SasA (FL) binds much more tightly than the isolated $SasA_{trx}$ domain (trx), suggesting that it relies on avidity for efficient binding to KaiC hexamer. Calculated K_D values extracted from data in panel **E** (mean ± SD, n = 3; pink or dark green) are compared to affinities from Valencia et al. (*31*) (mean ± SD, measured by SPR; red) for full-length SasA from *T. elongatus*. The affinity range of *S. elongatus* SasA calculated from the 2D titration data and our thermodynamic model (**Fig. 6**) is represented as a light green bar. (**G**) Full-length SasA does not display avidity and compete KaiB off of the KaiC-C1 monomer. Fluorescently labeled KaiB was bound to 10 μM monomeric KaiC-CI domain and subsequently titrated with full-length SasA as indicated. Anisotropy values for bound and unbound KaiB (dashed lines) were determined from curve fits in **Fig. S17A**.

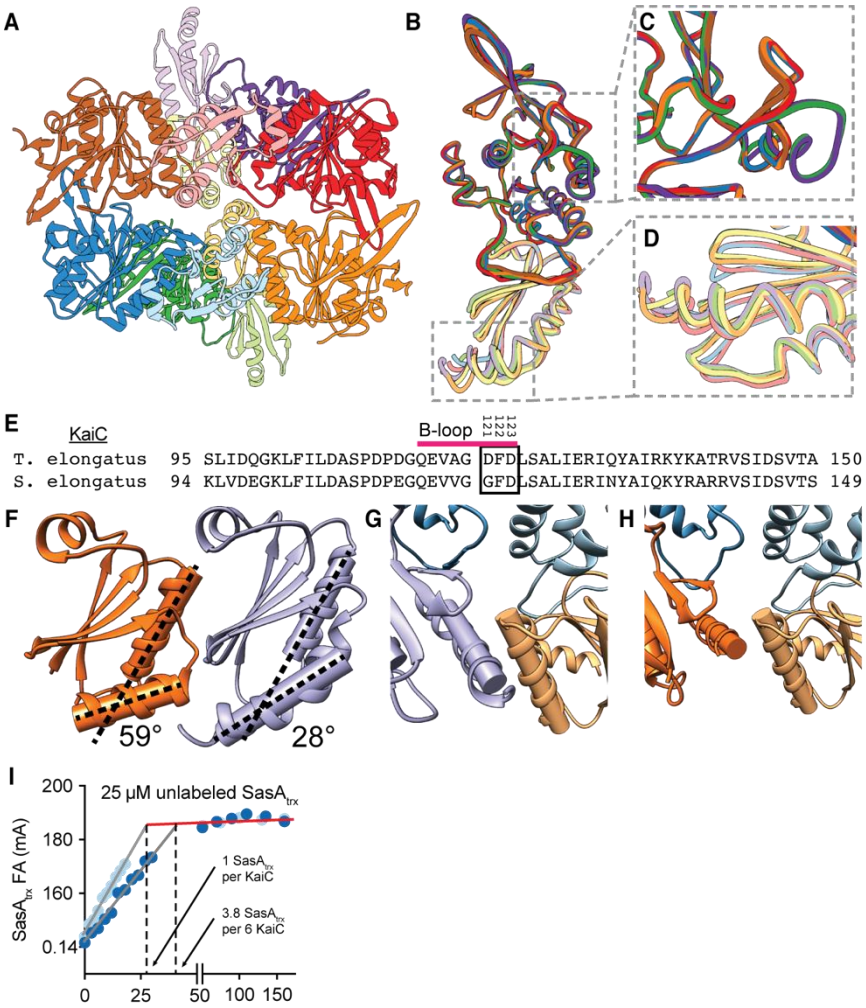

Figure S18. Structural details of the KaiC CI-SasAtrx complex.

(A) Asymmetric unit of the KaiC-C1-SasA$_{trx}$ crystal complex (PDB 6X61). Individual KaiC-CI-SasA$_{trx}$ pairs are depicted with SasA$_{trx}$ subunits in light hues and KaiC-CI subunits in dark hues. (**B-D**) Modest structural heterogeneity was observed between the complexes of the asymmetric unit. Backbone overlays of the 6 KaiC CI-SasA$_{trx}$ complexes from the asymmetric unit. Small differences are highlighted by the orientation of a loop comprising residues R185-V201 on the CI domain (panel **C**) or by the orientation of the α3 helix of SasA$_{trx}$ (panel **D**), with consensus among the complexes of chains CD and KL. (**E**) Sequence alignment of the B-loops (pink) and surrounding sequence from KaiC of *S. elongatus* and *T. elongatus*. Black box, residues at the shared KaiB and SasA-binding interface that were subjected to mutagenesis (**F**) SasA and fsKaiB diverge structurally at the α3 helix. The α1 and α3 helices of fsKaiB (PDB: 5JWO) and SasA$_{trx}$ (PDB: 6X61) are modeled as cylindrical axes with a radius of 1.8 Å, with the inter-axis crossing angle reported. (**G-H**) Orientation of the α3 helix is likely to affect binding of KaiB at

the adjacent KaiC protomer. Helical orientation of the $SasA_{trx}$ (purple, panel **G**) or fsKaiB (orange, panel **H**) domain relative to the α1 helix on the adjacent KaiB molecule at the CW interface (yellow). Helices are represented as in panel **F**. (**I**) Representative saturation binding titrations of the *T. elongatus* KaiC-CI monomer or KaiC-EE hexamer in the presence of 25 μM unlabeled $SasA_{trx}$. Stoichiometry of the saturated KaiC-$SasA_{trx}$ complex was calculated at 3.8 ± 0.3 (mean ± SD, n = 3) molecules of SasA per KaiC hexamer, consistent with measurements from native mass spectrometry (*32*). This calculation was made done by qualitatively separating the data into two linear regions and fitting each to a best fit line to describe the anisotropy after saturation (red line) and initial rate of anisotropy increase as a function of titrant concentration (gray line). The intersections of these lines (shown as dashed lines) represent the amount of KaiC needed to saturate the total SasA or KaiB concentration, which can be divided by the SasA concentration to give the KaiC to SasA ratio of the complex. We then assumed 1:1 binding between SasA and KaiC monomer to correct for errors in protein concentration and converted the ratio observed with hexamer to determine the number of SasA molecules per KaiC hexamer.

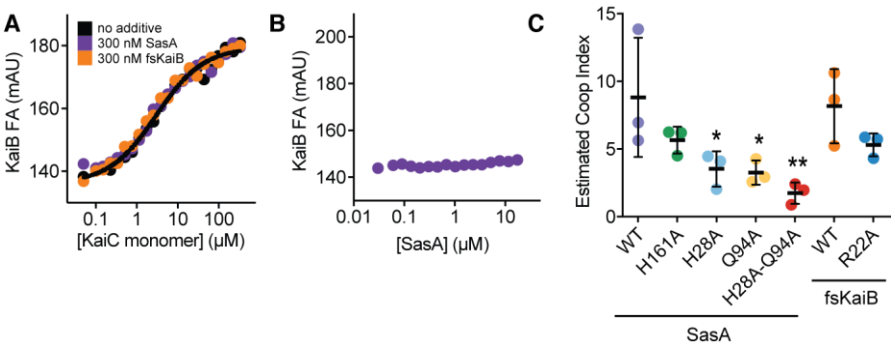

Figure S19. Validation of heterocooperative association model of KaiBC association. **(A)** SasA and fsKaiB additives do not affect binding of 50 nM fluorescently labeled KaiB to KaiC-CI monomer. Equilibrium binding titration of fluorescently labeled KaiB with *S. elongatus* KaiC-CI monomer (black) in the presence of 300 nM fsKaiB (orange) or full-length SasA (purple). (**B**) KaiC is required for KaiB-SasA interactions. Equilibrium titration of fluorescently labeled KaiB with full-length SasA (purple), showing that KaiB anisotropy is unaffected without KaiC present. (**C**) Comparison of estimated cooperativity indices (n = 3, ± SD) of various SasA and fsKaiB variants, as described in the main text (**Figure 7B**).

Figure S20. Multiple sequence alignment of KaiB and SasA$_{trx}$ from S. and T. elongatus. **(A)** Multiple sequence alignment of N-terminal (non-fold-switch) and C-terminal (fold-switch) halves of KaiB (orange box) and the structurally analogous SasA$_{trx}$ (purple box) from *S. elongatus* and *T. elongatus*. Red arrows (β-sheets) and blue lines (α-helices) indicate secondary structure from the KaiB tetramer (PDB: 2QKE), fsKaiB monomer (PDB: 5JWO) and SasA$_{trx}$ from the KaiC-CI-SasA$_{trx}$ structure (PDB: 6X61) reported here. Mutations tested in this study are depicted in bold.

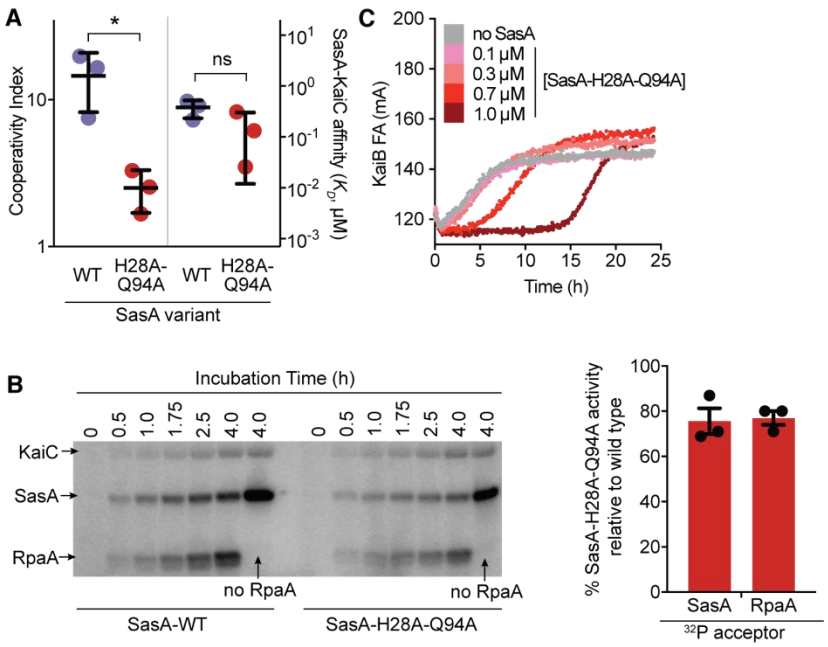

Figure S21. Biochemical characterization of various functions of the SasA-H28A-Q94A double mutant.

(**A**) Cooperativity index and KaiC affinity for wild-type SasA (purple dots) and SasA-H28A-Q94A double mutant (red dots) see Data S7. (**B**) Kinase assays were performed in the presence of γ-32P ATP as originally described in Takai et. al (*19*). These experiments were conducted with 5 μM KaiC-EE, 3.5 μM RpaA, and 2.5 μM SasA variant in 0.1 mM ATP. SasA-WT and SasA-H28A-Q94A were compared, tracking incorporation of ^{32}P into the proteins by SDS-PAGE and quantifying the result densitometrically. Slopes of the densitometry trajectories were compared in triplicate to estimate activity of the double mutant on RpaA as 77 ± 5% (mean ± standard deviation). A no-RpaA control was included to quantify the efficiency of initial histidine phosphorylation in the SasA variants, and triplicate densitometries were compared at a single timepoint, with SasA-H28A-Q94A autophosphorylation 76 ± 10% as efficient as wild-type. (**C**) Representative trajectory of SasA-H28A-Q94A, titrated in the presence of 50 nM labeled KaiB probe as well as 3.5 μM KaiC and 1.2 μM KaiA (as shown for wild type in **Figure 4E)**. SasA-H28A-Q94A were added here at a range of physiological and sub-physiological concentrations showing ~2-5 h delay in KaiB binding in presence of SasA-H28A-Q94A as compared to WT SasA.

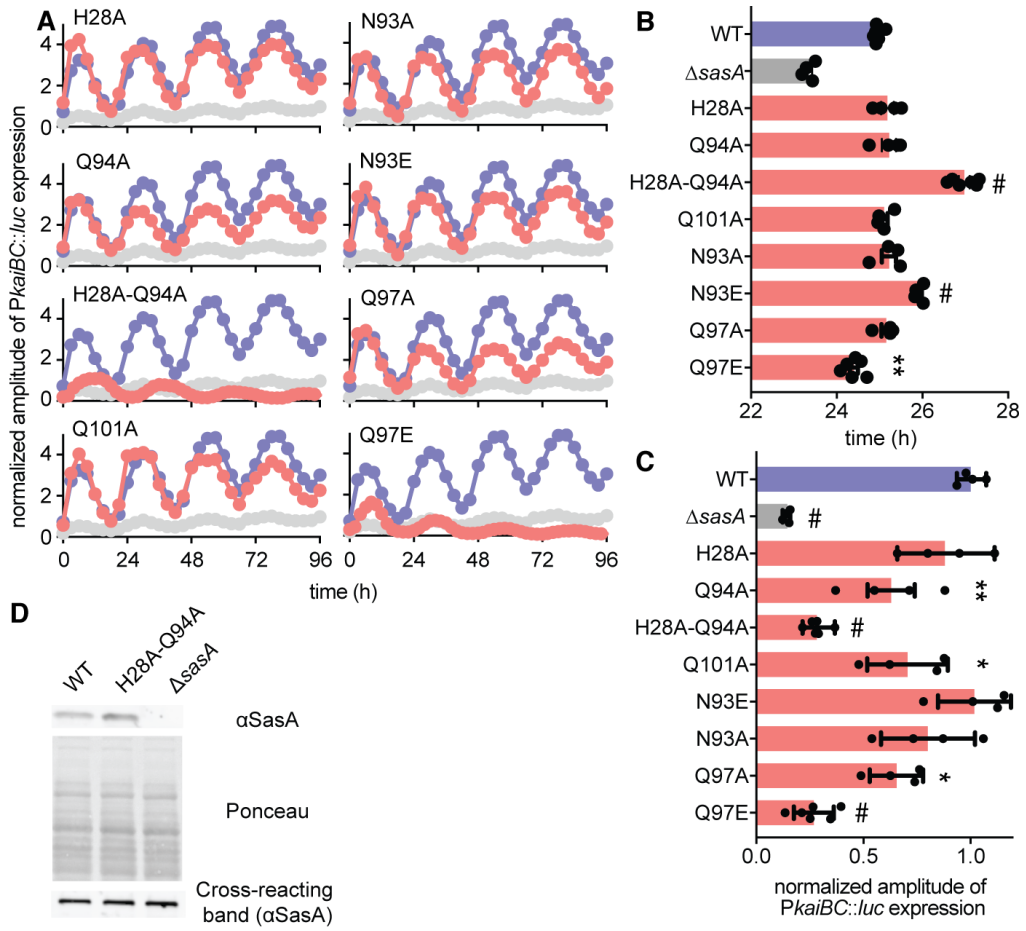

Figure S22. Mutations at the SasA-KaiB cooperativity interface alter circadian rhythms in S. elongatus.

(A) Bioluminescence traces produced by *S. elongatus* strains based on expression of firefly luciferase driven by the clock-controlled *kaiBC* promoter. Wild type (WT) and Δ*sasA* strains are compared to markerless CRISPR/Cas12a-edited *sasA* mutants, with the relevant amino acid substitutions indicated. Graphs display the averages of 6-12 wells, with standard deviation omitted for better visibility of multiple traces. WT (purple) and mutants, colored as in panel **B**. (**B-C**) Analysis of raw bioluminescence data was performed using BioDare2 to calculate the signal amplitude (in arbitrary units, a.u.) (panel **B**) and period length (panel **C**), with the average and standard deviation reported for 6-12 replicates. One-way ANOVA was performed to identify significant changes (*, $P < 0.05$; **, $P < 0.01$; #, $P < 0.0001$) in amplitude and period length relative to wild type. **D)** Western blot showing similar expression levels of SasA at CT 24 in WT

and *sasA*-H28A-Q94A double mutant strains. The cross-reacting band shown at the bottom serves as loading control.

Table S1. Constructs and shorthand names used in this study.

Shorthand name	organism	Protein full name
KaiC	*S. elongatus*	FLAG-seKaiC-1-519
KaiC-AA		FLAG-seKaiC-1-519-S431A-T432A
KaiC-AE		FLAG-seKaiC-1-519-S431A-T432E
KaiC-EE		FLAG-seKaiC-1-519-S431E-T432E
KaiC-EA		FLAG-seKaiC-1-519-S431E-T432A
KaiC-CI monomer		FLAG-seKaiC-16-246-R40A-K172A
KaiC-EE	*T. elongatus*	FLAG-teKaiC-1-518-S431E-T432E
KaiC-EE-D121A		FLAG-teKaiC-1-518-D121A-S431E-T432E
KaiC-EE-F122A		FLAG-teKaiC-1-518-F122A-S431E-T432E
KaiC-EE-D123A		FLAG-teKaiC-1-518-D123A-S431E-T432E
KaiC-CI monomer		FLAG-teKaiC-17-247-R41A-K173A
KaiB	*S. elongatus*	seKaiB-1-102-FLAG
G-KaiB		Gly-seKaiB-1-102-FLAG
KaiB-K25C-6IAF		sekaiB-1-102-K25C-FLAG-6-iodoacetamido-fluorescein
fsKaiB		seKaiB-1-99-Y7A-I87A-Y93A-FLAG
fsKaiB-R22A		seKaiB-1-99-Y7A-R22A-I87A-Y93A-FLAG
KaiA		seKaiA-1-284
G-KaiA		Gly-seKaiA-1-284
SasA		seSasA-1-387
G-SasA		Gly-seSasA-1-387
G-SasA-H161A		Gly-seSasA-1-387-H161A
SasA		seSasA-1-387-FLAG
SasA-H161A		seSasA-1-387-H161A-FLAG
SasA-H28A		seSasA-1-387-H28A-FLAG
SasA-Q94A		seSasA-1-387-Q94A-FLAG
SasA-H28A-Q94A		seSasA-1-387-H28A-Q94A-FLAG
$SasA_{trx}$-Q31C*		FLAG-seSasA-13-103-P13A-FLAG
		FLAG-seSasA-13-103-P13A-Q31C-FLAG
$SasA_{trx}$	*T. elongatus*	FLAG-teSasA-16-107-P16A-FLAG
$SasA_{trx}$-A35C*		FLAG-teSasA-16-107-P16A-A35C-FLAG
CikA	*S. elongatus*	FLAG-seCikA-1-754
CikA-LPTEGG-6IAF		FLAG-seCikA-1-754-LPET-GGGYC*(-6IAF)-N
CikA-H393A		FLAG-seCikA-1-754-H393A
CikA		FLAG-seCikA-1-754
$CikA_{psr}$		seCikA-S605-606-745-C644S-C686S-C742S
$CikA_{psr}$-S727C*		seCikA-S605-606-745-C644S-C686S-C742S-S727C
RpaA		seRpaA-1-249
GGG-RpaA		Gly_3-seRpaA-1-249
RpaA-R121Q		seRpaA-1-249-R121Q
G-RpaA-R121Q		Gly_3-seRpaA-1-249-R121Q

* Single cysteine residue for labeling with 6-iodoacetamido-fluorescein

Table S2. Protein expression and purification conditions

Protein construct	Expression temperature and duration	Ni-NTA Loading buffer	Ni-NTA Wash buffer	Ni-NTA Elution buffer	Gel Filtration Column and Elution Buffer
G-KaiA	30 ºC, 12 h	50 mM NaH_2PO_4, 500 mM NaCl, pH 8	50 mM NaH_2PO_4, 500 mM NaCl, 20 mM imidazole pH 8	50 mM NaH_2PO_4, 500 mM NaCl, 250 mM imidazole pH 8	Superdex-200-1660-pg 20 mM Tris, 150 mM NaCl, 5 mM $MgCl_2$, 1 mM ATP, pH 8
G-KaiB-FLAG	30 ºC, 12 h	50 mM NaH_2PO_4, 500 mM NaCl, pH 8	50 mM NaH_2PO_4, 500 mM NaCl, 20 mM imidazole pH 8	50 mM NaH_2PO_4, 500 mM NaCl, 250 mM imidazole pH 8	Superdex-75-1660-pg 20 mM Tris, 150 mM NaCl, 5 mM $MgCl_2$, 1 mM ATP, pH 8
FLAG-KaiC	30 ºC, 12 h	50 mM NaH_2PO_4, 500 mM NaCl, pH 8	50 mM NaH_2PO_4, 500 mM NaCl, 80 mM imidazole pH 8	50 mM NaH_2PO_4, 500 mM NaCl, 250 mM imidazole pH 8	Superdex-200-1660-pg 20 mM Tris, 150 mM NaCl, 5 mM $MgCl_2$, 1 mM ATP, pH 8
FLAG-KaiC-AA (S431A, T432A)	30 ºC, 12 h	50 mM NaH_2PO_4, 500 mM NaCl, pH 8	50 mM NaH_2PO_4, 500 mM NaCl, 80 mM imidazole pH 8	50 mM NaH_2PO_4, 500 mM NaCl, 250 mM imidazole pH 8	Superdex-200-1660-pg 20 mM Tris, 150 mM NaCl, 5 mM $MgCl_2$, 1 mM ATP, pH 8
FLAG-KaiC-AE (S431A, T432E)	30 ºC, 12 h	50 mM NaH_2PO_4, 500 mM NaCl, pH 8	50 mM NaH_2PO_4, 500 mM NaCl, 80 mM imidazole pH 8	50 mM NaH_2PO_4, 500 mM NaCl, 250 mM imidazole pH 8	Superdex-200-1660-pg 20 mM Tris, 150 mM NaCl, 5 mM $MgCl_2$, 1 mM ATP, pH 8
FLAG-KaiC-EE (S431E, T432E)	30 ºC, 12 h	50 mM NaH_2PO_4, 500 mM NaCl, pH 8	50 mM NaH_2PO_4, 500 mM NaCl, 80 mM imidazole pH 8	50 mM NaH_2PO_4, 500 mM NaCl, 250 mM imidazole pH 8	Superdex-200-1660-pg 20 mM Tris, 150 mM NaCl, 5 mM $MgCl_2$, 1 mM ATP, pH 8
FLAG-KaiC-EA	30 ºC, 12 h	50 mM NaH_2PO_4,	50 mM NaH_2PO_4, 500 mM	50 mM NaH_2PO_4, 500 mM NaCl, 250	Superdex-200-1660-pg

(S431E, T432A)		500 mM NaCl, pH 8	NaCl, 80 mM imidazole pH 8	mM imidazole pH 8	20 mM Tris, 150 mM NaCl, 5 mM $MgCl_2$,1 mM ATP, pH 8
G-SasA	30 ºC, 12 h	50 mM NaH_2PO_4, 500 mM NaCl, pH 8	50 mM NaH_2PO_4, 500 mM NaCl, 20 mM imidazole pH 8	50 mM NaH_2PO_4, 500 mM NaCl, 250 mM imidazole pH 8 + 10 mM TCEP	Superdex-200-1660-pg 20 mM Tris, 150 mM NaCl, 5 mM $MgCl_2$, 1 mM ATP, pH 8
G-SasA-H161A	30 ºC, 12 h	50 mM NaH_2PO_4, 500 mM NaCl, pH 8	50 mM NaH_2PO_4, 500 mM NaCl, 20 mM imidazole pH 8	50 mM NaH_2PO_4, 500 mM NaCl, 250 mM imidazole pH 8 + 10 mM TCEP	Superdex-200-1660-pg 20 mM Tris, 150 mM NaCl, 5 mM $MgCl_2$, 1 mM ATP, pH 8
FLAG-CikA-LPETGG	20 ºC, 22 h	50 mM NaH_2PO_4, 500 mM NaCl, pH 8	50 mM NaH_2PO_4, 500 mM NaCl, 20 mM imidazole pH 8	50 mM NaH_2PO_4, 500 mM NaCl, 250 mM imidazole pH 8 + 20 mM TCEP	Superdex-200-1660-pg 20 mM Tris, 150 mM NaCl, 5 mM $MgCl_2$, pH 8
FLAG-CikA-H393A	20 ºC, 22 h	50 mM NaH_2PO_4, 500 mM NaCl, pH 8	50 mM NaH_2PO_4, 500 mM NaCl, 20 mM imidazole pH 8	50 mM NaH_2PO_4, 500 mM NaCl, 250 mM imidazole pH 8 + 20 mM TCEP	Superdex-200-1660-pg 20 mM Tris, 150 mM NaCl, 5 mM $MgCl_2$, pH 8
GGG-RpaA	30 ºC, 12 h	50 mM NaH_2PO_4, 500 mM NaCl, pH 8	50 mM NaH_2PO_4, 500 mM NaCl, 20 mM imidazole pH 8	50 mM NaH_2PO_4, 500 mM NaCl, 250 mM imidazole pH 8	Superdex-75-1660-pg 20 mM Tris, 150 mM NaCl, 5 mM $MgCl_2$, 1 mM ATP, pH 8
GGG-RpaA-R121Q	30 ºC, 12 h	50 mM NaH_2PO_4, 500 mM NaCl, pH 8	50 mM NaH_2PO_4, 500 mM NaCl, 20 mM imidazole pH 8	50 mM NaH_2PO_4, 500 mM NaCl, 250 mM imidazole pH 8	Superdex-75-1660-pg 20 mM Tris, 150 mM NaCl, 5 mM $MgCl_2$, 1 mM ATP, pH 8

Table S3. Fluorophore labels and target proteins ligated using sortase-A

Target Protein	Label Position	Peptide with Fluorophore	Fluorophore Excitation Max (nm)	Fluorophore Emission Max (nm)
G-KaiA	N-terminal	C(Cy3)-LPETGG	554	568
G-KaiB-FLAG	N-terminal	5-FAM-LPETGG	480	520
G-SasA	N-terminal	5-FAM-LPETGG	480	520
GGG-RpaA	N-terminal	5-FAM-LPETGG	480	520
GGG-RpaA-R121Q	N-terminal	5-FAM-LPETGG	480	520
FLAG-CikA-LPETGG	C-terminal	GGGYC(6-IAF)-N	493	520
Fluorescently labeled synthetic DNA (Integrated DNA Technologies, Inc., Iowa, USA) (/4iCy3/ – internal labeling of DNA backbone with cyanoethyl phosphoramidite chemistry)				
P*kaiBC* 31-bp promoter sequence 5'-CCG/4iCy3/AGC TTA AGA CCT CCT TTA CCT TTT CAG G-3' 3'-GGC TCG AAT TCT GGA GGA AAT GGA AAA GTC C-5'			550	564

Initially, we labeled all the components with FAM. However, KaiA with N-terminal FAM produced noisy FA data. We empirically tested alternate fluorophores such as 6-IAF, Cy3, and Cy5, of which Cy3-labeled KaiA produced high quality FA data. For P*kaiBC* DNA, a FAM label conjugated to the 5'-end resulted in low signal-to-noise FA. In contrast, the Cy3-labeled P*kaiBC* produced high-quality FA data.

Table S4. In vitro clock reaction composition.

Component	Concentration
KaiA	1.20 μM
KaiB-FLAG	3.50 μM
FLAG-KaiC	3.50 μM
SasA	0.65 μM
FLAG-CikA	0.65 μM
RpaA	2.50 μM
P*kaiBC*,31-bp promoter DNA	100 nM

Cellular concentrations of SasA, CikA, and RpaA as determined by semi-quantitative Western blotting were used to optimize concentrations of these proteins for IVC reactions (*21*). Optimal concentrations for the Kai proteins are well established (*82*).

Table S5. Specific reaction conditions with designated protein constructs.

Experiment Type	Protein Construct Shorthand Name / Final Concentration (μM if not indicated)	Experimental Condition
KaiA Titration Fluorescence Assay (Fig. 3A)	1) KaiB-K25C-6IAF / 0.05 2) KaiC / 3.5 3) KaiB / 3.45 4) KaiA / varied (0.3, 0.6, 1.2, 2.4, 3.6, 4.8, and 6.0)	● Volume: 80 μL ● Buffer: 20 mM Tris, 150 mM NaCl, 5 mM $MgCl_2$, 1 mM ATP, 0.5 mM EDTA, pH 8.0 ● Temperature: 30 °C
KaiB Titration Fluorescence Assay (Fig. 3B)	1) KaiB-K25C-6IAF / 0.05 2) KaiC / 3.5 3) KaiB / varied (0.65, 0.825, 1.70, 3.45, 6.95, 10.45, and 17.45) 4) KaiA / 1.2	● Volume: 80 μL ● Buffer: 20 mM Tris, 150 mM NaCl, 5 mM $MgCl_2$, 1 mM ATP, 0.5 mM EDTA, pH 8.0 ● Temperature: 30 °C
SasA Titration Fluorescence Assay under different KaiB concentrations (Fig. 4)	1) KaiB-K25C-6IAF / 0.05 2) KaiC / 3.5 3) KaiB / fixed at 0.825, 1.70, and 3.45 4) KaiA / 1.2 5) SasA / varied (0.0, 0.1, 0.65, 1.0, 1.8, 3.5, and 5.0)	● Volume: 80 μL ● Buffer: 20 mM Tris, 150 mM NaCl, 5 mM $MgCl_2$, 1 mM ATP, 0.5 mM EDTA, pH 8.0 ● Temperature: 30 °C
CikA Titration Fluorescence Assay under different KaiA concentrations (Fig. 4)	1) KaiB-K25C-6IAF / 0.05 2) KaiC / 3.5 3) KaiB / 3.45 4) KaiA / fixed at 0.3 and 1.2 5) CikA / varied (0.0, 0.1, 0.65, 1.0, 1.8, 3.5, and 5.0)	● Volume: 80 μL ● Buffer: 20 mM Tris, 150 mM NaCl, 5 mM $MgCl_2$, 1 mM ATP, 0.5 mM EDTA, pH 8.0 ● Temperature: 30 °C
$SasA_{trx}$ Titration Fluorescence Assay under different KaiB concentrations (S15A)	1) KaiB-K25C-6IAF / 0.05 2) KaiC / 3.5 3) KaiB / fixed at 1.70 and 3.45 4) KaiA / 1.2 5) $SasA_{trx}$ / varied (0.0, 0.1, 0.65, 1.0, 1.8, 3.5, and 5.0)	● Volume: 80 μL ● Buffer: 20 mM Tris, 150 mM NaCl, 5 mM $MgCl_2$, 1 mM ATP, 0.5 mM EDTA, pH 8.0 ● Temperature: 30 °C
$CikA_{psr}$ Titration Fluorescence Assay under different KaiA concentrations (S15B)	1) KaiB-K25C-6IAF / 0.05 2) KaiC / 3.5 3) KaiB / 3.45 4) KaiA / fixed at 0.3 and 1.2 5) $CikA_{psr}$ / varied (0.0, 0.1, 0.65, 1.0, 1.8, 3.5, and 5.0)	● Volume: 80 μL ● Buffer: 20 mM Tris, 150 mM NaCl, 5 mM $MgCl_2$, 1 mM ATP, 0.5 mM EDTA, pH 8.0 ● Temperature: 30 °C

Table S6. Refinement statistics for structure determination of KaiC-CI-SasAtrx complex.

Data collection	
Space group	$P2_1$
Cell dimensions	
a, *b*, *c* (Å)	107.6, 121.58, 133.59
α, β, γ (º)	90.0, 108.78, 90.0
Resolution (Å)	49.05-3.2 (3.30-3.20) *
No. of total reflections	153257 (13790)
No. Unique Reflections	53267 (4637)
R_{merge}	16.5 (75.7)
R_{pim}	13.0 (57.5)
I/σI	5.5 (1.5)
Completeness (%)	98.8 (99.3)
$CC_{1/2}$	0.95 (0.58)
Wilson B-factor	58.3
Redundancy	2.9 (3.0)
Refinement	
Resolution (Å)	3.20
R_{work}/ R_{free}	22.2/26.6
No. atoms	
Protein	15469
Ligand/ion	30
B-factors	
Protein	61.3
Ligand/ion	46.1
R.m.s deviations	
Bond lengths (Å)	0.003
Bond angles (º)	0.78
Residues in favored regions (%)	93.1
Residues in outlier regions (%)	0.6

*Highest resolution shell is shown in parenthesis.
One crystal was used for data collection.
Data were collected at a wavelength of 1.0 Å.

Table S7. Period analysis, ordinary one-way ANOVA for fluorescence assays comparing different oscillator conditions.

Protein-concentration (μM) comparison with / altered protein-concentration	Mean Diff.	95.00% CI of diff.	Significant ?	Summary	Adjusted *P* Value
KaiB-3.5 / KaiB-1.75	-1.666	-3.238 to -0.09300	Yes	*	0.0354
KaiB-3.5 / KaiB-7.0	0.5423	-1.394 to 2.479	No	ns	0.8847
KaiB-3.5 / KaiB-10.5	0.5118	-1.561 to 2.584	No	ns	0.922
KaiB-3.5 / KaiB-17.5	1.244	-0.6920 to 3.181	No	ns	0.3047
SasA-0.0 / SasA-0.1	-0.498	-1.678 to 0.6824	No	ns	0.622
SasA-0.0 / SasA-0.3	-1.086	-2.266 to 0.09437	No	ns	0.0758
SasA-0.0 / SasA-0.65	-2.52	-3.700 to -1.340	Yes	***	0.0001
SasA-0.0 / SasA-1.0	-4.118	-5.298 to -2.938	Yes	#	<0.0001
SasA-0.0 / SasA-1.8	-12.76	-14.49 to -11.03	Yes	#	<0.0001
KaiB-1.75, SasA-0.0 / SasA-0.1	1.953	0.5292 to 3.377	Yes	**	0.0048
KaiB-1.75, SasA-0.0 / SasA-0.3	0.9688	-0.5609 to 2.498	No	ns	0.3415
KaiB-1.75, SasA-0.0 / SasA-0.65	-0.1362	-1.666 to 1.393	No	ns	0.9997
KaiB-1.75, SasA-0.0 / SasA-1.0	-1.861	-3.285 to -0.4367	Yes	**	0.0074
KaiB-1.75, SasA-0.0 / SasA-1.8	-8.009	-10.66 to -5.359	Yes	#	<0.0001
$SasA_{trx}$-0.0 / $SasA_{trx}$-0.1	-0.1257	-1.638 to 1.387	No	ns	0.9997
$SasA_{trx}$-0.0 / $SasA_{trx}$-0.3	-0.3682	-1.881 to 1.144	No	ns	0.9812
$SasA_{trx}$-0.0 / $SasA_{trx}$-0.65	-1.008	-2.521 to 0.5041	No	ns	0.3257
$SasA_{trx}$-0.0 / $SasA_{trx}$-1.0	-1.771	-3.283 to -0.2584	Yes	*	0.016
$SasA_{trx}$-0.0 / $SasA_{trx}$-1.8	-3.611	-5.123 to -2.098	Yes	#	<0.0001
$SasA_{trx}$-0.0 / $SasA_{trx}$-3.5	-7.318	-8.831 to -5.806	Yes	#	<0.0001
$SasA_{trx}$-0.0 / $SasA_{trx}$-5.0	-8.366	-10.03 to -6.701	Yes	#	<0.0001
KaiA-1.2 / KaiA-0.3	-5.433	-6.896 to -3.969	Yes	#	<0.0001
KaiA-1.2 / KaiA-0.6	-1.293	-2.833 to 0.2473	No	ns	0.1285
KaiA-1.2 / KaiA-2.4	0.5891	-0.9510 to 2.129	No	ns	0.8174
KaiA-1.2 / KaiA-3.6	0.9321	-0.7165 to 2.581	No	ns	0.4766
KaiA-1.2 / KaiA-4.8	-1.593	-3.702 to 0.5161	No	ns	0.2017
KaiA-1.2 / KaiA-6.0	-4.173	-6.985 to -1.361	Yes	**	0.002
CikA-0.0 / CikA-0.1	-0.04685	-0.1630 to 0.06934	No	ns	0.811
CikA-0.0 / CikA-0.3	-0.03718	-0.1534 to 0.07901	No	ns	0.9261
CikA-0.0 / CikA-0.65	-0.00668	-0.1229 to 0.1095	No	ns	0.9998
CikA-0.0 / CikA-1.0	0.04403	-0.07215 to 0.1602	No	ns	0.85
CikA-0.0 / CikA-1.8	0.1113	-0.004878 to 0.2275	No	ns	0.0654
CikA-0.0 / CikA-3.5	0.1006	-0.01555 to 0.2168	No	ns	0.1145
CikA-0.0 / CikA-5.0	0.1906	0.07439 to 0.3068	Yes	***	0.0004
KaiA-0.3, CikA-0.0 / CikA-0.1	0.75	-2.315 to 3.815	No	ns	0.9499
KaiA-0.3, CikA-0.0 / CikA-0.3	2.545	-0.5204 to 5.610	No	ns	0.1201
KaiA-0.3, CikA-0.0 / CikA-0.65	4.693	1.895 to 7.492	Yes	**	0.0014
KaiA-0.3, CikA-0.0 / CikA-1.0	5.02	2.222 to 7.818	Yes	***	0.0007

KaiA-0.3, CikA-0.0 / CikA-1.8	6.44	3.642 to 9.238	Yes	#	<0.0001
KaiA-0.3, CikA-0.0 / CikA-3.5	7.407	4.608 to 10.21	Yes	#	<0.0001
KaiA-0.3, CikA-0.0 / CikA-5.0	7.923	5.125 to 10.72	Yes	#	<0.0001
$CikA_{psr}$-0.0 / $CikA_{psr}$-0.1	3.01	2.132 to 3.889	Yes	#	<0.0001
$CikA_{psr}$-0.0 / $CikA_{psr}$-0.3	2.361	1.386 to 3.336	Yes	#	<0.0001
$CikA_{psr}$-0.0 / $CikA_{psr}$-0.65	1.658	0.7792 to 2.536	Yes	#	<0.0001
$CikA_{psr}$-0.0 / $CikA_{psr}$-1.0	0.8853	0.006697 to 1.764	Yes	*	0.0476
$CikA_{psr}$-0.0 / $CikA_{psr}$-1.8	0.6953	-0.1833 to 1.574	No	ns	0.1771
$CikA_{psr}$-0.0 / $CikA_{psr}$-3.5	0.5711	-0.4036 to 1.546	No	ns	0.4758
$CikA_{psr}$-0.0 / $CikA_{psr}$-5.0	-0.1997	-1.078 to 0.6789	No	ns	0.9893
KaiB-1.75, $SasA_{trx}$-0.0 / $SasA_{trx}$-0.1	2.256	-1.984 to 6.496	No	ns	0.4607
KaiB-1.75, $SasA_{trx}$-0.0 / $SasA_{trx}$-0.3	1.906	-2.334 to 6.146	No	ns	0.6179
KaiB-1.75, $SasA_{trx}$-0.0 / $SasA_{trx}$-0.65	1.131	-3.109 to 5.371	No	ns	0.9285
KaiB-1.75, $SasA_{trx}$-0.0 / $SasA_{trx}$-1.0	0.416	-3.824 to 4.656	No	ns	0.9996
KaiB-1.75, $SasA_{trx}$-0.0 / $SasA_{trx}$-1.8	-3.684	-7.924 to 0.5561	No	ns	0.0974
KaiB-1.75, $SasA_{trx}$-0.0 / $SasA_{trx}$-3.5	-11.24	-15.48 to -6.999	Yes	#	<0.0001
KaiA-0.3, $CikA_{psr}$-0.0 / $CikA_{psr}$-0.1	-0.065	-6.407 to 6.277	No	ns	>0.9999
KaiA-0.3, $CikA_{psr}$-0.0 / $CikA_{psr}$-0.3	0.505	-5.837 to 6.847	No	ns	0.9997
KaiA-0.3, $CikA_{psr}$-0.0 / $CikA_{psr}$-0.65	1.13	-5.212 to 7.472	No	ns	0.9937
KaiA-0.3, $CikA_{psr}$-0.0 / $CikA_{psr}$-1.0	1.905	-4.437 to 8.247	No	ns	0.9136
KaiA-0.3, $CikA_{psr}$-0.0 / $CikA_{psr}$-1.8	2.21	-4.132 to 8.552	No	ns	0.845
KaiA-0.3, $CikA_{psr}$-0.0 / $CikA_{psr}$-3.5	4.11	-2.232 to 10.45	No	ns	0.3006
KaiA-0.3, $CikA_{psr}$-0.0 / $CikA_{psr}$-5.0	4.47	-1.872 to 10.81	No	ns	0.2302

Ordinary one-way ANOVA performed with Dunnett's multiple comparisons test was used to compare period values under specified conditions: ns, not significant; *, $P < 0.05$; **, $P < 0.01$; ***, $P < 0.001$; #, $P < 0.0001$. If not specified, fluorescence assays were run with 1.2 μM KaiA, 3.45 μM KaiB, 3.5 μM KaiC, and 0.05 μM fluorescently labeled KaiB probe.

Table S8. Amplitude analysis, ordinary one-way ANOVA for fluorescence assays comparing different oscillator conditions.

Protein-concentration (μM) comparison with / altered protein-concentration	Mean Diff.	95.00% CI of diff.	Significant?	Summary	Adjusted *P* Value
KaiB-3.5 / KaiB-1.75	0.08743	-0.02121 to 0.1961	No	ns	0.1437
KaiB-3.5 / KaiB-7.0	0.04213	-0.07417 to 0.1584	No	ns	0.7636
KaiB-3.5 / KaiB-10.5	0.04656	-0.06209 to 0.1552	No	ns	0.6484
KaiB-3.5 / KaiB-17.5	0.434	0.3457 to 0.5222	Yes	#	<0.0001
SasA-0.0 / SasA-0.1	-0.03844	-0.1930 to 0.1162	No	ns	0.9098
SasA-0.0 / SasA-0.3	0.02229	-0.1323 to 0.1769	No	ns	0.989
SasA-0.0 / SasA-0.65	0.1149	-0.03974 to 0.2694	No	ns	0.1799
SasA-0.0 / SasA-1.0	0.2204	0.06584 to 0.3750	Yes	**	0.0047
SasA-0.0 / SasA-1.8	0.4423	0.2160 to 0.6686	Yes	***	0.0003
KaiB-1.75, SasA-0.0 / SasA-0.1	-0.4206	-0.6723 to -0.1688	Yes	***	0.0007
KaiB-1.75, SasA-0.0 / SasA-0.3	-0.5336	-0.8040 to -0.2632	Yes	#	<0.0001
KaiB-1.75, SasA-0.0 / SasA-0.65	-0.524	-0.7944 to -0.2535	Yes	***	0.0001
KaiB-1.75, SasA-0.0 / SasA-1.0	-0.3502	-0.6019 to -0.09843	Yes	**	0.0043
KaiB-1.75, SasA-0.0 / SasA-1.8	0.007592	-0.4608 to 0.4759	No	ns	>0.9999
$SasA_{trx}$-0.0 / $SasA_{trx}$-0.1	-0.04557	-0.1360 to 0.04490	No	ns	0.6219
$SasA_{trx}$-0.0 / $SasA_{trx}$-0.3	-0.03403	-0.1245 to 0.05644	No	ns	0.8555
$SasA_{trx}$-0.0 / $SasA_{trx}$-0.65	0.06425	-0.02622 to 0.1547	No	ns	0.2642
$SasA_{trx}$-0.0 / $SasA_{trx}$-1.0	0.1418	0.05135 to 0.2323	Yes	***	0.0009
$SasA_{trx}$-0.0 / $SasA_{trx}$-1.8	0.2437	0.1532 to 0.3341	Yes	#	<0.0001
$SasA_{trx}$-0.0 / $SasA_{trx}$-3.5	0.3859	0.2954 to 0.4763	Yes	#	<0.0001
$SasA_{trx}$-0.0 / $SasA_{trx}$-5.0	0.4243	0.3247 to 0.5239	Yes	#	<0.0001
KaiA-1.2 / KaiA-0.3	0.3983	0.1870 to 0.6096	Yes	***	0.0001
KaiA-1.2 / KaiA-0.6	0.1897	-0.02157 to 0.4010	No	ns	0.0919
KaiA-1.2 / KaiA-2.4	0.12	-0.09133 to 0.3313	No	ns	0.4707
KaiA-1.2 / KaiA-3.6	0.2376	0.01147 to 0.4638	Yes	*	0.0365
KaiA-1.2 / KaiA-4.8	0.4218	0.1324 to 0.7111	Yes	**	0.0025
KaiA-1.2 / KaiA-6.0	0.4745	0.08869 to 0.8602	Yes	*	0.0115
CikA-0.0 / CikA-0.1	-0.04685	-0.1630 to 0.06934	No	ns	0.811
CikA-0.0 / CikA-0.3	-0.03718	-0.1534 to 0.07901	No	ns	0.9261
CikA-0.0 / CikA-0.65	-0.00668	-0.1229 to 0.1095	No	ns	0.9998
CikA-0.0 / CikA-1.0	0.04403	-0.07215 to 0.1602	No	ns	0.85
CikA-0.0 / CikA-1.8	0.1113	-0.004878 to 0.2275	No	ns	0.0654
CikA-0.0 / CikA-3.5	0.1006	-0.01555 to 0.2168	No	ns	0.1145
CikA-0.0 / CikA-5.0	0.1906	0.07439 to 0.3068	Yes	***	0.0004
KaiA-0.3, CikA-0.0 / CikA-0.1	-0.09828	-0.3229 to 0.1263	No	ns	0.7137
KaiA-0.3, CikA-0.0 / CikA-0.3	-0.1326	-0.3571 to 0.09201	No	ns	0.4194
KaiA-0.3, CikA-0.0 / CikA-0.65	-0.05589	-0.2519 to 0.1401	No	ns	0.9446

KaiA-0.3, CikA-0.0 / CikA-1.0	-0.1135	-0.3095 to 0.08252	No	ns	0.4393
KaiA-0.3, CikA-0.0 / CikA-1.8	-0.1124	-0.3085 to 0.08358	No	ns	0.449
KaiA-0.3, CikA-0.0 / CikA-3.5	-0.1599	-0.3560 to 0.03607	No	ns	0.1412
KaiA-0.3, CikA-0.0 / CikA-5.0	-0.1116	-0.3076 to 0.08441	No	ns	0.4568
$CikA_{psr}$-0.0 / $CikA_{psr}$-0.1	0.01182	-0.2952 to 0.3189	No	ns	0.9999
$CikA_{psr}$-0.0 / $CikA_{psr}$-0.3	-0.0595	-0.3976 to 0.2786	No	ns	0.9971
$CikA_{psr}$-0.0 / $CikA_{psr}$-0.65	0.02002	-0.2870 to 0.3271	No	ns	0.9997
$CikA_{psr}$-0.0 / $CikA_{psr}$-1.0	0.06736	-0.2397 to 0.3744	No	ns	0.9899
$CikA_{psr}$-0.0 / $CikA_{psr}$-1.8	0.08699	-0.2201 to 0.3941	No	ns	0.9588
$CikA_{psr}$-0.0 / $CikA_{psr}$-3.5	0.196	-0.1420 to 0.5341	No	ns	0.4727
$CikA_{psr}$-0.0 / $CikA_{psr}$-5.0	0.1054	-0.2016 to 0.4125	No	ns	0.9001
KaiB-1.75, $SasA_{trx}$-0.0 / $SasA_{trx}$-0.1	-0.05691	-0.4526 to 0.3388	No	ns	0.9957
KaiB-1.75, $SasA_{trx}$-0.0 / $SasA_{trx}$-0.3	-0.2672	-0.6629 to 0.1285	No	ns	0.2498
KaiB-1.75, $SasA_{trx}$-0.0 / $SasA_{trx}$-0.65	-0.3274	-0.7231 to 0.06834	No	ns	0.1199
KaiB-1.75, $SasA_{trx}$-0.0 / $SasA_{trx}$-1.0	-0.1683	-0.5640 to 0.2275	No	ns	0.6662
KaiB-1.75, $SasA_{trx}$-0.0 / $SasA_{trx}$-1.8	-0.08904	-0.4848 to 0.3067	No	ns	0.9653
KaiB-1.75, $SasA_{trx}$-0.0 / $SasA_{trx}$-3.5	-0.06065	-0.4564 to 0.3351	No	ns	0.9946
KaiA-0.3, $CikA_{psr}$-0.0 / $CikA_{psr}$-0.1	-0.06478	-0.3795 to 0.2500	No	ns	0.9863
KaiA-0.3, $CikA_{psr}$-0.0 / $CikA_{psr}$-0.3	-0.06702	-0.3818 to 0.2477	No	ns	0.9833
KaiA-0.3, $CikA_{psr}$-0.0 / $CikA_{psr}$-0.65	-0.1085	-0.4233 to 0.2063	No	ns	0.851
KaiA-0.3, $CikA_{psr}$-0.0 / $CikA_{psr}$-1.0	-0.09977	-0.4145 to 0.2150	No	ns	0.892
KaiA-0.3, $CikA_{psr}$-0.0 / $CikA_{psr}$-1.8	-0.05927	-0.3740 to 0.2555	No	ns	0.9918
KaiA-0.3, $CikA_{psr}$-0.0 / $CikA_{psr}$-3.5	-0.134	-0.4487 to 0.1808	No	ns	0.7026
KaiA-0.3, $CikA_{psr}$-0.0 / $CikA_{psr}$-5.0	-0.1477	-0.4625 to 0.1670	No	ns	0.6145

Ordinary one-way ANOVA performed with Dunnett's multiple comparisons test was used to compare amplitude values under specified conditions: ns, not significant; *, $P < 0.05$; **, $P < 0.01$; ***, $P < 0.001$; #, $P < 0.0001$. If not specified, fluorescence assays were run with 1.2 μM KaiA, 3.45 μM KaiB, 3.5 μM KaiC, and 0.05 μM fluorescently labeled KaiB probe.

Table S9. Ordinary two-way ANOVA of period values from fluorescence assays with pairwise comparisons showing how core oscillator components modulate SasA or CikA effects.

[Fixed protein-concentration] protein-concentration comparison with / altered protein-concentration (μM)	Predicted (LS) mean diff.	95.00% CI of diff.	Significant ?	Summary	Adjusted P Value	N1	N2
[SasA-0.0] KaiB-3.5 / KaiB-1.75	-1.666	-2.798 to -0.5337	Yes	**	0.0021	7	12
[SasA-0.0] KaiB-3.5 / KaiB-7.0	0.5423	-0.8515 to 1.936	No	ns	0.6753	7	5
[SasA-0.0] KaiB-3.5 / KaiB-17.5	1.244	-0.1495 to 2.638	No	ns	0.0907	7	5
[SasA-0.1] KaiB-3.5 / KaiB-1.75	0.02	-1.493 to 1.533	No	ns	>0.9999	5	5
[SasA-0.1] KaiB-3.5 / KaiB-7.0	0.808	-0.9387 to 2.555	No	ns	0.5642	5	3
[SasA-0.1] KaiB-3.5 / KaiB-17.5	1.228	-0.5187 to 2.975	No	ns	0.2316	5	3
[SasA-0.3] KaiB-3.5 / KaiB-1.75	-0.3765	-1.983 to 1.230	No	ns	0.9059	5	4
[SasA-0.3] KaiB-3.5 / KaiB-7.0	0.826	-0.9225 to 2.575	No	ns	0.5504	5	3
[SasA-0.3] KaiB-3.5 / KaiB-17.5	1.069	-0.6792 to 2.818	No	ns	0.3404	5	3
[SasA-0.65] KaiB-3.5 / KaiB-1.75	-0.0475	-1.654 to 1.559	No	ns	0.9997	5	4
[SasA-0.65] KaiB-3.5 / KaiB-7.0	0.56	-1.189 to 2.309	No	ns	0.7967	5	3
[SasA-0.65] KaiB-3.5 / KaiB-17.5	1.103	-0.6452 to 2.852	No	ns	0.3152	5	3
[SasA-1.0] KaiB-3.5 / KaiB-1.75	-0.174	-1.687 to 1.339	No	ns	0.9868	5	5
[SasA-1.0] KaiB-3.5 / KaiB-7.0	1.041	-0.7054 to 2.788	No	ns	0.3594	5	3
[SasA-1.0] KaiB-3.5 / KaiB-17.5	0.8813	-0.8654 to 2.628	No	ns	0.4959	5	3
[SasA-1.8] KaiB-3.5 / KaiB-1.75	2	-0.2738 to 4.274	No	ns	0.0925	2	2
[SasA-1.8] KaiB-3.5 / KaiB-7.0	3.375	0.5902 to 6.160	Yes	*	0.0149	2	1
[CikA-0.0] KaiA-1.2 / KaiA-0.3	-5.433	-6.313 to -4.552	Yes	#	<0.0001	7	6
[CikA-0.0] KaiA-1.2 / KaiA-0.6	-1.293	-2.220 to -0.3661	Yes	**	0.0031	7	5
[CikA-0.0] KaiA-1.2 / KaiA-2.4	0.5891	-0.3376 to 1.516	No	ns	0.3347	7	5
[CikA-0.0] KaiA-1.2 / KaiA-3.6	0.9321	-0.05985 to 1.924	No	ns	0.0719	7	4
[CikA-0.1] KaiA-1.2 / KaiA-0.3	-4.394	-5.728 to -3.060	Yes	#	<0.0001	5	2
[CikA-0.1] KaiA-1.2 / KaiA-0.6	-1.441	-2.605 to -0.2764	Yes	**	0.0098	5	3
[CikA-0.1] KaiA-1.2 / KaiA-2.4	0.4493	-0.7150 to 1.614	No	ns	0.7689	5	3
[CikA-0.1] KaiA-1.2 / KaiA-3.6	-0.174	-1.920 to 1.572	No	ns	0.9979	5	1
[CikA-0.3] KaiA-1.2 / KaiA-0.3	-2.871	-4.205 to -1.537	Yes	#	<0.0001	5	2
[CikA-0.3] KaiA-1.2 / KaiA-0.6	-1.113	-2.277 to 0.05163	No	ns	0.0659	5	3
[CikA-0.3] KaiA-1.2 / KaiA-2.4	0.3707	-0.7936 to 1.535	No	ns	0.8669	5	3
[CikA-0.3] KaiA-1.2 / KaiA-3.6	0.274	-1.472 to 2.020	No	ns	0.9885	5	1
[CikA-0.65] KaiA-1.2 / KaiA-0.3	-1.215	-2.209 to -0.2202	Yes	*	0.012	5	3
[CikA-0.65] KaiA-1.2 / KaiA-0.6	-0.908	-1.902 to 0.08644	No	ns	0.0824	5	3
[CikA-0.65] KaiA-1.2 / KaiA-2.4	0.222	-0.7724 to 1.216	No	ns	0.9194	5	3
[CikA-1.0] KaiA-1.2 / KaiA-0.3	-1.308	-2.302 to -0.3136	Yes	**	0.0061	5	3
[CikA-1.0] KaiA-1.2 / KaiA-0.6	-0.5813	-1.576 to 0.4131	No	ns	0.3817	5	3
[CikA-1.0] KaiA-1.2 / KaiA-2.4	0.05533	-0.9391 to 1.050	No	ns	0.9985	5	3
[CikA-1.8] KaiA-1.2 / KaiA-0.3	-0.55	-1.713 to 0.6129	No	ns	0.6158	5	3

[CikA-1.8] KaiA-1.2 / KaiA-0.6	-0.87	-2.033 to 0.2929	No	ns	0.2068	5	3
[CikA-1.8] KaiA-1.2 / KaiA-2.4	-0.04667	-1.210 to 1.116	No	ns	0.9999	5	3
[CikA-1.8] KaiA-1.2 / KaiA-3.6	-1.51	-3.254 to 0.2344	No	ns	0.1114	5	1
[CikA-3.5] KaiA-1.2 / KaiA-0.3	0.1247	-0.8698 to 1.119	No	ns	0.9839	5	3
[CikA-3.5] KaiA-1.2 / KaiA-0.6	-0.1687	-1.163 to 0.8258	No	ns	0.962	5	3
[CikA-3.5] KaiA-1.2 / KaiA-2.4	0.3213	-0.6731 to 1.316	No	ns	0.7969	5	3
[CikA-5.0] KaiA-1.2 / KaiA-0.3	0.1613	-1.002 to 1.324	No	ns	0.9926	5	3
[CikA-5.0] KaiA-1.2 / KaiA-0.6	-0.1953	-1.358 to 0.9676	No	ns	0.9847	5	3
[CikA-5.0] KaiA-1.2 / KaiA-2.4	-0.132	-1.295 to 1.031	No	ns	0.9965	5	3
[CikA-5.0] KaiA-1.2 / KaiA-3.6	-4.302	-6.046 to -2.558	Yes	#	<0.0001	5	1

Ordinary two-way ANOVA performed with Dunnett's multiple comparisons test was used to compare pairwise period values under specified conditions: ns, not significant; *, $P < 0.05$; **, $P < 0.01$; ***, $P < 0.001$; #, $P < 0.0001$. Predicted least squared (LS) mean difference is reported instead of mean due to comparing means with different number of independent experiments. N1 and N2 specify the number of independent experiments that were able to be fit by FFT-NLLS with the online BioDare suite for the first and second conditions being compared, respectively (*60*, *61*). If not specified, oscillators were run with 1.2 μM KaiA, 3.45 μM KaiB, 3.5 μM KaiC, and 0.05 μM fluorescently labeled KaiB probe.

Table S10. Ordinary two-way ANOVA of amplitude values from fluorescence assays with pairwise comparisons showing how core oscillator components modulate SasA or CikA effects.

[Fixed protein-concentration] protein-concentration comparison with / altered protein-concentration (μM)	Predicted (LS) mean diff.	95.00% CI of diff.	Significant ?	Summary	Adjusted P Value	N1	N2
[SasA-0.0] KaiB-3.5 / KaiB-1.75	0.434	0.3145 to 0.5535	Yes	#	<0.0001	7	12
[SasA-0.0] KaiB-3.5 / KaiB-7.0	0.04656	-0.1006 to 0.1937	No	ns	0.7909	7	5
[SasA-0.0] KaiB-3.5 / KaiB-17.5	0.08743	-0.05971 to 0.2346	No	ns	0.3543	7	5
[SasA-0.1] KaiB-3.5 / KaiB-1.75	0.04169	-0.1180 to 0.2014	No	ns	0.8745	5	5
[SasA-0.1] KaiB-3.5 / KaiB-7.0	0.06957	-0.1148 to 0.2540	No	ns	0.7056	5	3
[SasA-0.1] KaiB-3.5 / KaiB-17.5	0.1301	-0.05432 to 0.3145	No	ns	0.2293	5	3
[SasA-0.3] KaiB-3.5 / KaiB-1.75	-0.1321	-0.3016 to 0.03751	No	ns	0.164	5	4
[SasA-0.3] KaiB-3.5 / KaiB-7.0	0.04368	-0.1409 to 0.2283	No	ns	0.9036	5	3
[SasA-0.3] KaiB-3.5 / KaiB-17.5	0.07517	-0.1094 to 0.2598	No	ns	0.6589	5	3
[SasA-0.65] KaiB-3.5 / KaiB-1.75	-0.215	-0.3845 to -0.04541	Yes	**	0.0089	5	4
[SasA-0.65] KaiB-3.5 / KaiB-7.0	-0.05956	-0.2442 to 0.1250	No	ns	0.7932	5	3
[SasA-0.65] KaiB-3.5 / KaiB-17.5	0.01352	-0.1711 to 0.1981	No	ns	0.9966	5	3
[SasA-1.0] KaiB-3.5 / KaiB-1.75	-0.1468	-0.3065 to 0.01293	No	ns	0.0792	5	5
[SasA-1.0] KaiB-3.5 / KaiB-7.0	0.04559	-0.1388 to 0.2300	No	ns	0.8907	5	3
[SasA-1.0] KaiB-3.5 / KaiB-17.5	0.03213	-0.1523 to 0.2165	No	ns	0.9571	5	3
[SasA-1.8] KaiB-3.5 / KaiB-1.75	0.01854	-0.2246 to 0.2617	No	ns	0.9792	2	2
[SasA-1.8] KaiB-3.5 / KaiB-7.0	-0.01082	-0.3086 to 0.2869	No	ns	0.9952	2	1
[CikA-0.0] KaiA-1.2 / KaiA-0.3	0.3983	0.2520 to 0.5447	Yes	#	<0.0001	7	5
[CikA-0.0] KaiA-1.2 / KaiA-0.6	0.1897	0.04336 to 0.3361	Yes	**	0.0066	7	5
[CikA-0.0] KaiA-1.2 / KaiA-2.4	0.12	-0.02640 to 0.2663	No	ns	0.1407	7	5
[CikA-0.0] KaiA-1.2 / KaiA-3.6	0.2376	0.08098 to 0.3943	Yes	**	0.0012	7	4
[CikA-0.1] KaiA-1.2 / KaiA-0.3	0.3469	0.1364 to 0.5574	Yes	***	0.0004	5	2
[CikA-0.1] KaiA-1.2 / KaiA-0.6	0.1197	-0.06407 to 0.3034	No	ns	0.325	5	3
[CikA-0.1] KaiA-1.2 / KaiA-2.4	0.0546	-0.1291 to 0.2383	No	ns	0.8923	5	3
[CikA-0.1] KaiA-1.2 / KaiA-3.6	0.2974	0.02178 to 0.5730	Yes	*	0.0299	5	1
[CikA-0.3] KaiA-1.2 / KaiA-0.3	0.3029	0.09246 to 0.5134	Yes	**	0.0021	5	2
[CikA-0.3] KaiA-1.2 / KaiA-0.6	0.08615	-0.09757 to 0.2699	No	ns	0.626	5	3
[CikA-0.3] KaiA-1.2 / KaiA-2.4	0.06877	-0.1150 to 0.2525	No	ns	0.7871	5	3
[CikA-0.3] KaiA-1.2 / KaiA-3.6	0.4703	0.1947 to 0.7459	Yes	***	0.0002	5	1
[CikA-0.65] KaiA-1.2 / KaiA-0.3	0.3491	0.1872 to 0.5111	Yes	#	<0.0001	5	3
[CikA-0.65] KaiA-1.2 / KaiA-0.6	0.06287	-0.09909 to 0.2248	No	ns	0.6955	5	3
[CikA-0.65] KaiA-1.2 / KaiA-2.4	0.08232	-0.07964 to 0.2443	No	ns	0.4976	5	3
[CikA-1.0] KaiA-1.2 / KaiA-0.3	0.2408	0.07883 to 0.4027	Yes	**	0.0017	5	3
[CikA-1.0] KaiA-1.2 / KaiA-0.6	0.06642	-0.09553 to 0.2284	No	ns	0.6594	5	3
[CikA-1.0] KaiA-1.2 / KaiA-2.4	0.0411	-0.1209 to 0.2031	No	ns	0.8874	5	3
[CikA-1.8] KaiA-1.2 / KaiA-0.3	0.1746	-0.008936 to 0.3581	No	ns	0.0675	5	3

[CikA-1.8] KaiA-1.2 / KaiA-0.6	-0.03042	-0.2139 to 0.1531	No	ns	0.9854	5	3
[CikA-1.8] KaiA-1.2 / KaiA-2.4	0.08793	-0.09558 to 0.2714	No	ns	0.6045	5	3
[CikA-1.8] KaiA-1.2 / KaiA-3.6	0.262	-0.01327 to 0.5373	No	ns	0.0673	5	1
[CikA-3.5] KaiA-1.2 / KaiA-0.3	0.1377	-0.02421 to 0.2997	No	ns	0.1154	5	3
[CikA-3.5] KaiA-1.2 / KaiA-0.6	-0.03605	-0.1980 to 0.1259	No	ns	0.92	5	3
[CikA-3.5] KaiA-1.2 / KaiA-2.4	0.1386	-0.02338 to 0.3005	No	ns	0.1124	5	3
[CikA-5.0] KaiA-1.2 / KaiA-0.3	0.09614	-0.08737 to 0.2796	No	ns	0.5253	5	3
[CikA-5.0] KaiA-1.2 / KaiA-0.6	-0.02335	-0.2069 to 0.1602	No	ns	0.9947	5	3
[CikA-5.0] KaiA-1.2 / KaiA-2.4	0.07869	-0.1048 to 0.2622	No	ns	0.6934	5	3
[CikA-5.0] KaiA-1.2 / KaiA-3.6	0.2078	-0.06747 to 0.4830	No	ns	0.1999	5	1

Ordinary two-way ANOVA performed with Dunnett's multiple comparisons test was used to compare pairwise amplitude values under specified conditions: ns, not significant; *, $P < 0.05$; **, $P < 0.01$; ***, $P < 0.001$; #, $P < 0.0001$. Predicted least squared (LS) mean difference is reported instead of mean due to comparing means with different number of independent experiments. N1 and N2 specify the number of independent experiments that were able to be fit by FFT-NLLS with the online BioDare suite for the first and second conditions being compared, respectively (*60, 61*). If not specified, oscillators were run with 1.2 μM KaiA, 3.45 μM KaiB, 3.5 μM KaiC, and 0.05 μM fluorescently labeled KaiB probe.

Table S11. Cyanobacterial strains used in this study.

Strain	Genotype (NS denotes neutral site)	Antibiotic resistance	Source
WT (AMC541)	NSII-P$_{kaiBC}$*::luc*	Cm	Lab collection
Δ*sasA* (AMC1192)	NSII-P$_{kaiBC}$*::luc ΔsasA*	Cm	Lab collection
sasA-H28A	NSII-P$_{kaiBC}$*::luc. sasA*-H28A	Cm	This study
sasA-N93A	NSII-P$_{kaiBC}$*::luc. sasA*-N93A	Cm	This study
sasA-N93E	NSII-P$_{kaiBC}$*::luc. sasA*-N93E	Cm	This study
sasA-Q94A	NSII-P$_{kaiBC}$*::luc sasA*-Q94A	Cm	This study
sasA-H28A-Q94A	NSII-P$_{kaiBC}$*::luc sasA*-H28A-Q94A	Cm	This study
sasA-Q97A	NSII-P$_{kaiBC}$*::luc. sasA*-Q97A	Cm	This study
sasA-Q97E	NSII-P$_{kaiBC}$*::luc. sasA*-Q97E	Cm	This study
sasA-Q101A	NSII-P$_{kaiBC}$*::luc sasA*-Q101A	Cm	This study
AMC704	Δ*kaiC* / NSII-P*kaiBC::luc*	Cm	Lab collection
AMC1722	Tn*5* 8S15-E11 in AMC541	Cm	Boyd et al., 2013 (*43*)
Δ*rpaA*	*rpaA*::Gm / NSII-P*kaiBC::luc*	Cm	This study
rpaA-R121Q	*rpaA*(G362->A) / NSII-P*kaiBC::luc*	Cm	This study

Table S12. Plasmids and primers used in generating cyanobacterial strains.

Plasmids	**Description**	**Source**
pSL2680	CRISPR/Cas12a plasmid; Km resistance	Addgene (#85581)
pSL2680-HA	pSL2680 + SasA H28A substitution	This study
pSL2680-NA	pSL2680 + SasA N93A substitution	This study
pSL2680-NE	pSL2680 + SasA N93E substitution	This study
pSL2680-94	pSL2680 + SasA Q94A substitution	This study
pSL2680-HA/94	pSL2680 + SasA H28A and Q94A substitutions	This study
pSL2680-97	pSL2680 + SasA Q97A substitution	This study
pSL2680-QE	pSL2680 + SasA Q97E substitution	This study
pSL2680-101	pSL2680 + SasA Q101A substitution	This study
pSL2680	RSF1010-backbone, Cas12a and CRISPR assay from *Francisella novicida*, Km^R	Ungerer and Pakrasi, 2016 (*44*)
AM4523	Deletion construct containing *rpaA*::Gm flanked by *S. elongatus* gDNA	Lab collection
pDE32	pSL2680 with gRNA targeting *rpaA* and HDR encoding *rpaA* (G362->A)	This study
Primers	**Sequence (5'-3')**	

Primers used for pSL2680-HA	
H28A gRNA F	AGATTGCAGCGGGTTAAAAATATT
H28A gRNA R	AGACAATATTTTTAACCCGCTGCA
H28A homology arm upstream F	TAGCTTTAATGCGGTAGTTGGTACCATGATCGACGCCTGTCGA
H28A homology arm upstream R	TTTAACCCGCTGCACGATGGCCTGTGACAGGGGCCG
H28A homology arm downstream F	CGGCCCCTGTCACAGGCCATCGTGCAGCGGGTTAAA
Primers used for pSL2680-NA	
N93A gRNA F	AGATGCTAATTGATCGGTGAGGTC
N93A gRNA R	AGACGACCTCACCGATCAATTAGC
N93A homology arm upstream F	CATTTTTTTGTCTAGCTTTAATGCGGTAGTTGGTACC CTGGCGATGGACTTGCACTCA
N93A homology arm upstream R	CTGGGGCAACTGGGCGGCTAATTGATCGGT
N93A homology arm downstream F	ACCGATCAATTAGCCGCCCAGTTGCCCCAG
N93A homology arm downstream R	GCCCGGATTACAGATCCTCTAGAGTCGACGGTACC TTAGCAGGGCATGGTGTAGC
Primers used for pSL2680-NE	
N93E gRNA F	AGATGCTAATTGATCGGTGAGGTC
N93E gRNA R	AGACGACCTCACCGATCAATTAGC
N93E homology arm upstream F	CATTTTTTTGTCTAGCTTTAATGCGGTAGTTGGTACC CTGGCGATGGACTTGCACTCA
N93E homology arm upstream R	CTGGGGCAACTGCTCGGCTAATTGATCGGT
N93E homology arm downstream F	ACCGATCAATTAGCCGAGCAGTTGCCCCAG
N93E homology arm downstream R	GCCCGGATTACAGATCCTCTAGAGTCGACGGTACC TTAGCAGGGCATGGTGTAGC
Primers used for pSL2680-94	
Q94A gRNA F	AGATGTTGGCTAATTGATCGGTGA
Q94AgRNA R	AGACTCACCGATCAATTAGCCAAC
Q94A homology arm upstream F	CATTTTTTTGTCTAGCTTTAATGCGGTAGTTGGTACC CTGGCGATGGACTTGCACTCA
Q94A homology arm upstream R	CCACTGGGGCAACGCGTTGGCTAATTG
Q94A homology arm downstream F	CAATTAGCCAACGCGTTGCCCCAGTGG
Q94A homology arm downstream R	GCCCGGATTACAGATCCTCTAGAGTCGACGGTACC TTAGCAGGGCATGGTGTAGC
Primers used for pSL2680 HA/94	
HA/94 gRNA F	AGATACGAAGAAAGCTCAGTGAGC
HA/94 gRNA R	AGACGCTCACTGAGCTTTCTTCGT

HA/94 homology arm upstream F	CATTTTTTTGTCTAGCTTTAATGCGGTAGTTGGTACC CTGGCGATGGACTTGCACTCA
HA/94 homology arm upstream R	GCTCACTGAGCTTTCTTCGTGTATCCGCCAAATTGT
HA94 homology arm downstream F	ACAATTTGGCGGATACACGAAGAAAGCTCAGTGAGC
HA94 homology arm downstream R	CAGATCCTCTAGAGTCGACGGTACC ATCGTGCCTGATCGAACA
Primers used for pSL2680-97	
Q97A gRNA F	AGATGGGCAACTGGTTGGCTAATT
Q97A gRNA R	AGACAATTAGCCAACCAGTTGCCC
Q97A homology arm upstream F	CATTTTTTTGTCTAGCTTTAATGCGGTAGTTGGTACC CTGGCGATGGACTTGCACTCA
Q97A homology arm upstream R	CTGAACCAGCCACGCGGGCAACTGGTT
Q97A homology arm downstream F	AACCAGTTGCCCGCGTGGCTGGTTCAG
Q97A homology arm downstream R	GCCCGGATTACAGATCCTCTAGAGTCGACGGTACC TTAGCAGGGCATGGTGTAGC
Primers used for pSL2680-QE	
Q97E gRNA F	AGATTGAGTGGCATCGACCTCACC
Q97E gRNA R	AGACGGTGAGGTCGATGCCACTCA
Q97E homology arm upstream F	CATTTTTTTGTCTAGCTTTAATGCGGTAGTTGGTACC CTGGCGATGGACTTGCACTCA
Q97E homology arm upstream R	GGCTAATTGATCGGTGAGGTCGATGCCACTCAGCACTTGGC
Q97E homology arm downstream F	ACCTCACCGATCAATTAGCCAACCAGTTGCCCGAGTGGCTGG
Q97E homology arm downstream R	GCCCGGATTACAGATCCTCTAGAGTCGACGGTACC TTAGCAGGGCATGGTGTAGC
Primers used for pSL2680-101	
Q101A gRNA F	AGATAACCAGCCACTGGGGCAACT
Q101A gRNA R	AGACAGTTGCCCCAGTGGCTGGTT
Q101A homology arm upstream F	CATTTTTTTGTCTAGCTTTAATGCGGTAGTTGGTACC CTGGCGATGGACTTGCACTCA
Q101A homology arm upstream R	AAAGGCCTCTTGCGCAACCAGCCACTG
Q101A homology arm downstream F	CAGTGGCTGGTTGCGCAAGAGGCCTTT
Q101A homology arm downstream R	GCCCGGATTACAGATCCTCTAGAGTCGACGGTACC TTAGCAGGGCATGGTGTAGC
Primers used for colony PCR	
sasA1_SNP_chkF	CGAGTTAATGGGAGAGTCTCTGTC
sasA1_SNP_chkR	GGCCTAGCTCCGTGAACG
Primer used for construction of RpaA-R121Q mutant stains	

rpaA_gRNA_F	AGATGCTGAACAGCTAAAGCCTGA
rpaA_gRNA_R	AGACTCAGGCTTTAGCTGTTCAGC
rpaA_HDR-UP_F	CATTTTTTTGTCTAGCTTTAATGCGGTAGTTGGTACCGAGTCC TGAGCTGCTACTGCC
rpaA_HDR-UP_R	GGTCAGGCTTTAGCTGTGCAGCTCGTTCCCGACCTGAT
rpaA_HDR-DWN_F	ATCAGGTCGGGAACGAGCTGCACAGCTAAAGCCTGACC
rpaA_HDR-DWN_R	GCCCGGATTACAGATCCTCTAGAGTCGACGGTACCGCCATGT CAAACTCAATCAAGCG
rpaA_cPCR_F	GAACAGGCTGAAACGATGGC
rpaA_cPCR_R	GGATTGAGTAATTTGATGGTTGACTGC

References and Notes

1. J. C. Dunlap, J. J. Loros, P. J. DeCoursey, Eds., *Chronobiology: Biological Timekeeping* (Sinauer Associates, 2004).

2. M. A. Woelfle, Y. Ouyang, K. Phanvijhitsiri, C. H. Johnson, The adaptive value of circadian clocks: An experimental assessment in cyanobacteria. *Curr. Biol.* **14**, 1481–1486 (2004). doi:10.1016/j.cub.2004.08.023 Medline

3. T. Kondo, C. A. Strayer, R. D. Kulkarni, W. Taylor, M. Ishiura, S. S. Golden, C. H. Johnson, Circadian rhythms in prokaryotes: Luciferase as a reporter of circadian gene expression in cyanobacteria. *Proc. Natl. Acad. Sci. U.S.A.* **90**, 5672–5676 (1993). doi:10.1073/pnas.90.12.5672 Medline

4. M. Ishiura, S. Kutsuna, S. Aoki, H. Iwasaki, C. R. Andersson, A. Tanabe, S. S. Golden, C. H. Johnson, T. Kondo, Expression of a gene cluster *kaiABC* as a circadian feedback process in cyanobacteria. *Science* **281**, 1519–1523 (1998). doi:10.1126/science.281.5382.1519 Medline

5. J. Tomita, M. Nakajima, T. Kondo, H. Iwasaki, No transcription-translation feedback in circadian rhythm of KaiC phosphorylation. *Science* **307**, 251–254 (2005). doi:10.1126/science.1102540 Medline

6. M. Nakajima, K. Imai, H. Ito, T. Nishiwaki, Y. Murayama, H. Iwasaki, T. Oyama, T. Kondo, Reconstitution of circadian oscillation of cyanobacterial KaiC phosphorylation in vitro. *Science* **308**, 414–415 (2005). doi:10.1126/science.1108451 Medline

7. M. J. Rust, J. S. Markson, W. S. Lane, D. S. Fisher, E. K. O'Shea, Ordered phosphorylation governs oscillation of a three-protein circadian clock. *Science* **318**, 809–812 (2007). doi:10.1126/science.1148596 Medline

8. T. Nishiwaki, Y. Satomi, Y. Kitayama, K. Terauchi, R. Kiyohara, T. Takao, T. Kondo, A sequential program of dual phosphorylation of KaiC as a basis for circadian rhythm in cyanobacteria. *EMBO J.* **26**, 4029–4037 (2007). doi:10.1038/sj.emboj.7601832 Medline

9. H. Iwasaki, T. Nishiwaki, Y. Kitayama, M. Nakajima, T. Kondo, KaiA-stimulated KaiC phosphorylation in circadian timing loops in cyanobacteria. *Proc. Natl. Acad. Sci. U.S.A.* **99**, 15788–15793 (2002). doi:10.1073/pnas.222467299 Medline

10. S. B. Williams, I. Vakonakis, S. S. Golden, A. C. LiWang, Structure and function from the circadian clock protein KaiA of *Synechococcus elongatus*: A potential clock input mechanism. *Proc. Natl. Acad. Sci. U.S.A.* **99**, 15357–15362 (2002). doi:10.1073/pnas.232517099 Medline

11. Y. Kitayama, H. Iwasaki, T. Nishiwaki, T. Kondo, KaiB functions as an attenuator of KaiC phosphorylation in the cyanobacterial circadian clock system. *EMBO J.* **22**, 2127–2134 (2003). doi:10.1093/emboj/cdg212 Medline

12. Y. Xu, T. Mori, C. H. Johnson, Cyanobacterial circadian clockwork: Roles of KaiA, KaiB and the *kaiBC* promoter in regulating KaiC. *EMBO J.* **22**, 2117–2126 (2003). doi:10.1093/emboj/cdg168 Medline

13. Y.-G. Chang, R. Tseng, N.-W. Kuo, A. LiWang, Rhythmic ring-ring stacking drives the circadian oscillator clockwise. *Proc. Natl. Acad. Sci. U.S.A.* **109**, 16847–16851 (2012). doi:10.1073/pnas.1211508109 Medline

14. Y.-G. Chang, N.-W. Kuo, R. Tseng, A. LiWang, Flexibility of the C-terminal, or CII, ring of KaiC governs the rhythm of the circadian clock of cyanobacteria. *Proc. Natl. Acad. Sci. U.S.A.* **108**, 14431–14436 (2011). doi:10.1073/pnas.1104221108 Medline

15. J. Abe, T. B. Hiyama, A. Mukaiyama, S. Son, T. Mori, S. Saito, M. Osako, J. Wolanin, E. Yamashita, T. Kondo, S. Akiyama, Atomic-scale origins of slowness in the cyanobacterial circadian clock. *Science* **349**, 312–316 (2015). doi:10.1126/science.1261040 Medline

16. H. Iwasaki, S. B. Williams, Y. Kitayama, M. Ishiura, S. S. Golden, T. Kondo, A KaiC-interacting sensory histidine kinase, SasA, necessary to sustain robust circadian oscillation in cyanobacteria. *Cell* **101**, 223–233 (2000). doi:10.1016/S0092-8674(00)80832-6 Medline

17. O. Schmitz, M. Katayama, S. B. Williams, T. Kondo, S. S. Golden, CikA, a bacteriophytochrome that resets the cyanobacterial circadian clock. *Science* **289**, 765–768 (2000). doi:10.1126/science.289.5480.765 Medline

18. N. B. Ivleva, T. Gao, A. C. LiWang, S. S. Golden, Quinone sensing by the circadian input kinase of the cyanobacterial circadian clock. *Proc. Natl. Acad. Sci. U.S.A.* **103**, 17468–17473 (2006). doi:10.1073/pnas.0606639103 Medline

19. N. Takai, M. Nakajima, T. Oyama, R. Kito, C. Sugita, M. Sugita, T. Kondo, H. Iwasaki, A KaiC-associating SasA-RpaA two-component regulatory system as a major circadian timing mediator in cyanobacteria. *Proc. Natl. Acad. Sci. U.S.A.* **103**, 12109–12114 (2006). doi:10.1073/pnas.0602955103 Medline

20. J. S. Markson, J. R. Piechura, A. M. Puszynska, E. K. O'Shea, Circadian control of global gene expression by the cyanobacterial master regulator RpaA. *Cell* **155**, 1396–1408 (2013). doi:10.1016/j.cell.2013.11.005 Medline

21. A. Gutu, E. K. O'Shea, Two antagonistic clock-regulated histidine kinases time the activation of circadian gene expression. *Mol. Cell* **50**, 288–294 (2013). doi:10.1016/j.molcel.2013.02.022 Medline

22. K. Ito-Miwa, Y. Furuike, S. Akiyama, T. Kondo, Tuning the circadian period of cyanobacteria up to 6.6 days by the single amino acid substitutions in KaiC. *Proc. Natl. Acad. Sci. U.S.A.* **117**, 20926–20931 (2020). doi:10.1073/pnas.2005496117 Medline

23. E. Leypunskiy, J. Lin, H. Yoo, U. Lee, A. R. Dinner, M. J. Rust, The cyanobacterial circadian clock follows midday in vivo and in vitro. *eLife* **6**, e23539 (2017). doi:10.7554/eLife.23539 Medline

24. G. K. Chow, A. G. Chavan, J. C. Heisler, Y.-G. Chang, A. LiWang, R. D. Britt, Monitoring protein–protein interactions in the cyanobacterial circadian clock in real time via electron paramagnetic resonance spectroscopy. *Biochemistry* **59**, 2387–2400 (2020). doi:10.1021/acs.biochem.0c00279 Medline

25. J. Heisler, A. Chavan, Y.-G. Chang, A. LiWang, Real-time in vitro fluorescence anisotropy of the cyanobacterial circadian clock. *Methods Protoc.* **2**, 42 (2019). doi:10.3390/mps2020042 Medline

26. C. S. Theile, M. D. Witte, A. E. M. Blom, L. Kundrat, H. L. Ploegh, C. P. Guimaraes, Site-specific N-terminal labeling of proteins using sortase-mediated reactions. *Nat. Protoc.* **8**, 1800–1807 (2013). doi:10.1038/nprot.2013.102 Medline

27. C. P. Guimaraes, M. D. Witte, C. S. Theile, G. Bozkurt, L. Kundrat, A. E. M. Blom, H. L. Ploegh, Site-specific C-terminal and internal loop labeling of proteins using sortase-mediated reactions. *Nat. Protoc.* **8**, 1787–1799 (2013). doi:10.1038/nprot.2013.101 Medline

28. B. Guo, P. S. Gurel, R. Shu, H. N. Higgs, M. Pellegrini, D. F. Mierke, Monitoring ATP hydrolysis and ATPase inhibitor screening using ^{1}H NMR. *Chem. Commun.* **50**, 12037–12039 (2014). doi:10.1039/C4CC04399E Medline

29. K. Terauchi, Y. Kitayama, T. Nishiwaki, K. Miwa, Y. Murayama, T. Oyama, T. Kondo, ATPase activity of KaiC determines the basic timing for circadian clock of cyanobacteria. *Proc. Natl. Acad. Sci. U.S.A.* **104**, 16377–16381 (2007). doi:10.1073/pnas.0706292104 Medline

30. R. M. Smith, S. B. Williams, Circadian rhythms in gene transcription imparted by chromosome compaction in the cyanobacterium *Synechococcus elongatus*. *Proc. Natl. Acad. Sci. U.S.A.* **103**, 8564–8569 (2006). doi:10.1073/pnas.0508696103 Medline

31. S. E. Cohen, S. S. Golden, Circadian rhythms in cyanobacteria. *Microbiol. Mol. Biol. Rev.* **79**, 373–385 (2015). doi:10.1128/MMBR.00036-15 Medline

32. H. Kageyama, T. Kondo, H. Iwasaki, Circadian formation of clock protein complexes by KaiA, KaiB, KaiC, and SasA in cyanobacteria. *J. Biol. Chem.* **278**, 2388–2395 (2003). doi:10.1074/jbc.M208899200 Medline

33. R. Tseng, Y.-G. Chang, I. Bravo, R. Latham, A. Chaudhary, N.-W. Kuo, A. Liwang, Cooperative KaiA-KaiB-KaiC interactions affect KaiB/SasA competition in the circadian clock of cyanobacteria. *J. Mol. Biol.* **426**, 389–402 (2014). doi:10.1016/j.jmb.2013.09.040 Medline

34. P. B. Straughn, L. R. Vass, C. Yuan, E. N. Kennedy, C. A. Foster, R. B. Bourret, Modulation of response regulator CheY reaction kinetics by two variable residues that affect conformation. *J. Bacteriol.* **202**, e00089-20 (2020). doi:10.1128/JB.00089-20 Medline

35. A. H. West, A. M. Stock, Histidine kinases and response regulator proteins in two-component signaling systems. *Trends Biochem. Sci.* **26**, 369–376 (2001). doi:10.1016/S0968-0004(01)01852-7 Medline

36. R. Tseng, N. F. Goularte, A. Chavan, J. Luu, S. E. Cohen, Y.-G. Chang, J. Heisler, S. Li, A. K. Michael, S. Tripathi, S. S. Golden, A. LiWang, C. L. Partch, Structural basis of the day-night transition in a bacterial circadian clock. *Science* **355**, 1174–1180 (2017). doi:10.1126/science.aag2516 Medline

37. Y.-G. Chang, S. E. Cohen, C. Phong, W. K. Myers, Y.-I. Kim, R. Tseng, J. Lin, L. Zhang, J. S. Boyd, Y. Lee, S. Kang, D. Lee, S. Li, R. D. Britt, M. J. Rust, S. S. Golden, A. LiWang,

A protein fold switch joins the circadian oscillator to clock output in cyanobacteria. *Science* **349**, 324–328 (2015). doi:10.1126/science.1260031 Medline

38. N. B. Ivleva, M. R. Bramlett, P. A. Lindahl, S. S. Golden, LdpA: A component of the circadian clock senses redox state of the cell. *EMBO J.* **24**, 1202–1210 (2005). doi:10.1038/sj.emboj.7600606 Medline

39. Y. Taniguchi, N. Takai, M. Katayama, T. Kondo, T. Oyama, Three major output pathways from the KaiABC-based oscillator cooperate to generate robust circadian *kaiBC* expression in cyanobacteria. *Proc. Natl. Acad. Sci. U.S.A.* **107**, 3263–3268 (2010). doi:10.1073/pnas.0909924107 Medline

40. M. J. Rust, S. S. Golden, E. K. O'Shea, Light-driven changes in energy metabolism directly entrain the cyanobacterial circadian oscillator. *Science* **331**, 220–223 (2011). doi:10.1126/science.1197243 Medline

41. Y.-I. Kim, D. J. Vinyard, G. M. Ananyev, G. C. Dismukes, S. S. Golden, Oxidized quinones signal onset of darkness directly to the cyanobacterial circadian oscillator. *Proc. Natl. Acad. Sci. U.S.A.* **109**, 17765–17769 (2012). doi:10.1073/pnas.1216401109 Medline

42. M. L. Paddock, J. S. Boyd, D. M. Adin, S. S. Golden, Active output state of the *Synechococcus* Kai circadian oscillator. *Proc. Natl. Acad. Sci. U.S.A.* **110**, E3849–E3857 (2013). doi:10.1073/pnas.1315170110 Medline

43. J. S. Boyd, J. R. Bordowitz, A. C. Bree, S. S. Golden, An allele of the *crm* gene blocks cyanobacterial circadian rhythms. *Proc. Natl. Acad. Sci. U.S.A.* **110**, 13950–13955 (2013). doi:10.1073/pnas.1312793110 Medline

44. J. Ungerer, H. B. Pakrasi, Cpf1 is a versatile tool for CRISPR genome editing across diverse species of cyanobacteria. *Sci. Rep.* **6**, 39681 (2016). doi:10.1038/srep39681 Medline

45. M. Nakajima, H. Ito, T. Kondo, *In vitro* regulation of circadian phosphorylation rhythm of cyanobacterial clock protein KaiC by KaiA and KaiB. *FEBS Lett.* **584**, 898–902 (2010). doi:10.1016/j.febslet.2010.01.016 Medline

46. J. Chew, E. Leypunskiy, J. Lin, A. Murugan, M. J. Rust, High protein copy number is required to suppress stochasticity in the cyanobacterial circadian clock. *Nat. Commun.* **9**, 3004 (2018). doi:10.1038/s41467-018-05109-4 Medline

47. J. Lin, J. Chew, U. Chockanathan, M. J. Rust, Mixtures of opposing phosphorylations within hexamers precisely time feedback in the cyanobacterial circadian clock. *Proc. Natl. Acad. Sci. U.S.A.* **111**, E3937–E3945 (2014). doi:10.1073/pnas.1408692111 Medline

48. M. Kaur, A. Ng, P. Kim, C. Diekman, Y.-I. Kim, CikA modulates the effect of KaiA on the period of the circadian oscillation in KaiC phosphorylation. *J. Biol. Rhythms* **34**, 218–223 (2019). doi:10.1177/0748730419828068 Medline

49. R. Murakami, R. Mutoh, R. Iwase, Y. Furukawa, K. Imada, K. Onai, M. Morishita, S. Yasui, K. Ishii, J. O. Valencia Swain, T. Uzumaki, K. Namba, M. Ishiura, The roles of the dimeric and tetrameric structures of the clock protein KaiB in the generation of circadian oscillations in cyanobacteria. *J. Biol. Chem.* **287**, 29506–29515 (2012). doi:10.1074/jbc.M112.349092 Medline

50. J. Valencia S., K. Bitou, K. Ishii, R. Murakami, M. Morishita, K. Onai, Y. Furukawa, K. Imada, K. Namba, M. Ishiura, Phase-dependent generation and transmission of time information by the KaiABC circadian clock oscillator through SasA-KaiC interaction in cyanobacteria. *Genes Cells* **17**, 398–419 (2012). doi:10.1111/j.1365-2443.2012.01597.x Medline

51. J. Snijder, J. M. Schuller, A. Wiegard, P. Lössl, N. Schmelling, I. M. Axmann, J. M. Plitzko, F. Förster, A. J. R. Heck, Structures of the cyanobacterial circadian oscillator frozen in a fully assembled state. *Science* **355**, 1181–1184 (2017). doi:10.1126/science.aag3218 Medline

52. R. Murakami, Y. Yunoki, K. Ishii, K. Terauchi, S. Uchiyama, H. Yagi, K. Kato, Cooperative binding of KaiB to the KaiC hexamer ensures accurate circadian clock oscillation in cyanobacteria. *Int. J. Mol. Sci.* **20**, 4550 (2019). doi:10.3390/ijms20184550 Medline

53. J. Snijder, R. J. Burnley, A. Wiegard, A. S. J. Melquiond, A. M. J. J. Bonvin, I. M. Axmann, A. J. R. Heck, Insight into cyanobacterial circadian timing from structural details of the KaiB-KaiC interaction. *Proc. Natl. Acad. Sci. U.S.A.* **111**, 1379–1384 (2014). doi:10.1073/pnas.1314326111 Medline

54. R. G. Garces, N. Wu, W. Gillon, E. F. Pai, Anabaena circadian clock proteins KaiA and KaiB reveal a potential common binding site to their partner KaiC. *EMBO J.* **23**, 1688–1698 (2004). doi:10.1038/sj.emboj.7600190 Medline

55. Y. Xu, T. Mori, C. H. Johnson, Circadian clock-protein expression in cyanobacteria: Rhythms and phase setting. *EMBO J.* **19**, 3349–3357 (2000). doi:10.1093/emboj/19.13.3349 Medline

56. C. K. Holtman, Y. Chen, P. Sandoval, A. Gonzales, M. S. Nalty, T. L. Thomas, P. Youderian, S. S. Golden, High-throughput functional analysis of the *Synechococcus elongatus* PCC 7942 genome. *DNA Res.* **12**, 103–115 (2005). doi:10.1093/dnares/12.2.103 Medline

57. K. Imai, Y. Kitayama, T. Kondo, Elucidation of the role of Clp protease components in circadian rhythm by genetic deletion and overexpression in cyanobacteria. *J. Bacteriol.* **195**, 4517–4526 (2013). doi:10.1128/JB.00300-13 Medline

58. H. Liu, J. H. Naismith, An efficient one-step site-directed deletion, insertion, single and multiple-site plasmid mutagenesis protocol. *BMC Biotechnol.* **8**, 91 (2008). doi:10.1186/1472-6750-8-91 Medline

59. C. A. Schneider, W. S. Rasband, K. W. Eliceiri, NIH Image to ImageJ: 25 years of image analysis. *Nat. Methods* **9**, 671–675 (2012). doi:10.1038/nmeth.2089 Medline

60. A. Moore, T. Zielinski, A. J. Millar, Online period estimation and determination of rhythmicity in circadian data, using the BioDare data infrastructure. *Methods Mol. Biol.* **1158**, 13–44 (2014). doi:10.1007/978-1-4939-0700-7_2 Medline

61. T. Zielinski, A. M. Moore, E. Troup, K. J. Halliday, A. J. Millar, Strengths and limitations of period estimation methods for circadian data. *PLOS ONE* **9**, e96462 (2014). doi:10.1371/journal.pone.0096462 Medline

62. S. R. Mackey, J. L. Ditty, E. M. Clerico, S. S. Golden, Detection of rhythmic bioluminescence from luciferase reporters in cyanobacteria. *Methods Mol. Biol.* **362**, 115–129 (2007). doi:10.1007/978-1-59745-257-1_8 Medline

63. A. Taton, F. Unglaub, N. E. Wright, W. Y. Zeng, J. Paz-Yepes, B. Brahamsha, B. Palenik, T. C. Peterson, F. Haerizadeh, S. S. Golden, J. W. Golden, Broad-host-range vector system for synthetic biology and biotechnology in cyanobacteria. *Nucleic Acids Res.* **42**, e136 (2014). doi:10.1093/nar/gku673 Medline

64. E. M. Clerico, J. L. Ditty, S. S. Golden, Specialized techniques for site-directed mutagenesis in cyanobacteria. *Methods Mol. Biol.* **362**, 155–171 (2007). doi:10.1007/978-1-59745-257-1_11 Medline

65. J. Elhai, A. Vepritskiy, A. M. Muro-Pastor, E. Flores, C. P. Wolk, Reduction of conjugal transfer efficiency by three restriction activities of Anabaena sp. strain PCC 7120. *J. Bacteriol.* **179**, 1998–2005 (1997). doi:10.1128/jb.179.6.1998-2005.1997 Medline

66. J. Elhai, C. P. Wolk, "Conjugal transfer of DNA to cyanobacteria" in *Cyanobacteria*, vol. 167 of *Methods in Enzymology*, L. Packer, A. N. Glazer, Eds. (Elsevier, 1988), pp. 747–754.

67. S. S. Golden, L. A. Sherman, Optimal conditions for genetic transformation of the cyanobacterium Anacystis nidulans R2. *J. Bacteriol.* **158**, 36–42 (1984). doi:10.1128/jb.158.1.36-42.1984 Medline

68. A. Taton, E. Lis, D. M. Adin, G. Dong, S. Cookson, S. A. Kay, S. S. Golden, J. W. Golden, Gene transfer in *Leptolyngbya* sp. strain BL0902, a cyanobacterium suitable for production of biomass and bioproducts. *PLOS ONE* **7**, e30901 (2012). doi:10.1371/journal.pone.0030901 Medline

<jrn>69. N. B. Ivleva, S. S. Golden, Protein extraction, fractionation, and purification from cyanobacteria. *Methods Mol. Biol.* **362**, 365–373 (2007). doi:10.1007/978-1-59745-257-1_26 Medline</jrn>

70. D. G. Welkie, B. E. Rubin, Y.-G. Chang, S. Diamond, S. A. Rifkin, A. LiWang, S. S. Golden, Genome-wide fitness assessment during diurnal growth reveals an expanded role of the cyanobacterial circadian clock protein KaiA. *Proc. Natl. Acad. Sci. U.S.A.* **115**, E7174–E7183 (2018). doi:10.1073/pnas.1802940115 Medline

71. T. G. G. Battye, L. Kontogiannis, O. Johnson, H. R. Powell, A. G. W. Leslie, *iMOSFLM*: A new graphical interface for diffraction-image processing with *MOSFLM*. *Acta Crystallogr. D* **67**, 271–281 (2011). doi:10.1107/S0907444910048675 Medline

72. P. R. Evans, G. N. Murshudov, How good are my data and what is the resolution? *Acta Crystallogr. D* **69**, 1204–1214 (2013). doi:10.1107/S0907444913000061 Medline

73. A. J. McCoy, R. W. Grosse-Kunstleve, P. D. Adams, M. D. Winn, L. C. Storoni, R. J. Read, *Phaser* crystallographic software. *J. Appl. Crystallogr.* **40**, 658–674 (2007). doi:10.1107/S0021889807021206 Medline

74. D. Liebschner, P. V. Afonine, M. L. Baker, G. Bunkóczi, V. B. Chen, T. I. Croll, B. Hintze, L.-W. Hung, S. Jain, A. J. McCoy, N. W. Moriarty, R. D. Oeffner, B. K. Poon, M. G. Prisant, R. J. Read, J. S. Richardson, D. C. Richardson, M. D. Sammito, O. V. Sobolev,

D. H. Stockwell, T. C. Terwilliger, A. G. Urzhumtsev, L. L. Videau, C. J. Williams, P. D. Adams, Macromolecular structure determination using X-rays, neutrons and electrons: Recent developments in *Phenix*. *Acta Crystallogr. D* **75**, 861–877 (2019). doi:10.1107/S2059798319011471 Medline

75. P. Emsley, B. Lohkamp, W. G. Scott, K. Cowtan, Features and development of *Coot*. *Acta Crystallogr. D* **66**, 486–501 (2010). doi:10.1107/S0907444910007493 Medline

76. E. F. Pettersen, T. D. Goddard, C. C. Huang, G. S. Couch, D. M. Greenblatt, E. C. Meng, T. E. Ferrin, UCSF Chimera—A visualization system for exploratory research and analysis. *J. Comput. Chem.* **25**, 1605–1612 (2004). doi:10.1002/jcc.20084 Medline

77. M. F. Sanner, A. J. Olson, J. C. Spehner, Reduced surface: An efficient way to compute molecular surfaces. *Biopolymers* **38**, 305–320 (1996). doi:10.1002/(SICI)1097-0282(199603)38:3<305:AID-BIP4>3.0.CO;2-Y Medline

78. E. F. Pettersen, T. D. Goddard, C. C. Huang, E. C. Meng, G. S. Couch, T. I. Croll, J. H. Morris, T. E. Ferrin, UCSF ChimeraX: Structure visualization for researchers, educators, and developers. *Protein Sci.* **30**, 70–82 (2021). doi:10.1002/pro.3943 Medline

79. C. R. Bagshaw, *Biomolecular Kinetics: A Step-by-Step Guide* (CRC Press, 2017).

80. P. Kuzmič, Program DYNAFIT for the analysis of enzyme kinetic data: Application to HIV proteinase. *Anal. Biochem.* **237**, 260–273 (1996). doi:10.1006/abio.1996.0238 Medline

81. J. A. Goodrich, J. F. Kugel, *Binding and Kinetics for Molecular Biologists* (Cold Spring Harbor Laboratory Press, 2007).

82. H. Kageyama, T. Nishiwaki, M. Nakajima, H. Iwasaki, T. Oyama, T. Kondo, Cyanobacterial circadian pacemaker: Kai protein complex dynamics in the KaiC phosphorylation cycle in vitro. *Mol. Cell* **23**, 161–171 (2006). doi:10.1016/j.molcel.2006.05.039 Medline